RETROFITTING OF EXTERIOR BEAM-COLUMN JOINTS USING CFRP

BY

DANISH AHMED

A Thesis Presented to the
DEANSHIP OF GRADUATE STUDIES

KING FAHD UNIVERSITY OF PETROLEUM & MINERALS

DHAHRAN, SAUDI ARABIA

In Partial Fulfillment of the
Requirements for the Degree of

MASTER OF SCIENCE

In

CIVIL ENGINEERING

NOVEMBER, 2012

KING FAHD UNIVERSITY OF PETROLEUM & MINERALS

DHAHRAN- 31261, SAUDI ARABIA

DEANSHIP OF GRADUATE STUDIES

This thesis, written by **Danish Ahmed** under the direction of his thesis advisor and approved by his thesis committee, has been presented and accepted by the Dean of Graduate Studies, in partial fulfillment of the requirements for the degree of **MASTER OF SCIENCE IN CIVIL ENGINEERING.**

Dr. Mohammed H. Baluch
(Advisor)

26 DEC 2012

Dr. Nedal T. Ratrout
Department Chairman

CEE Chairman
For Dr. Muhammad K. Rahman
(Co-Advisor) 26 DEC 2012

Dr. Salam A. Zummo
Dean of Graduate Studies

Dr. Ali H. Al-Gadhib
(Member)

30/12/12
Date

Dr. Hussain J.Al-Gahtani
(Member)

Dr. Al Farabi M. Sharif
(Member)

Dedicated to my family and friends

ACKNOWLEDGMENTS

In the name of ALLAH, the Beneficent the Most Merciful

All honor and grandeur goes to Allah Almighty who gave me the strength and endurance to carry out this work.

First of all I would like to show my gratitude to esteemed university, **King Fahd University of Petroleum and Minerals**, and its learned faculty members for providing me with quality education that paved my way through my Master's studies and thesis work.

I would like to pay my immense regard and appreciation to my thesis advisor **Dr.Mohammed H. Baluch** for his consistent guidance, motivation and feedback during the course of this research work. Beside research work, he is always there to provide me advice on shaping up my career and future goals.

I would like to express my appreciation to my co-advisor **Dr**. **Muhammad K. Rahman** for helping me with my research work. I am heartily thankful to the efforts he put in while encouraging and mentoring me. I extend my deepest gratitude to my thesis committee members Dr. Ali H. Al-Gadhib, Dr. Hussain J.Al-Gahtani & Dr. Al Farabi M. Sharif who gave astute comments and reviewed my work.

I am also thankful to AFI (Alaa for Industry) who was the manufacturer for our lab testing equipments and Al-Yamama Company for helping me casting my specimens.

Thanks are due to the laboratory personnel Engr. Omer Hussein, Engr. Syed Imran Ali & Mr. M. Mukarram Khan. I owe thanks to my seniors Mr. Basheer Algohi, Mr. Halahla, Abdulsamee, Mr. Mohammed Osta, Mr. Mohammed Tholaia whose consistent guidance and support helped me during the course of Master's studies and research work. I would also like to thanks all my friends here at KFUPM who made my stay at KFUPM pleasant.

I would also like to thanks my (always there friends) friends Ajmal, Saad and Zubair whose consistent support and encouragement made my stay at Saudi Arabia a lot pleasant. Thanks guys, you were always there for me.

Last, but most important, I thank my family: my father and my mother for indescribable support, love and confidence they provided during course of my foreign studies. My wife for being always there for listening, encouraging, motivating me. My brothers for giving me immense support and motivation.

TABLE OF CONTENTS

LIST OF TABLES

LIST OF FIGURES

ABSTRACT

Full Name : Danish Ahmed

Thesis Title : RETROFITTING OF EXTERIOR BEAM-COLUMN JOINTS USING CFRP

Major Field : Civil Engineering

Date of Degree : November, 2012

Beam column joint is an important component of reinforced concrete frames and these joints should be designed and detailed properly, especially for cyclic loading, as for example when the frame is subjected to earthquake loading. Recent awareness of a potential seismic event in low to moderate seismicity regions of Saudi Arabia have led to concerns of the safety and vulnerability of reinforced concrete buildings, in which ductile detailing has not been provided explicitly in the design process. Most of the buildings designed in these regions are based on gravity load and wind loads and their behavior would be non-ductile in case of a seismic event and which could lead to loss of human life and severe economic disruption.

The objective of this study is to investigate the behavior of poor detailed beam-column joints under vertical cyclic & static load. These beam-column joints are representative of existing detailed building in seismically active area of Saudi Arabia.

Three types of specimens were tested with different detailing and reinforcement, out of which two were having with small "ρ" and one with higher "ρ", experimental result shows two type of failure between small and high "ρ", the specimens with lower "ρ" fails due to flexural failure and specimens with high "ρ" fails due to failure of joint under

shear which is validated by the mechanistic /experimental computations and also by DIANA modeling using Drucker-Prager with tension cut-off and tension softening.

CFRP retrofitting of beam column joints were also studied by modeling the ITU specimens with very low compressive strength concrete in DIANA and the Finite Element analysis shows very good correlation with experimental results for both control and retrofitted specimens.

الملخص

الاسم الكامل:دانش أحمد

عنوان الرسالة: التعديل التحديثي للمفاصل الخارج شعاع- العمود باستخدام

الرئيسية الميدانية: الهندسة المدنية

تاريخ الدرجة العلمية: نوفمبر، 2012

شعاع العمود المشترك هو عنصر هام من الإطارات الخرسانة المسلحة ويجب أن تصمم هذه المفاصل ومفصلة بشكل صحيح، وخاصة بالنسبة للتحميل دوري، كما هو الحال مثلا عندما يتعرض الإطار لتحميل الزلزال. وقد أدت الوعي مؤخرا الحدث الزلزالي المحتملة في مناطق منخفضة إلى معتدلة الزلزالية للمملكة العربية السعودية مخاوف من سلامة والضعف للمنشآت الخرسانية المسلحة، والتي لم يتم تفصيل الدكتايل المنصوص عليها صراحة في عملية التصميم. وتستند معظم المباني في هذه المناطق مصممة على الحمل الجاذبية والرياح الأحمال والسلوك من شأنه أن يكون غير قابل للسحب في حالة وجود الحدث الزلزالي والتي يمكن أن تؤدي إلى خسائر في الأرواح والاضطراب الاقتصادي الشديد.

والهدف من هذه الدراسة هو التحقيق في سلوك الفقراء المفاصل شعاع عمود مفصلة تحت رأسي ودوري حمولة ساكنة. هذه المفاصل هي الحزم العمود ممثل بناء مفصلة الموجودة في منطقة نشطة زلزاليا في المملكة العربية السعودية.

" ρ" الصغيرة واحد مع "ρتم اختبار ثلاثة أنواع من العينات مع تفاصيل مختلفة وتعزيز، منها اثنان من وجود مع " " فشل بسبب ρ" الصغيرة وعالية، والعينات مع انخفاض "ρأعلى، نتيجة التجريبية يظهر النوع الثاني من الفشل بين " " عالية فشل بسبب فشل المشترك في إطار من القص الذي يتم التحقق من صحة ρعدم الانحناء والعينات مع " -دراكر براجر مع التوتر وقطع DIANAالحسابات من قبل الآلية / تجريبية وأيضا عن طريق استخدام النمذجة

تخفيف التوترز

التعديل التحديثي للمفاصل العمود شعاع عبر الاقتداء العينات مع الاتحاد الدولي للاتصالات CFRPودرس أيضا وتحليل العناصر المحدودة يبين علاقة جيدة جدا مع النتائج التجريبية DIANAمنخفضة جدا ملموسة في قوة الضغط لكل من السيطرة والعينات التعديلي.

CHAPTER 1

INTRODUCTION

1.1 GENERAL

In the past few decades, many investigations have been carried out to evaluate the performance of reinforced concrete structures subjected to seismic loading all over the world. For many reinforced concrete buildings and bridges, a significant majority of the structural failures could be attributed to inadequate seismic design of columns and the beam-column joints and/or the deterioration of concrete structures.

All the building structures before 1980's were mostly design for the gravity load all over the world, these structures perform well under gravity loads but there performance are questionable under earthquake. Several recent earthquakes such as in Taiwan (1999), in Turkey (1999) and in Japan (2010) causes extensive building damage and collapse of RC structures because of old design and poor reinforcement detailing as shown in "Figure 1"

Shear failure of beam-column joints is defined as one of the causes of damage and collapse of these existing RC buildings due to poor reinforcement detailing within the beam column joint region.

Figure 1 Damages Due to Earthquake in Japan Earthquake (2010) Taiwan Earthquake (1999) and Turkey Earthquake (1999)

This thesis research is done under the collaborative research project between King Fahd University of Petroleum and Minerals (KFUPM) and Istanbul Technical University (ITU), in the area of seismic behavior of RC Structures to study the behavior of External beam-column joints with poor reinforcement detailing and retrofitting of these beam-column joints. Some of the specimens were tested at ITU lab and their results used to verify the Finite Element Modeling of beam-column joints and other detailed experimental program was conducted in KFUPM structures lab on old reinforcement detailed beam-column joints. Details, test results and finite element modeling of these beam-column joints are presented in further chapters.

1.2 SEISMICITY OF SAUDI ARABIA

Recently, there has been an increasing concern about the seismic activity along the western coast of the Kingdom. Several studies were conducted to estimate the level of the seismic risk in the Kingdom. The seismic hazard analysis for the Kingdom was performed. A zonation map, as shown in “Figure 2”, was developed for the Kingdom

based on the peak ground acceleration, (PGA), values calculated for 50 years service lifetime with 10% probability of being exceeded.

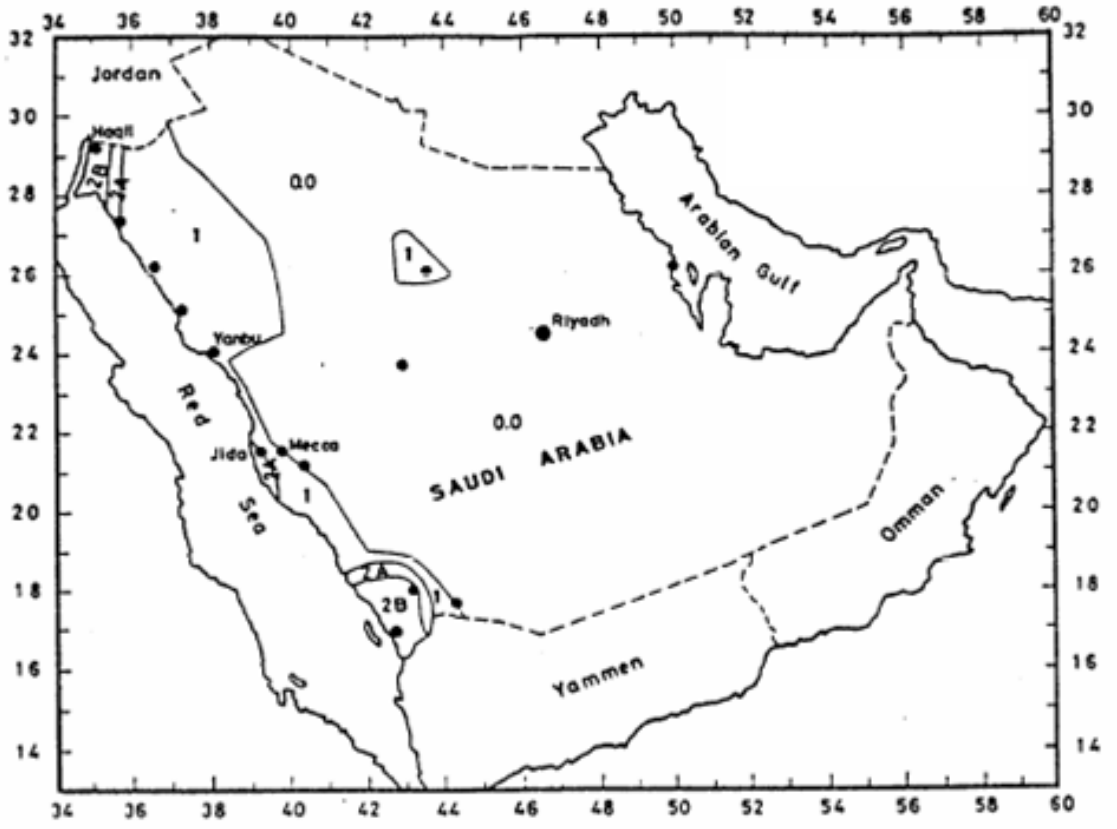

Figure2 Seismic Zonation Map for the Kingdom

Following the Uniform Building Code (UBC 1991) model, the Kingdom was divided into four zones with seismic zone numbers (SZN) of 0, 1, 2A and 2B as shown in table [1]

Table 1 Seismic Zone Number (SZN) and Corresponding PGA According to UBC

SZN	PGA in g's
0	<0.05
1	0.05 to 0.10
2A	0.10 to 0.15
2B	0.15 – and above

The framework of ACI 318M-95 code was adopted for the design of reinforced concrete structures in the Kingdom. According to the ACI 318M table number R21.2.1, the zones of SZN = 0 and 1 are considered of no and low risk levels, respectively. The zones of SZN = 2A and 2B are considered as areas with moderate risk level whereas the zones of SZN = 3 and 4 are considered to be high seismic risk areas. Thus according to the seismic zonation map most of the Kingdom regions fall in the zone of no and low risk level. Areas along the western coast, especially in the northwest and southwest, are considered to be of moderate risk level.

Some large cities in the Eastern Part of Saudi Arabia are located close to fault zones. As the population increases and new areas are developed, the seismic risk to human life and infrastructure increases. Geologists in an interview with the Asharq Al Awasat have explained that the cause of frequent earthquakes in recent years in the Arabian Peninsula is attributed to the fact that the region is located near active seismic borders on both the north-eastern and western borders. They stated that the Arab plate which includes the GCC states, Yemen and parts of Iran and Greater Syria collides with the Iranian plate (the Zagros Mountains) and the Turkish plate (the mountains of Anatolia). In turn, this causes

the movement of the Arab plate by two centimeters annually causing an expansion to the Red Sea area and causing friction between the two plates in the eastern region of the Arab plate.

In September 2005, an earthquake measuring 3.7 on the Richter scale shook Mecca and caused panic amongst the citizens of Otaibah, a neighborhood situated near the Holy Mosque. Official statements regarding the intensity of the tremor contradicted each other and this led to a decision by the Saudi cabinet to assign the responsibility of monitoring seismic activity to the Geological Survey, which is to include all centers affiliated to King Abdul Aziz City for Science and Technology, King Abdul Aziz University, King Saud University and King Fahd University for Petroleum and Minerals under the umbrella of the Geological Survey. Following this, in the year 2006 in Jeddah, Asharq Al-Awsat reported an earthquake measuring 4.1 on the Richter scale that shook the city of Haradh in Eastern Saudi Arabia. To reduce the damage of building and loss of life due to earthquakes there are two approaches to overcome this problem: the first is to build new structures using the new building code and design specifications specially for beam-column joints: or to strengthen the existing structures and heritage buildings by using the different techniques available.

1.3 IMPORTANCE OF BEAM-COLUMN JOINTS IN BUILDING

In the Kingdom of Saudi Arabia, most of the existing buildings that were built in the early eighties were for gravity and wind loads. These buildings are prone to severe

damage in case of an earthquake event because of the poor performance of beam-column joints of these existing buildings .Beam-column joints in a reinforced concrete moment resisting frame are crucial zones for transfer of loads effectively between the connecting elements (i.e. beams and columns) in the structure.

Portions of columns that are common to beams at their intersections are called beam-column joint. Beam-column joints perform a fundamental role integrating the structural system. It is the most critical component in the structure, especially in regions of medium to high seismicity. Shear failure of beam-column joints is identified as one of the main causes of collapse of many moment resisting reinforced concrete frames, particularly those constructed before 1980's. These frames were not seismic resistant due to the low-strength concrete and improper reinforcement details within the beam-column joint regions as given in "Figure 3"

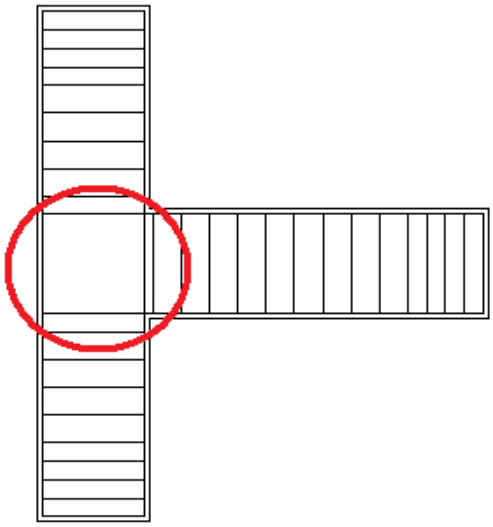

Figure 3 Non-Seismic Detailing of Joints

Unsafe design and detailing within the joint region can jeopardize the entire structure as shown in "Figure 4", even if other structural members conform to the design requirements. Since past three decades, extensive research has been carried out on studying the behaviour of joints under seismic conditions through experimental and analytical studies.

Figure 4 Example of Joint Failure

Various international codes of practice have been undergoing periodic revisions to incorporate the research findings into practice. In addition to above, to reduce the cost and simultaneously ensuring the seismic safety, retrofitting methods and techniques need to be developed. Significant progress is also being made in this area.

1.4 NEED OF RESEARCH

Recent awareness of a potential seismic event in low to moderate seismicity regions of Saudi Arabia have led to concerns of the safety and vulnerability of reinforced concrete buildings. Most of the buildings designed in these regions are based on gravity load their behavior would be non-ductile in case of a seismic event and which could lead to loss of

human life and severe economic disruption. Mostly in the gravity load design RC buildings beam column joints are the weakest member of the structure because of poor detailing of reinforcement in the joint region.

This research was planned to study the non ductile behavior of beam-column joint collaboration between King Fahd University of Petroleum and Minerals (KFUPM), Saudi Arabia and Istanbul Technical University (ITU), Turkey.

1.5 OBJECTIVE OF RESEARCH

The primary objective of this research is to investigate the behavior of reinforced concrete (RC) external beam-column joints under cyclic load. The beam column joints are representative of existing detailed buildings in seismically active areas of Saudi Arabia

The other objectives of this research involves

1. Experimental test on three types of RC beam-column joint with (a) Bent up joint detail, (b) Bent in joint detail and (c) bent in joint detail with flexural strength capacity.
2. Finite element modeling of beam-column joint specimens tested in KFUPM lab.
3. Finite element modeling of beam-column joint with experimental test results conducted in Istanbul Technical University
4. Finite element modeling of strengthened beam-column joint with CFRP tested at Istanbul Technical University.

CHAPTER 2

LITERATURE REVIEW

2.1 STUDIES FOR EXTERIOR BEAM COLUMN JOINTS EXPERIMENTAL TEST AND RETROFITTING.

Hakuto et al [1] studied the exterior and interior beam column joints which were designed as pre 70's specification with less reinforcement detailing in joint region and also tested one of the retrofitted interior beam column joints to see the improve ductility of interior specimens as shown in "Figure 5", For exterior beam column joints they investigated difference of reinforcement detailing of longitudinal top and bottom beam bars end hooks in the joint. In old practice the end hooks of beam bar in joint were bent up and in the current practice bars are bent down in the joint and the test shows the improvement in performance of joint with beam bars anchored according to current practice as shown in "Figure 6 and 7"

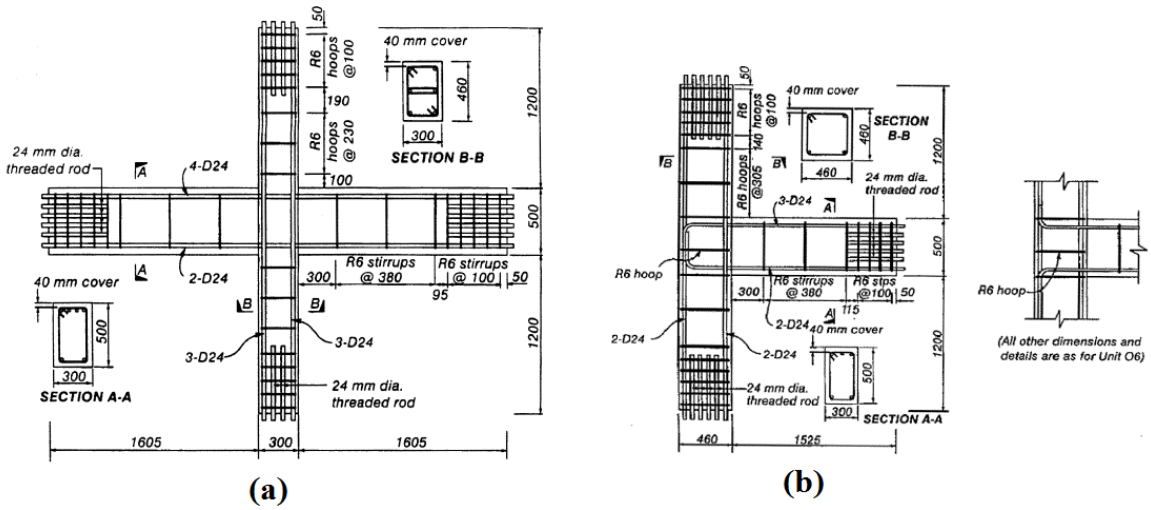

Figure 5 Interior and Exterior Beam Column Joints Size and Reinforcement Detailing [1]

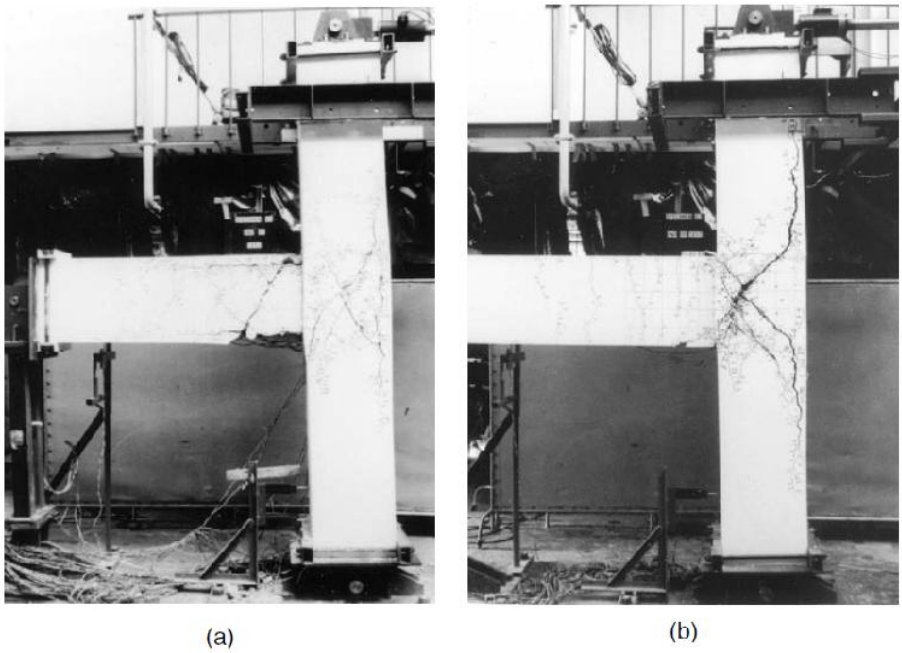

Figure 6 crack Pattern for (a) Bent Down and (b) Bent Up Specimens [1]

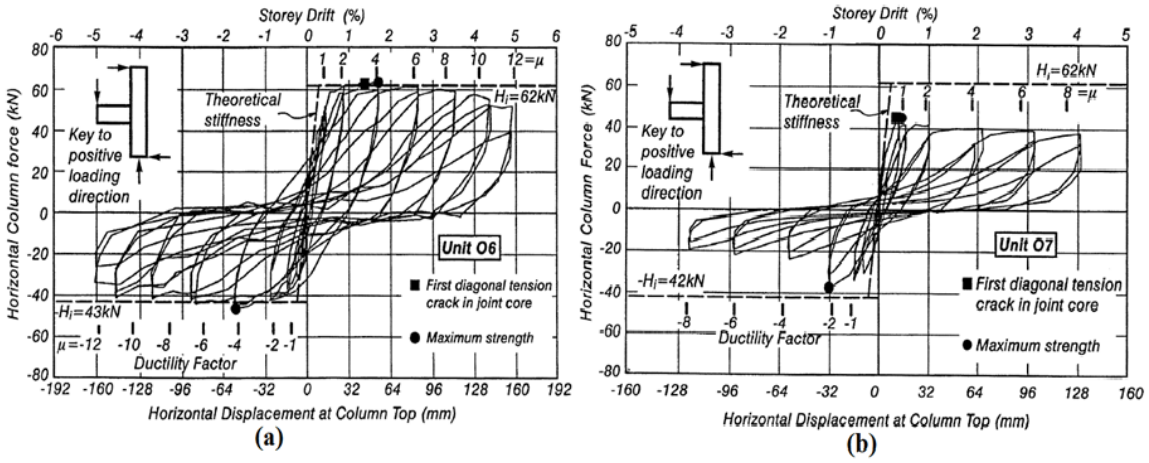

Figure 7 Horizontal Column Force Versus Horizontal Displacement at Top of Column Relationship Measured For (a) Bent Down And (b) Bent Up Specimen [1]

Chris et al [2] tested two half scale corner beam column joint to investigate the diagonal tension failure in joint in control specimen and to see the increase in shear capacity of joint in retrofitted specimen as shown in "Figure 8". These specimens were tested under the quasi-static cyclic loading and their performance were examined in terms of peak lateral load capacity, ductility, drift, axial load bearing capacity of the column at high levels of drift, and in terms of crack widths. The behavior of the FRP composite retrofitted joint was found significantly improved in terms of lateral load capacity, ductility and axial load bearing capacity at high levels of drift as shown in "Figure 9" In addition, the joint shear strength of the FRP retrofitted joint was 45% higher than that of the control.

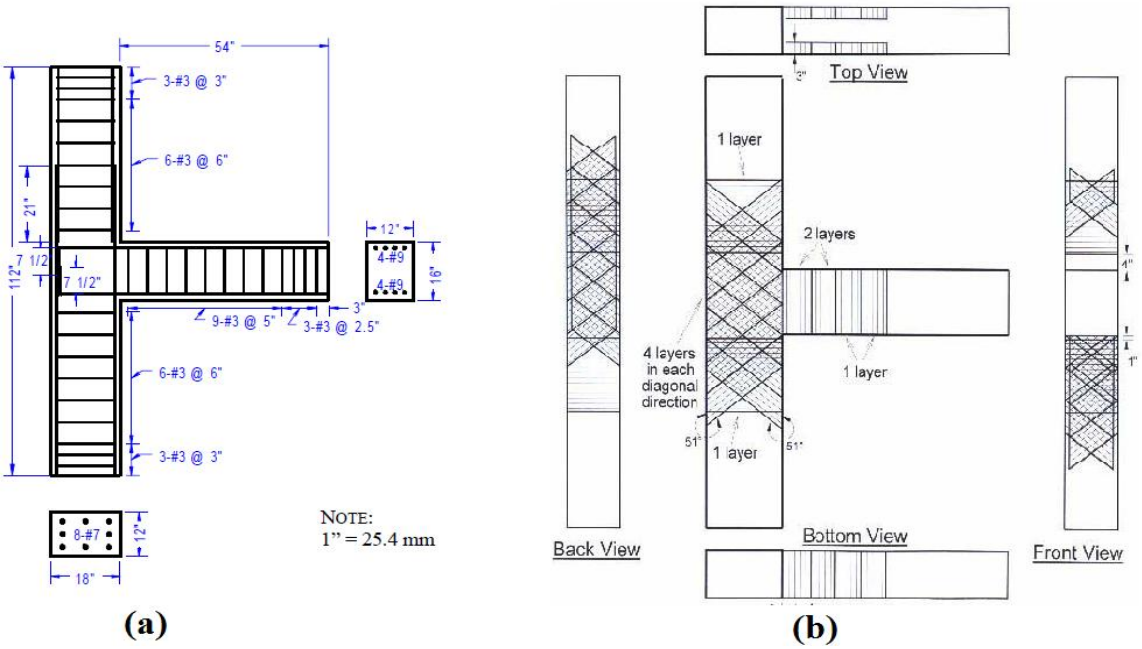

Figure 8(a) Specimen Dimensions and Reinforcement Details (b) Composite Retrofit Layout [2]

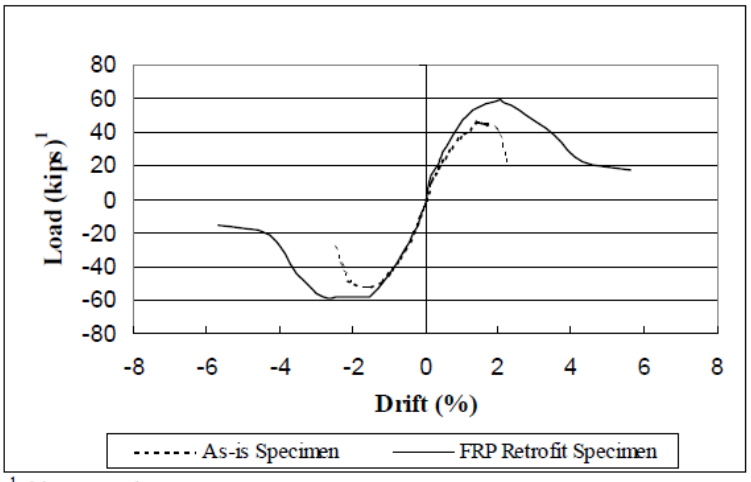

[1]1kip = 4.45 kN

Figure 9 Backbone Curve for as-is and FRP Retrofit Specimen [2]

Gencoglua et al [3] investigated four half scale exterior beam column joints under cyclic loading with constant load on the column of 90KN, one of the specimen were designed according to the ACI 318-02 and two were rehabilitated with CFRP fabrics on the tension face of column and beam and both column and beam were wrapped and last one was considered as control specimen as given in "Figure 10 & 11 (a)". The test result indicates that the retrofitted specimens have more load carrying capacity, ultimate beam tip displacements and absorbed more total energy amount then ACI 318-02 design and control specimens as shown in "Figure 11(b)".

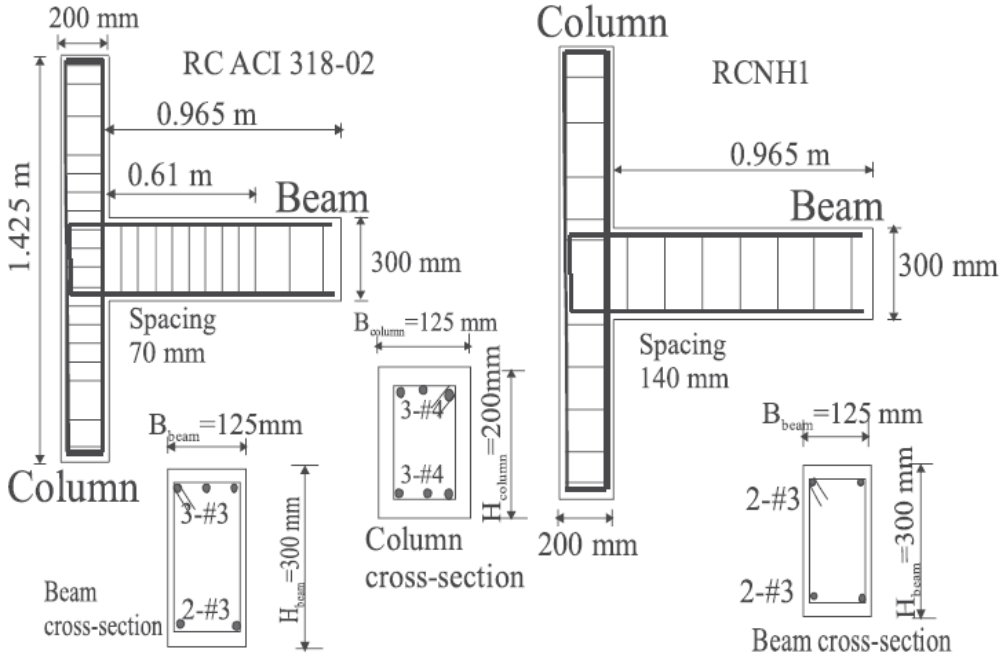

Figure 10 Reinforcement Details of Exterior Beam-Column Joint Specimens [3]

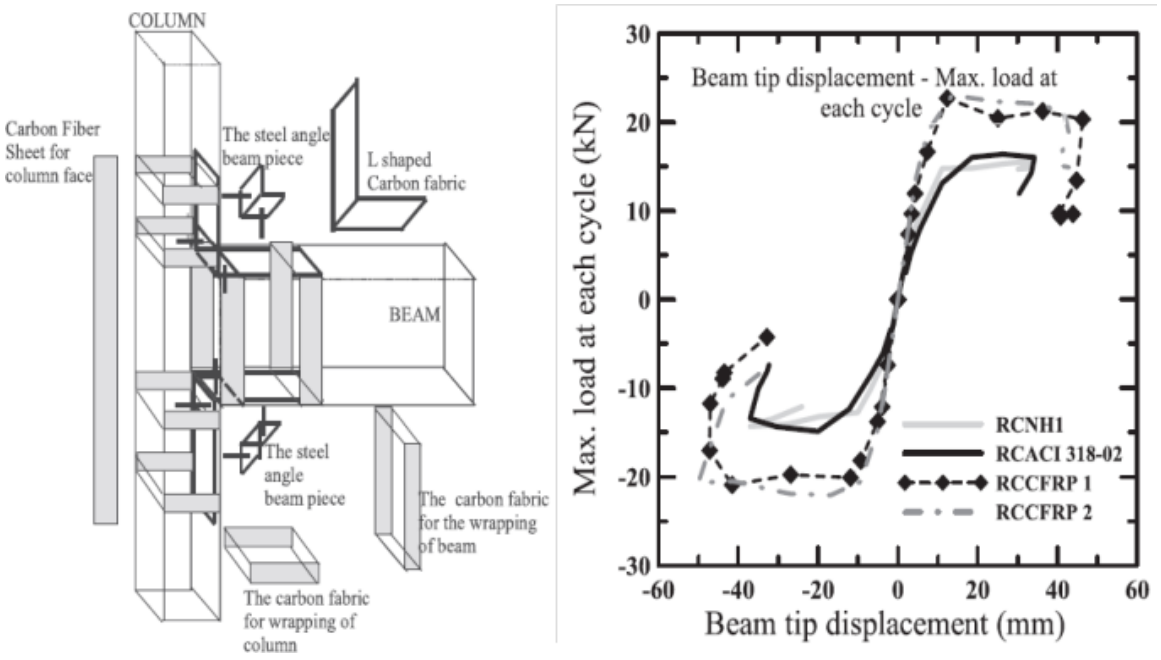

Figure 11 (A) Details Of Strengthening Process By CFRP (B) The Envelopes Of Beam Tip Displacement-Cyclic Loads Of Beam-Column Joint Specimens [3]

Kien et al [4] studied eight 1/3 scale exterior reinforced concrete beam column joints including a non-seismic, seismic and six retrofitted specimens with CFRP on different configuration as shown in "Figure 12 and 13" to find out the effective way of use of CFRP for strengthening the beam column joints with CFRP to increase the lateral strength and ductility. According to the test results the x-shape configuration of warping, the strip on the column and two layers of the CFRP sheets show better performance in terms of ductility and strength as shown in "Figure 14"

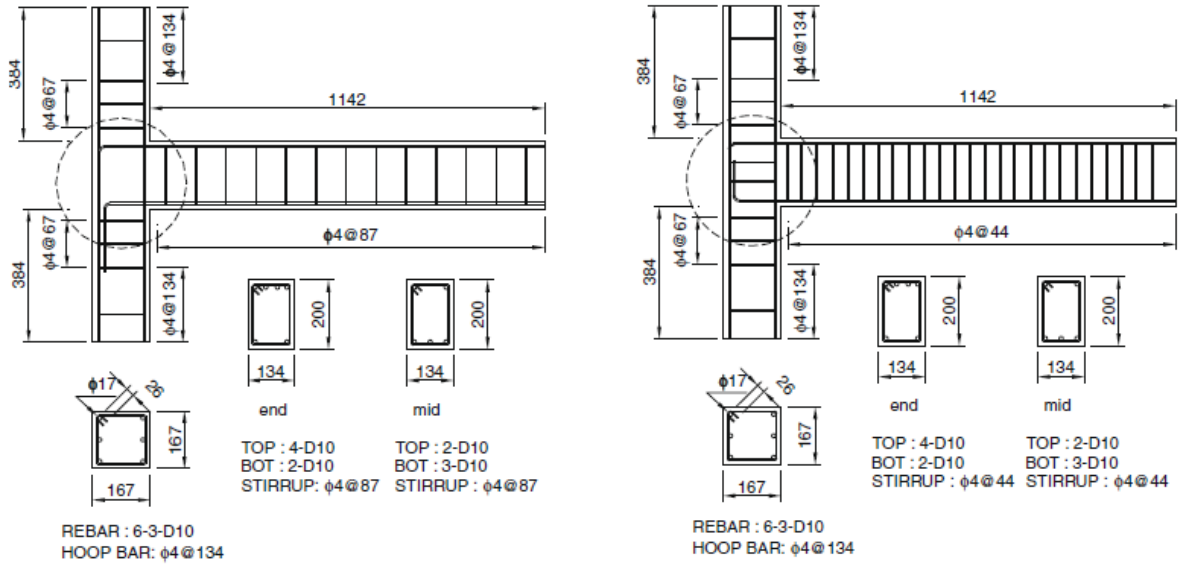

Figure 12 (a) Non-Seismic And (b)Seismic Details of The Test Specimens [4]

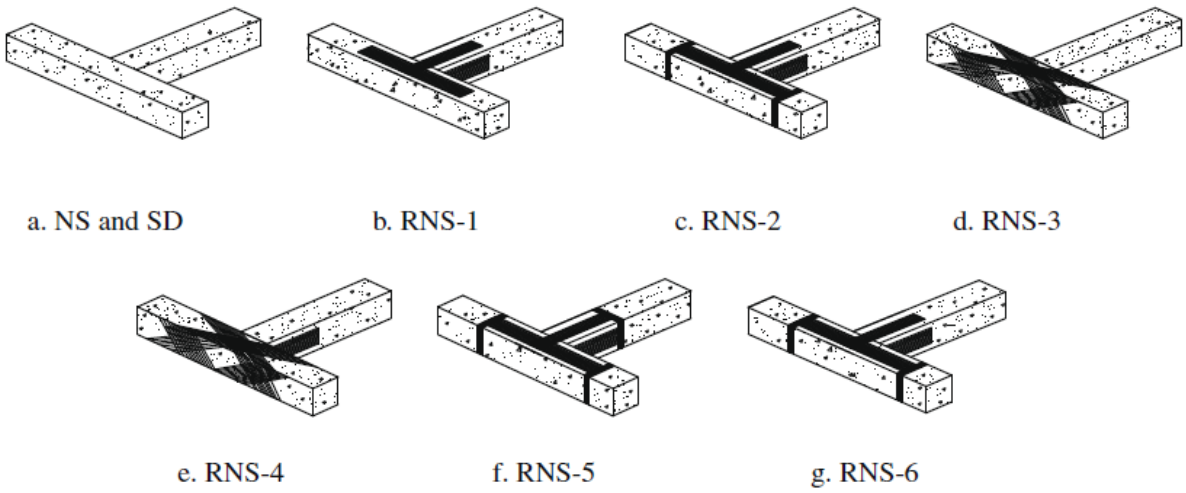

Figure 13 Description of All Test Specimens [4]

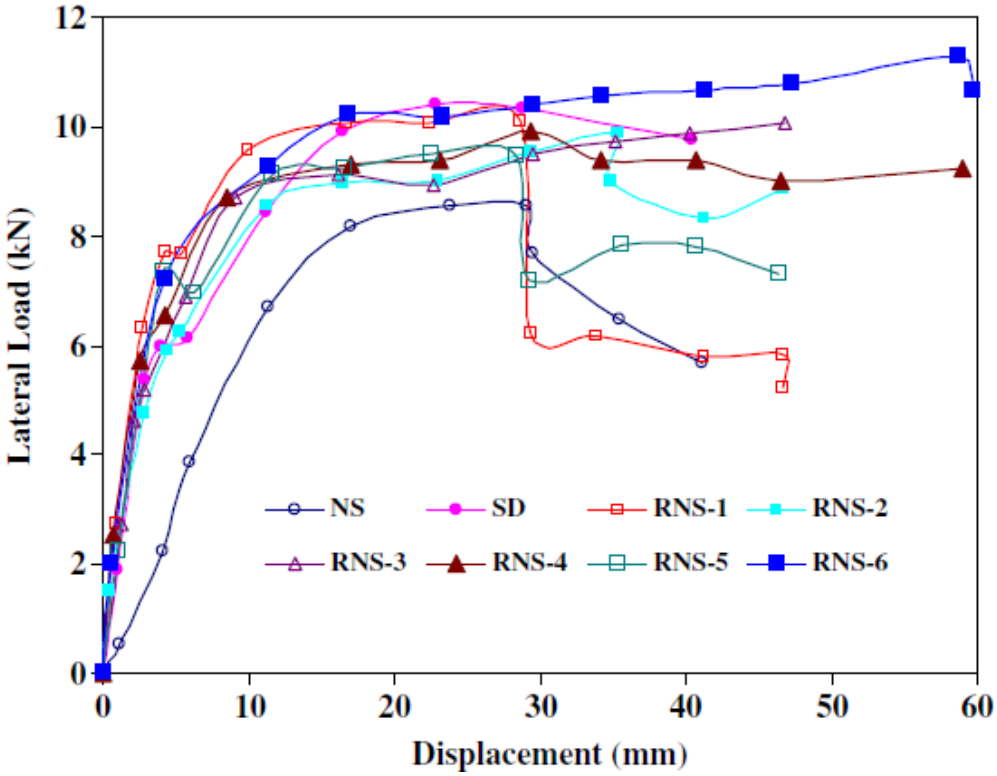

Figure 14 Positive Lateral Load versus Displacement Envelop for All Specimens [4]

Pampanin et al [5] have investigated seismic behavior of six 2/3 scaled reinforced concrete beam column joints designed for gravity load in which two were exterior knee joints, two exterior tee-joints and two interior cruciform joints using smooth bars with deficient anchorage hook-end bars and in-adequate detailing in the joint region as shown in "Figure 15". Experimental results showed the slippage of bars stress concentration at the end bars hook-end which results in concrete wedge at the joint in the exterior specimens as given in "Figure 16".

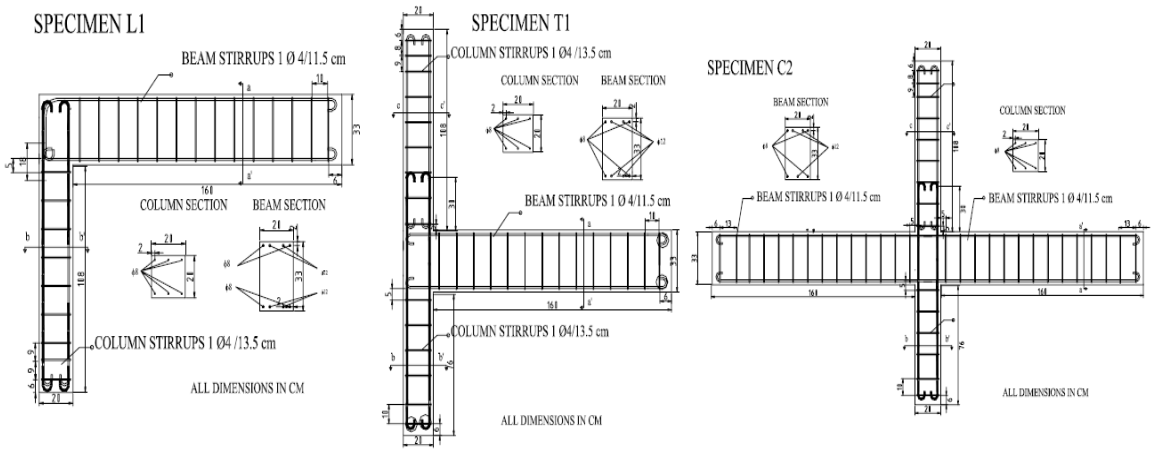

Figure 15 (a) Knee Joint (b) Tee Joint and (c) Interior Joint Sizes and Reinforcement Details [5]

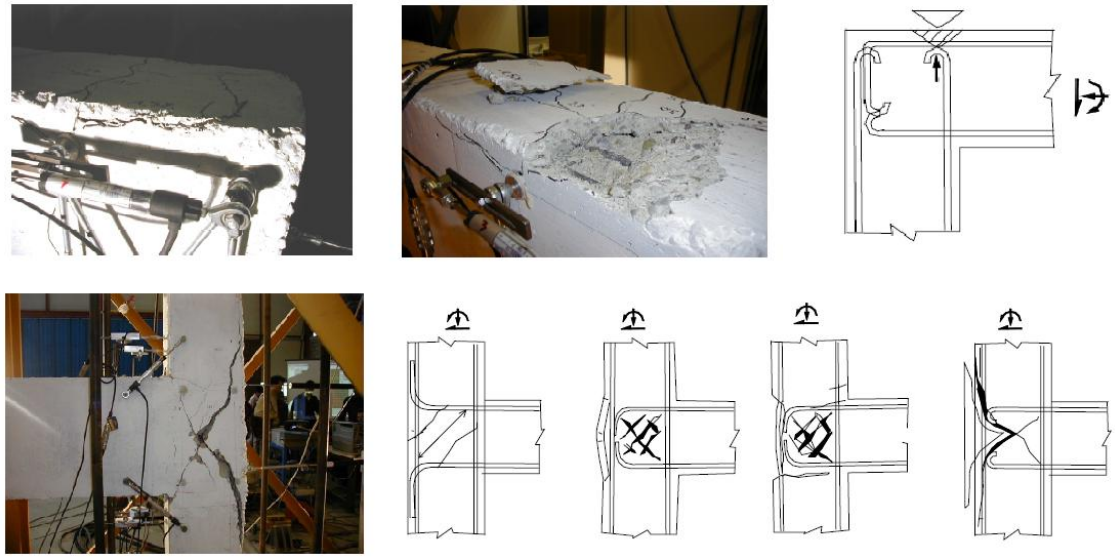

Figure 16 Knee and Tee Joint Failure Mechanisms [5]

Ravi et al. [6] conducted an experimental investigation on influence of development length in retrofitted reinforced concrete beam-column joints. Nine controlled reinforced concrete beam-column joints specimens were cast, in which six specimens had design and details as per the code IS 456:2000. The remaining three specimens had design and details as per the code IS 13920:1993 as shown in "Figure 17". Retrofitting was done on

failed specimens with details as per code IS 456:2000.Three specimens were wrapped with GFRP and remaining three with CFRP. Static load test was conducted on control and retrofitted specimens. They concluded that there was an increase in load carrying capacity by 14.5% and an increase in energy absorption capacity by 10% as the development length was increased based on code IS 13920:1993 as given in “Figure 18”

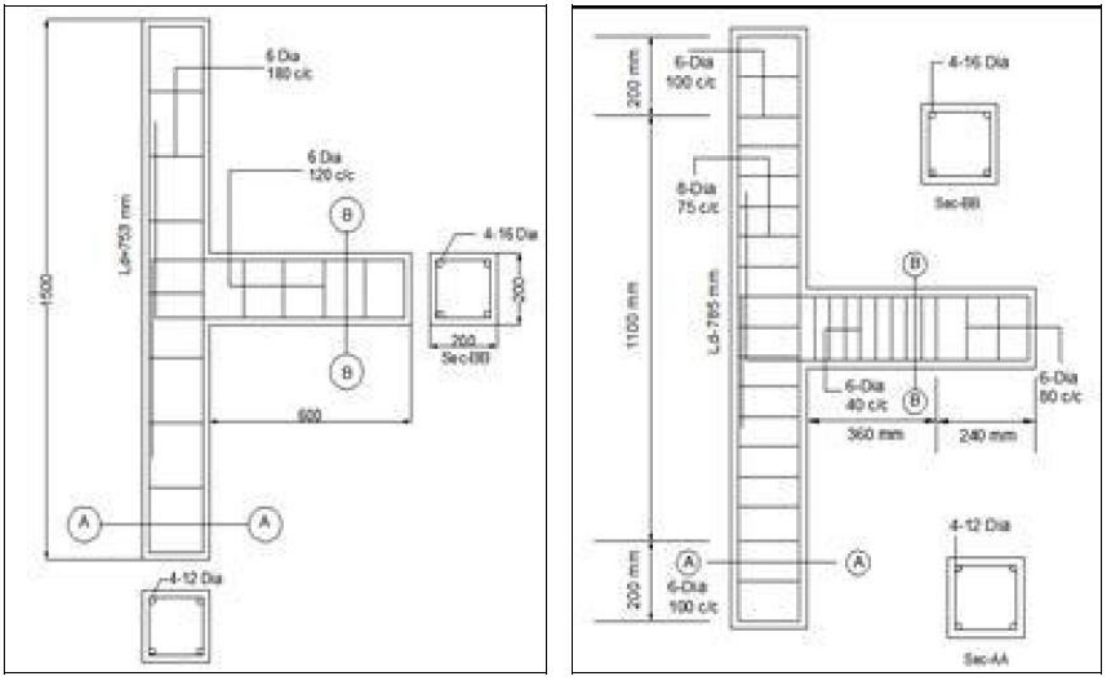

Figure 17 (a) IS 13920 and (b) IS 456 Specimens Size and Reinforcement Details [6]

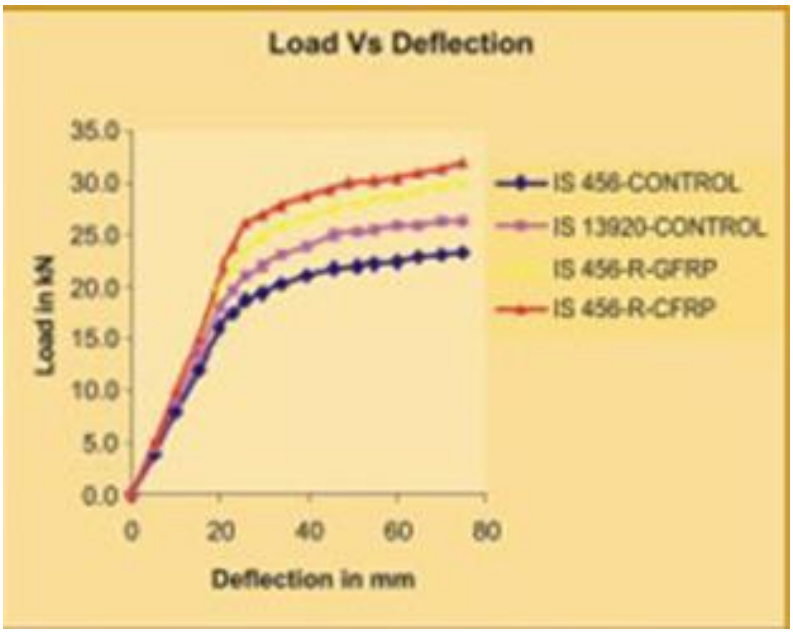

Figure 18 load Deflection Curve for Control and Retrofitted Specimens [6]

Ghobarah et al [7] conducted the cyclic load test on the exterior beam column joints designed for gravity load only without transverse reinforcement in the joint region, three reinforced concrete beam column joints were TO, TR1 and TR2 where TO is control and TR1 & TR2 were rehabilitated with GFRP as shown in "Figure 19 & 20" Results shows that the joint rehabilitation eliminated the brittle joint failure and improved the bond conditions of beam top reinforcement, delayed slippage of bottom steel, increase the energy distribution of joints also improve the ductility and load carrying capacity of specimens as shown in "Figure 21"

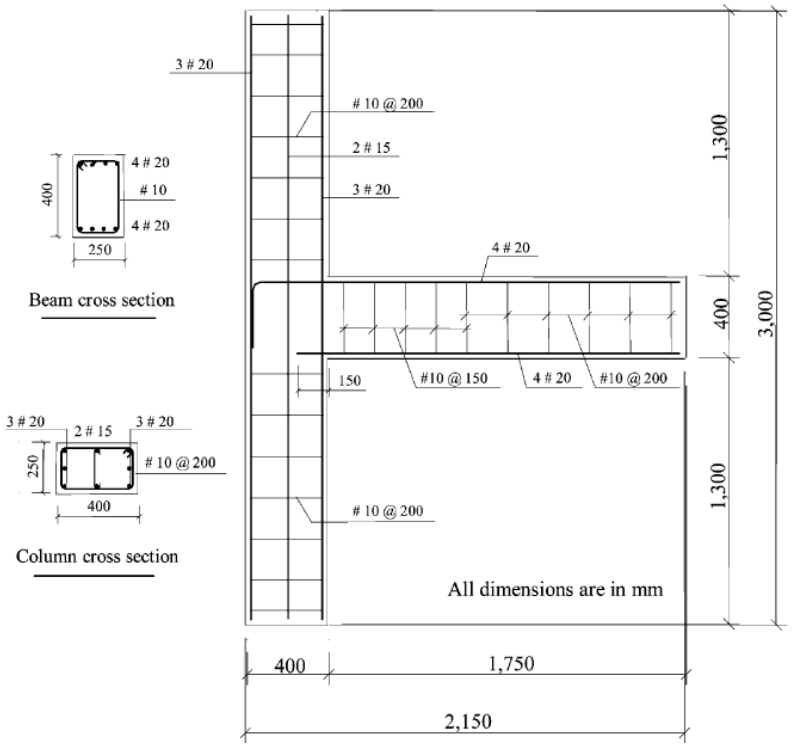

Figure 19 Specimen Dimensions and Reinforcement Details [7]

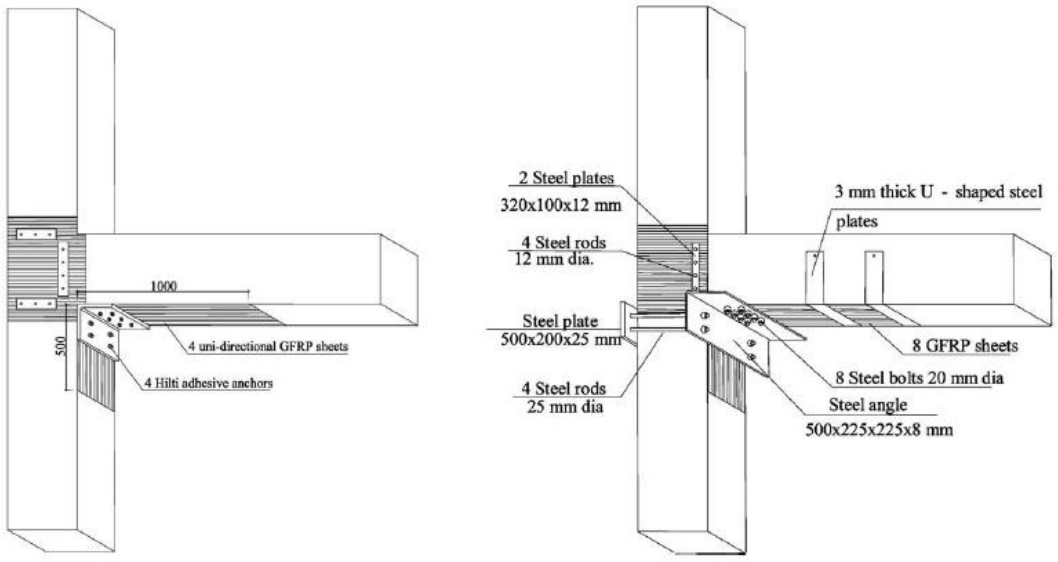

Figure 20 Retrofitting Schemes: (a) Specimen TR1, (b) Specimen TR2 [7]

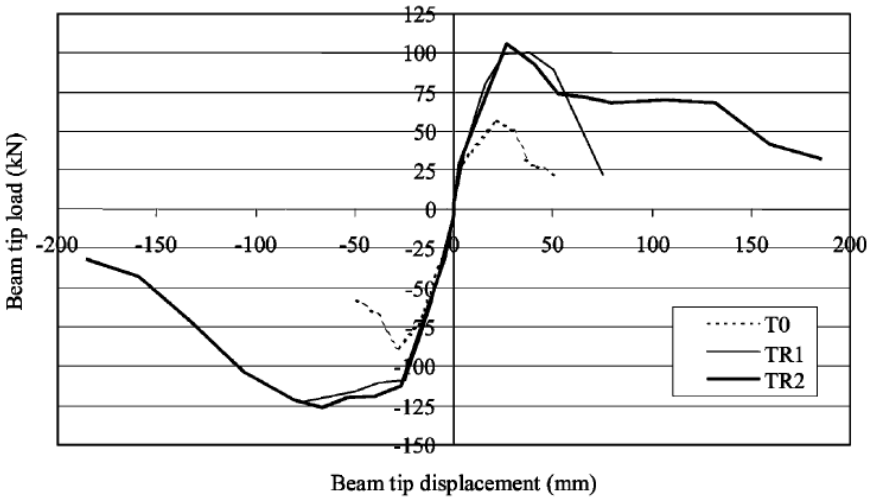

Figure 21 Hysteretic Loop Envelopes of the Test Specimens [7]

Franco et al [8] studied the inelastic seismic behavior of reinforced concrete existing buildings with smooth bars and low strength concrete by testing four internal and exterior reinforced concrete beam column joints under increasing cyclic horizontal displacement up to the failure. Results shows the bond slips of longitudinal bars and shear failure in exterior as shown in “Figure 22”.

Figure 22 T-Joint Specimen: Beam and Joint Panel Cracks Pattern at Failure [8]

Sasmal et al [9] investigated the aspects of repair and retrofitting techniques adopted for reinforced concrete beam column joint specimen under cyclic loading, specimens were designed under seismic specification of Indian standard but without adopting ductile detailing (Non-Ductile) and repaired with epoxy mortar and grout using low viscous polymer and retrofitted using FRP wrapping and steel plate as shown in "Figure 23". The test results shows that retrofitted specimens regain its stiffness and shows that cumulative energy dissipation obtained from retrofitted specimens was almost 25% more than that of original specimen as shown in "Figure 24".

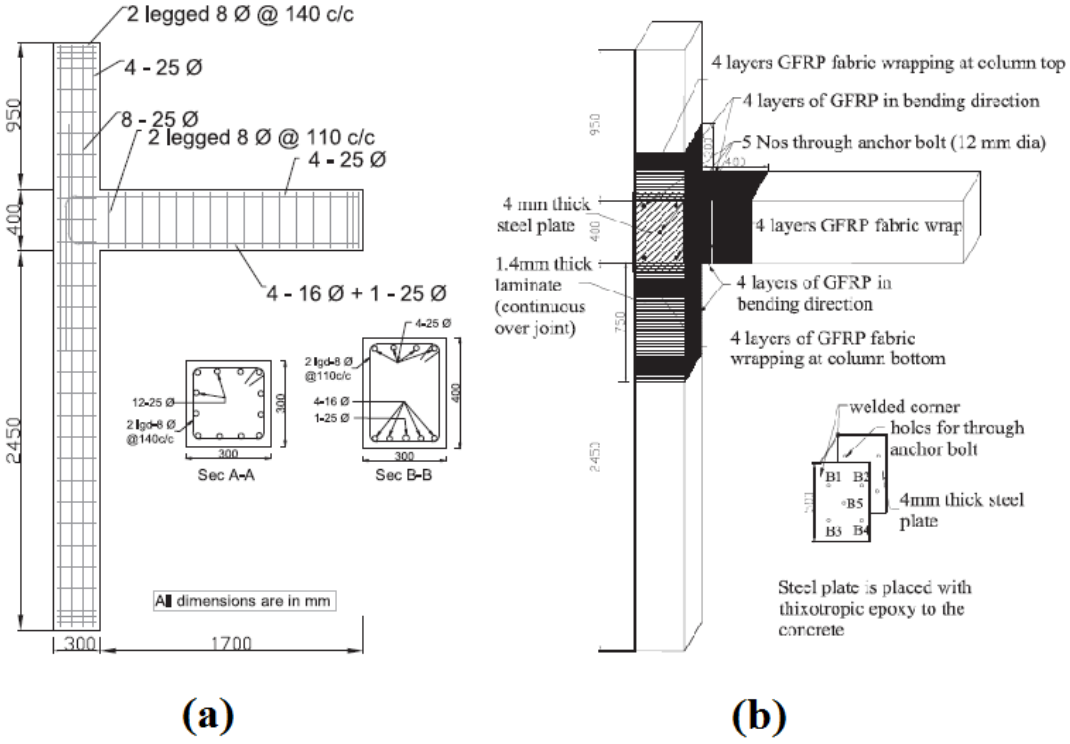

Figure 23 Reinforcement details of 'NonDuctile' Specimen and (b) Retrofitting scheme for damaged 'NonDuctile' specimen [9]

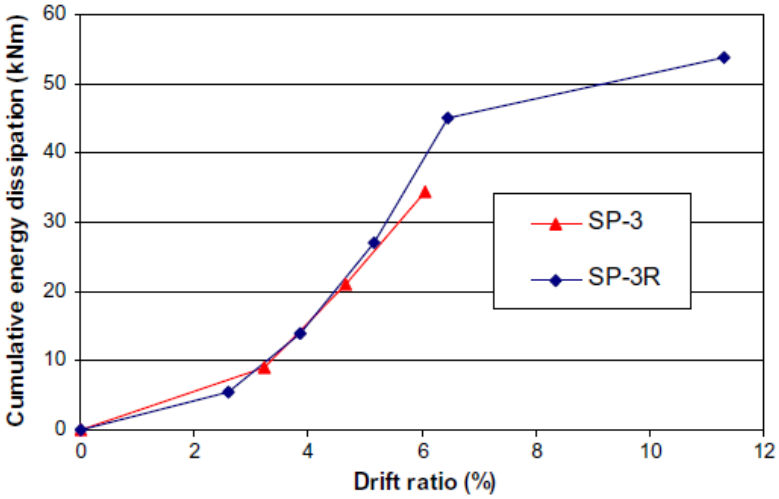

Figure 24Comparison of Cumulative Energy Dissipation [9]

Al-Sayed et al [10] have presented a practical technique for the seismic rehabilitation of poorly detailed beam-column corner joint using FRP composite sheets as shown in "Figure 25 & 26". A full scale corner beam-column sub-assemblage with inadequate joint shear strength and no transverse reinforcement in the joint is tested under reversed cyclic lateral load. The tests results indicate improve shear capacity, ductility, higher load carrying capacity "Figure 27" and slower stiffness degradation after FRP retrofit.

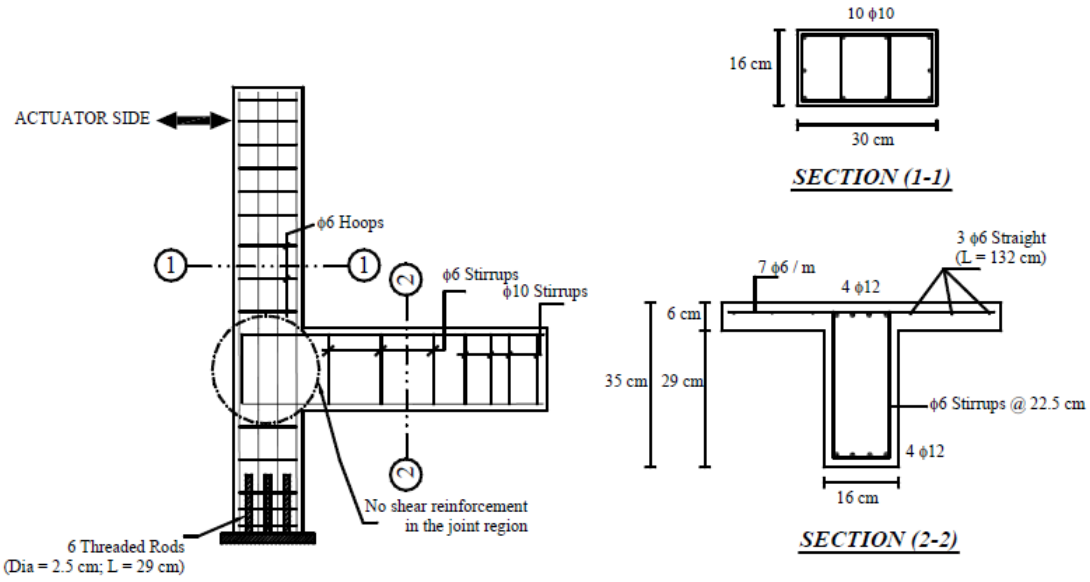

Figure 25 Reinforcement Details of the As-Built Specimen [10]

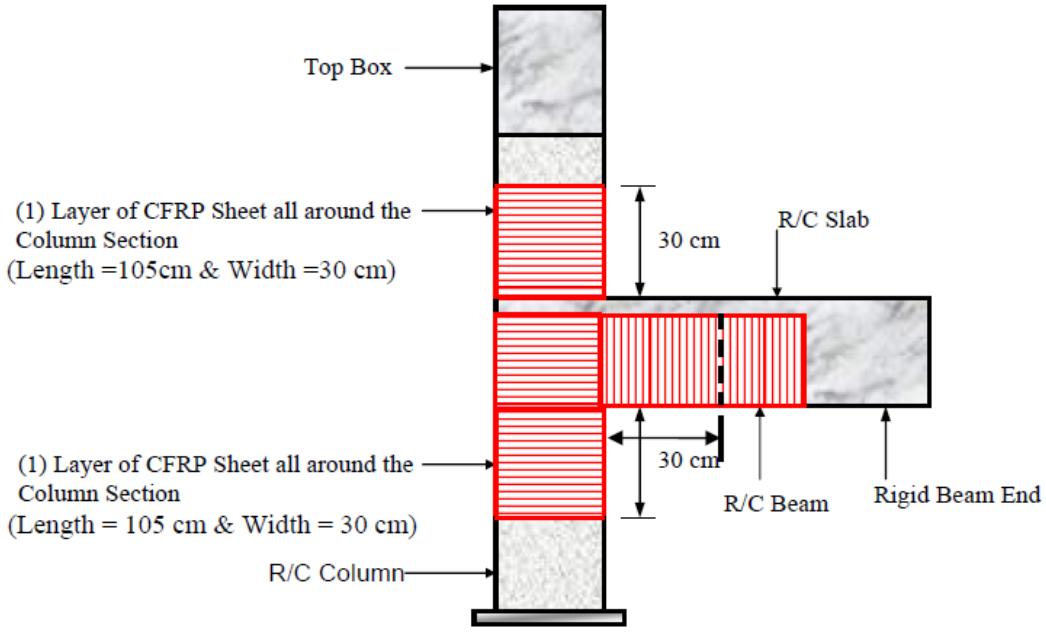

Figure 26 Final Schematic Representation of FRP Scheme Applied To As Built Exterior Joint [10]

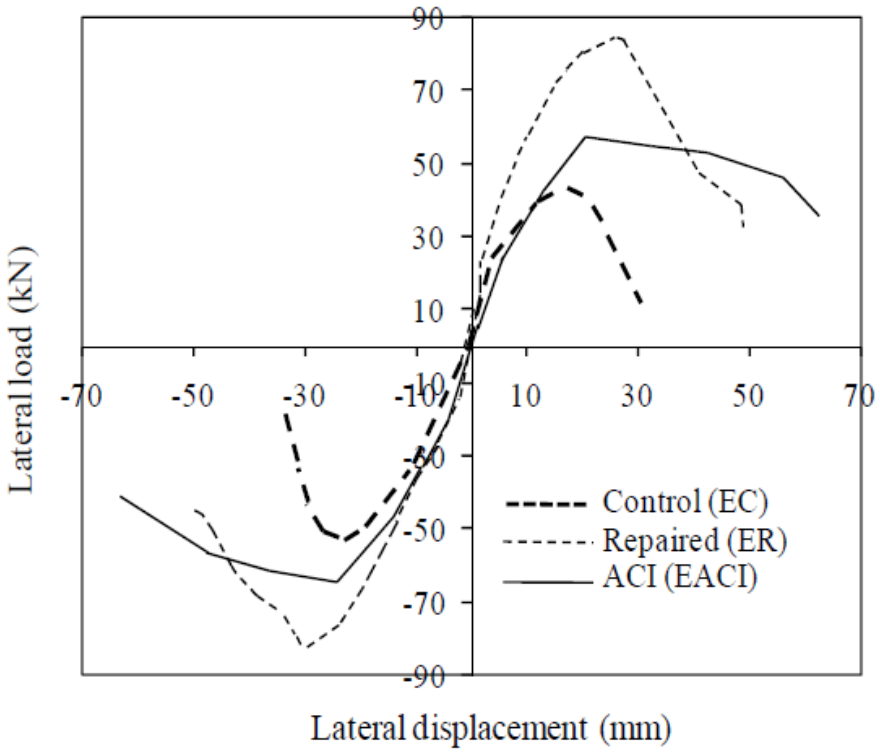

Figure 27 Envelopes of Hysteretic Plots for As-Built Control, Repaired and ACI Based Designed Specimens [10]

2.2 FINITE ELEMENT INVESTIGATION OF BEAM-COLUMN JOINTS

Mostofinejad et al [11] modeled and non-linearly analyzed the reinforced concrete beam column joint with FRP overlays in ANSYS as shown in "Figure 28(a)", model consist the effect of anchorage slip and anchorage extension of steel. Results indicate the good match in the experimental and model prediction as shown in "Figure 28(a)"

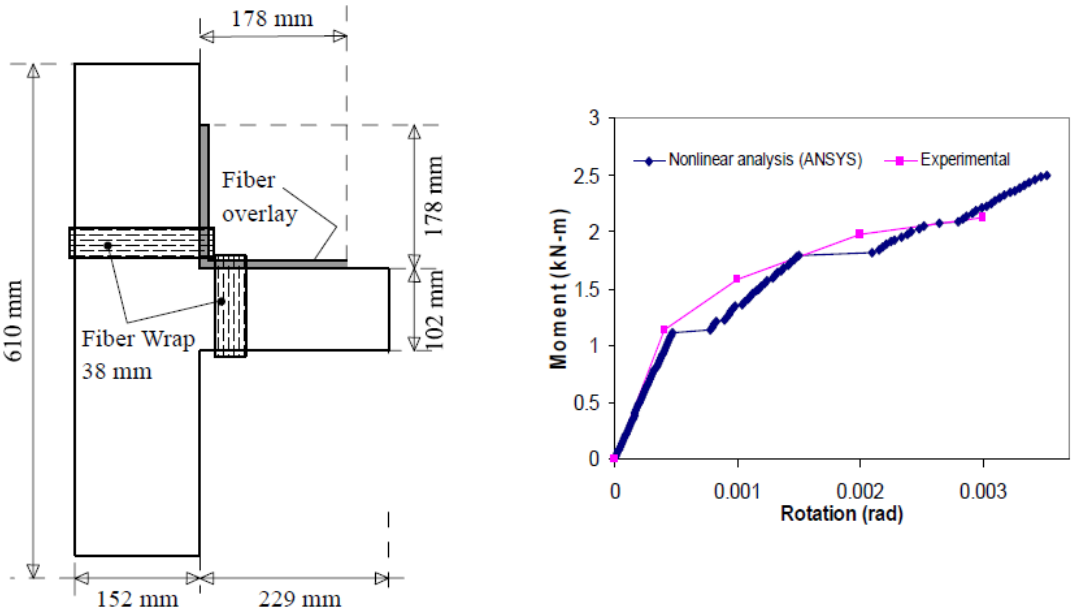

Figure 28 (a) FRP Strengthening Plan and (b) Moment-Rotation Curve for the Joint [11]

Ravi et al [12] modeled and analyzed three specimens using ANSYS in which one of the specimens has the seismic detailing and other two have non-seismic detailing for reinforcement, one of the non-seismic detail specimens were retrofit with CFRP as shown in "Figure 29". The in this study the performance of Exterior beam column joints were compared with control specimen as shown in "Figure 30".

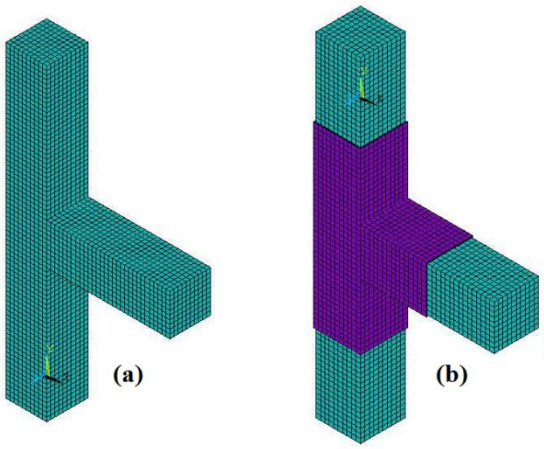

Figure 29 (a) Typical Meshed (b) Typical Meshed Control Specimen Retrofitted Specimen [12]

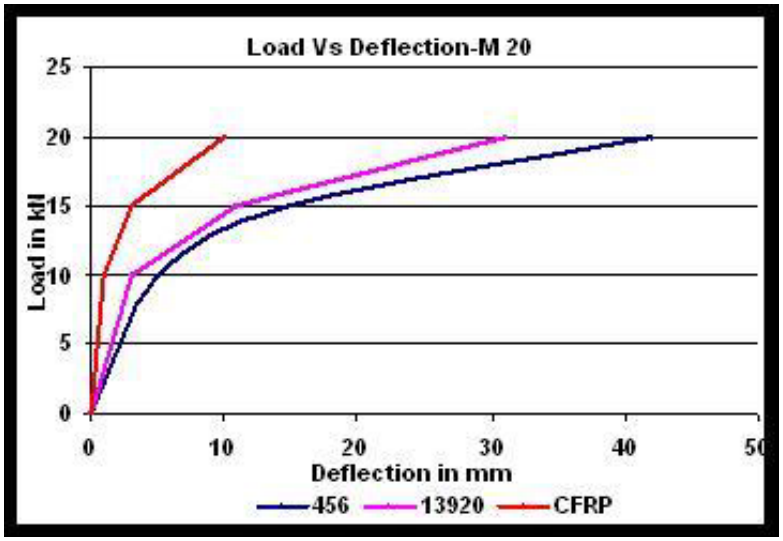

Figure 30 Load Deflection Curve for the Retrofitted Specimen Control and Retrofitted Specimen [12]

Sagbas et al [13] investigate the cyclic response of interior and exterior seismically and non-seismically designed beam column joint subassemblies by modeling and analyzing these specimens in FEM program VecTor2. The analysis shows the good response in predicting the failure mode of all specimens as shown in "Figure 31 & 32".

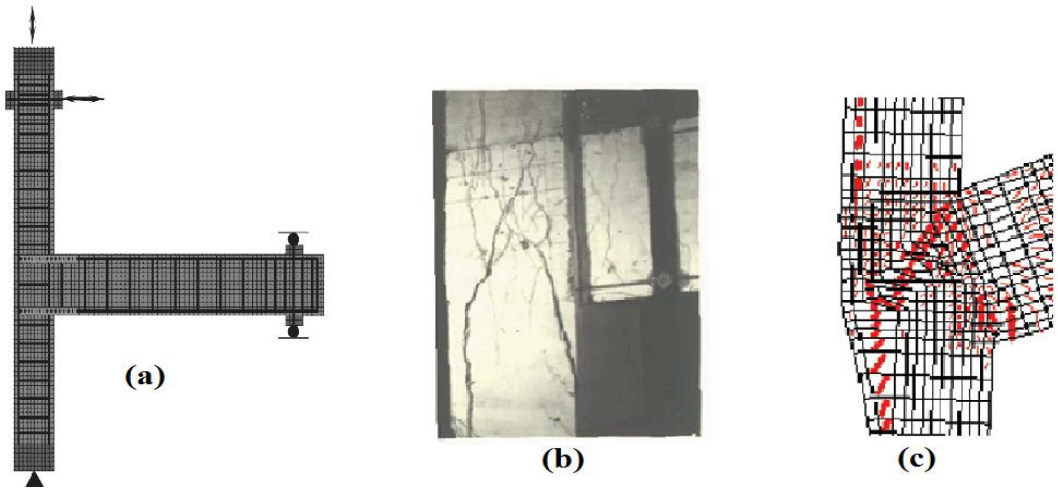

Figure 31(a) Finite Element Model (b) Comparison of Final Failure Mode of Experiment and (c) Analytical of Exterior Beam Column Joint [13]

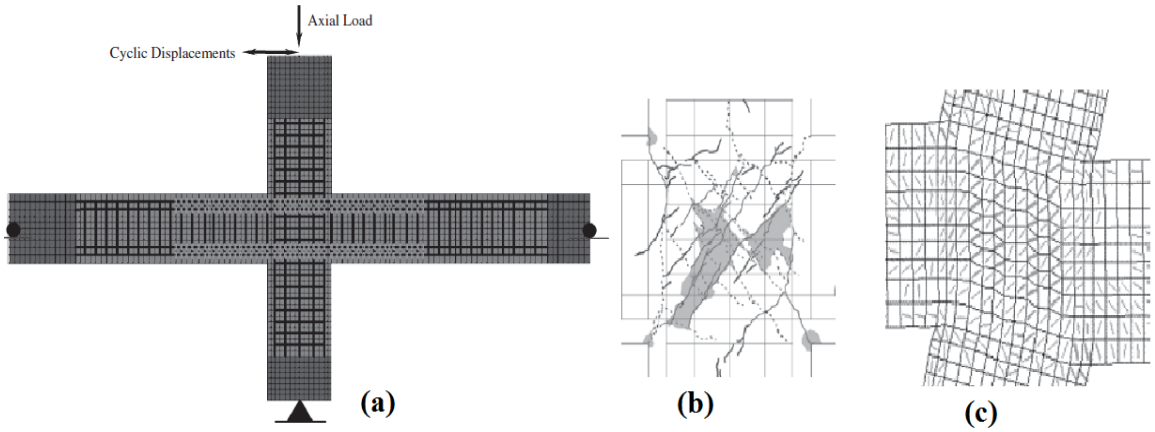

Figure 32 (a) Finite Element Model (b) Comparison of Final Failure Mode of Experiment and (c) Analytical Interior Beam Column Joint [13]

Bindhu et al [14] tested four beam column joints in two groups, group A comprises of two joints with reinforced detailing as per Indian construction practice code IS 456:2000 and group B comprises of two specimens having additional cross bearing reinforcement for joint detail with the same IS 456:2000 as shown in "Figure 33". Finite element program ANSYS was used to model and analyze these specimens to validate the experimental results as given in "Figure 34".

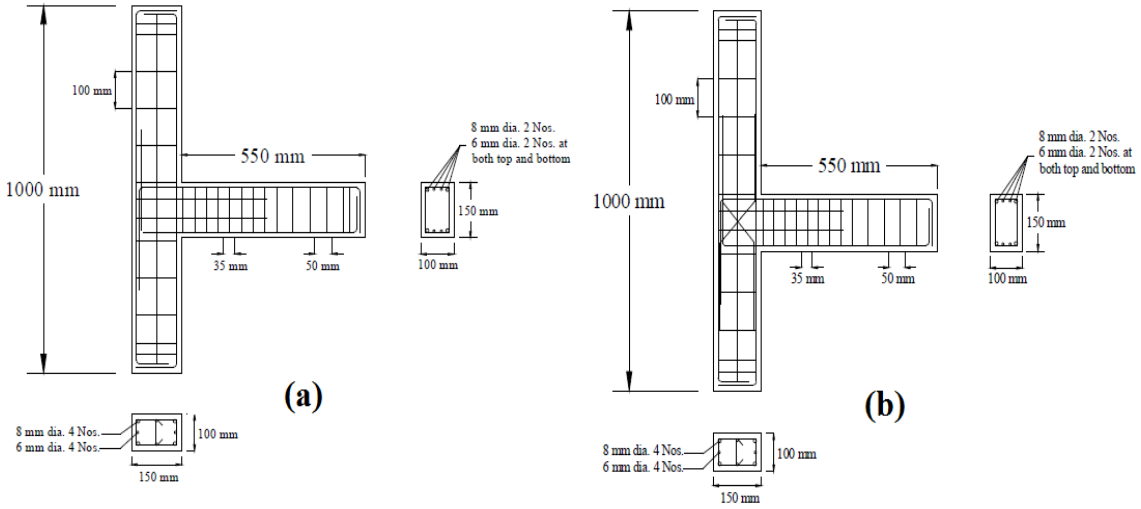

Figure 33 Reinforcement Details of the Specimens (a) Group A (As Per IS: 456-2000) (b) Group B (As Per IS: 456-2000 with Non-Conventional Reinforcement) [14]

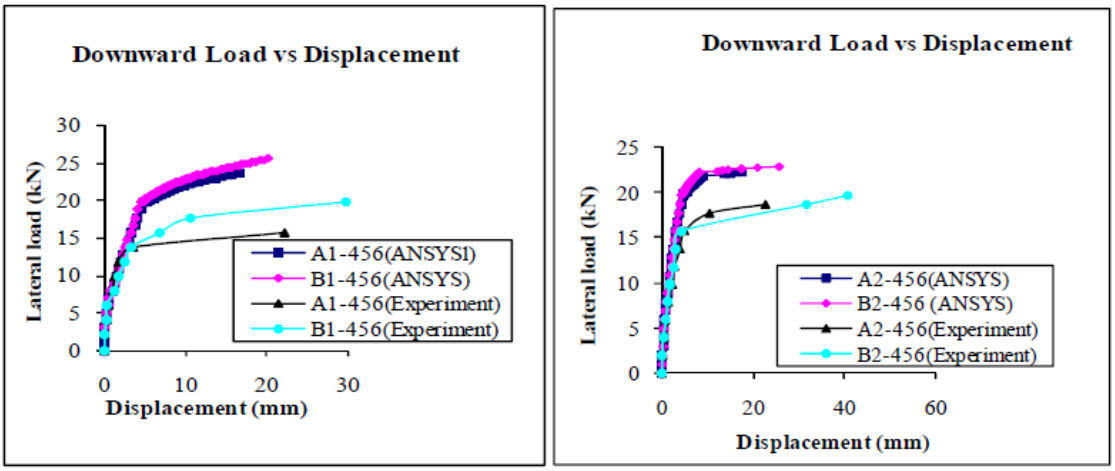

Figure 34 Comparison of Load-Displacement Relations of Models and Specimens [14]

Mitra et al [15] used DIANA 9.1 software and modeled the joint as 2D to simulate the experimental response of two interior beam column joints which represent the range of expected global behavior of joint as shown in load deflection response "Figure 35" and compression stress distribution "Figure 36".

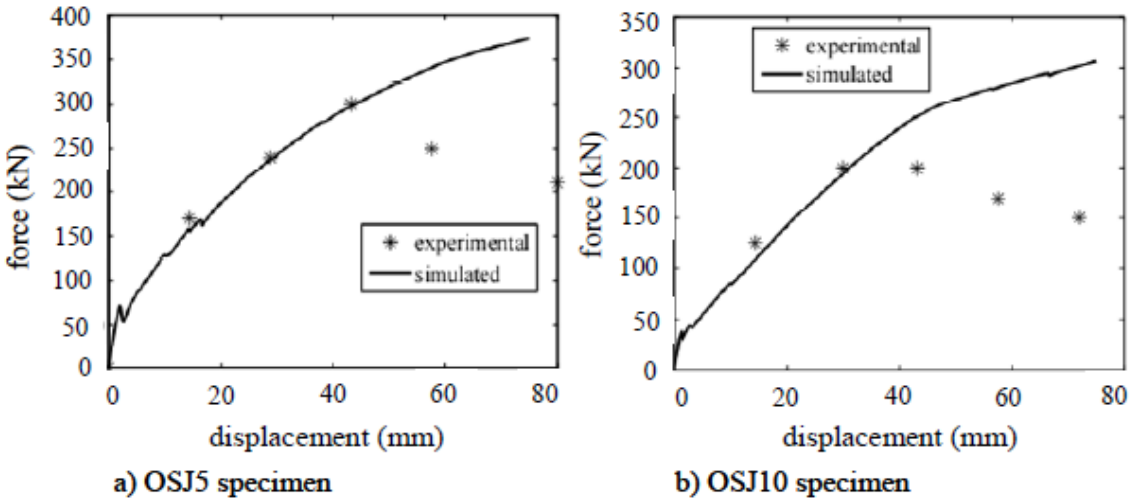

Figure 35 Load Deformation Response of the Simulated Specimen [15]

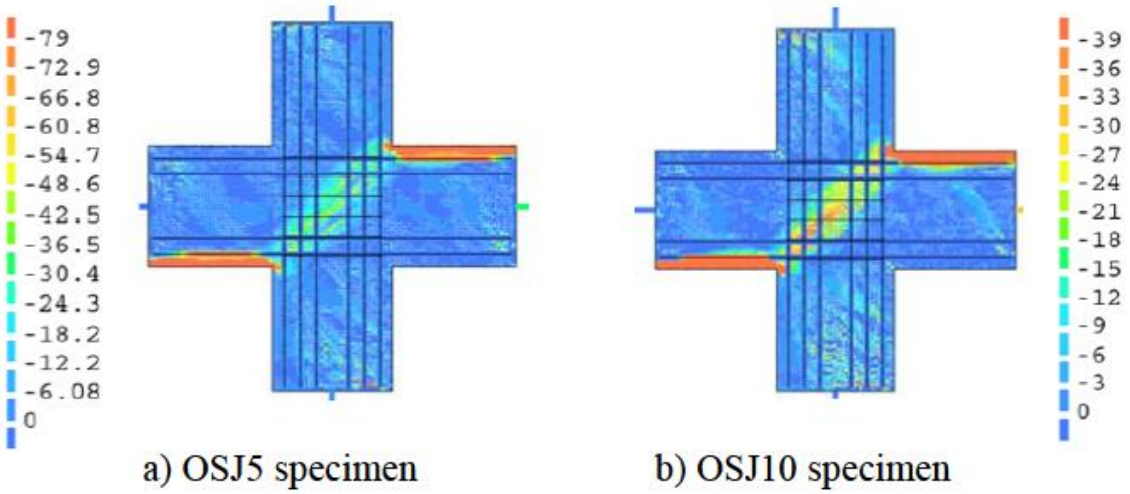

Figure 36 Compressive Stress Distribution in the Connection Region [15]

CHAPTER 3

MECHANISTIC MODEL FOR STRESS DISTRIBUTION AND FAILURE MODEL IN EXTERIOR BEAM COLUMN JOINTS

3.1 FORCES IN EXTERIOR BEAM COLUMN JOINTS

The behavior of beam column joint region in a reinforced concrete structure is not easily understood. Number of stresses adjoining members converges at one point. Bending moments and shear stresses are transferred into the joint from the beam and axial and shear stresses are transferred into the joint region from the column. To understand joint forces we need to know the loading on beams and columns.

3.1.1 Loading on Beams

The moment reaction at the joint interface, M_n equation [3.1]

$$M_n = P \times l_b \tag{3.1}$$

Where:

P is the load

lb is the distance from the tip of the beam where the load in applied to the column face as shown in “Figure 37”.

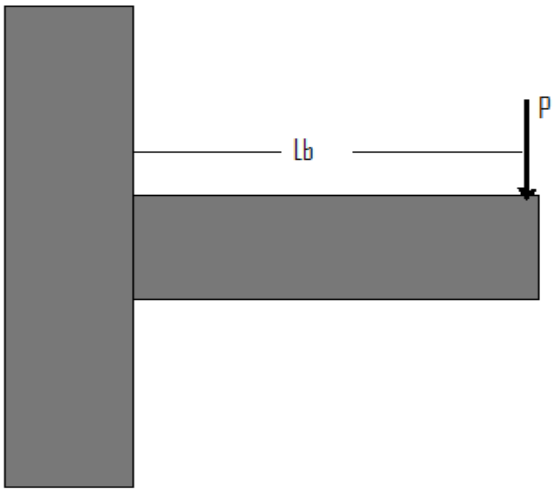

Figure 37 loading at the Tip of Beam

3.1.2 Loadings on Column

An assumption is made that at the midpoint between floors there are inflection points in the column where the bending moment is zero; moment within the column at the beam-column joint is the same as the moment at the end of the beam, M_n.

So, the shear force in the column can be calculated by equation [3.2]

$$V_C' = {M_n}/{l_{pc}} \tag{3.2}$$

Where:

V'_c is the shear force in the column, and l_{pc} is the distance between inflection points as given in "Figure 38".

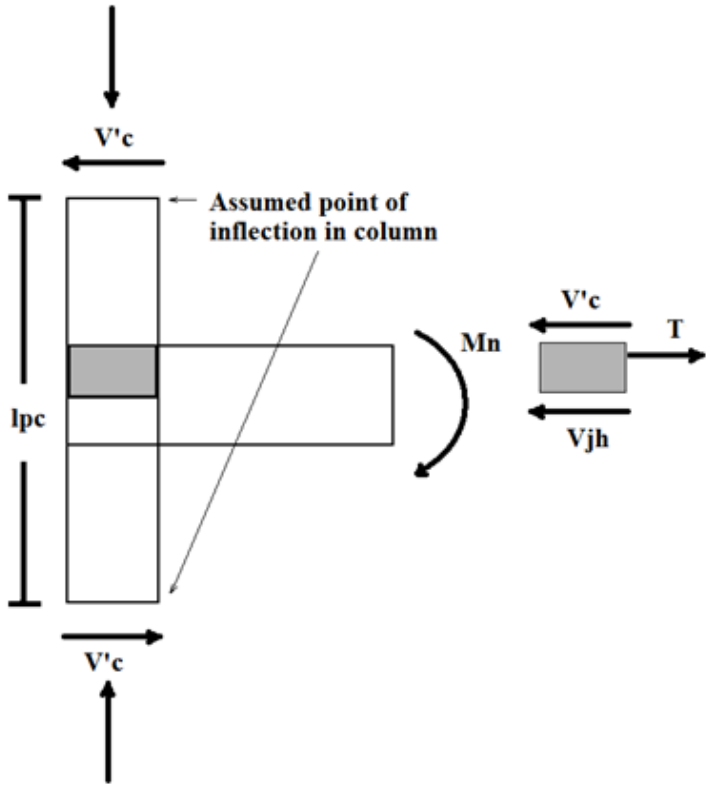

Figure 38 Forces in Beam-Column Joints

"Figure 39" shows that horizontal shear force is a combination of the shear carried down through the column and tensile force in the beam reinforcement framing into the joint. as shown in equation [3.3]

$$V_{jh} = T - V_C' \tag{3.3}$$

Where:

T is equal to the tensile force in the beam longitudinal reinforcement and V'_c is the total shear in the column above the joint.

The strength of the beam-column joint is governed by the shear strength and this shear is the combination of horizontal shear force V_{jh} and vertical shear force as shown in "Figure 39", considering the free body diagram in mid width of the joint the vertical shear force V_{jv} is given in equation [3.4]

$$V_{jv} = T' + C_C^{"} + C_S^{"} - V_b \tag{3.4}$$

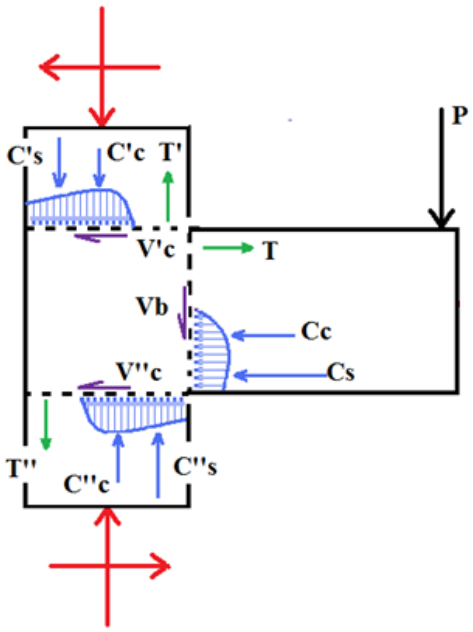

Figure 39 Stresses in Beam-Column Joints

3.2 EXTERIOR BEAM COLUMN JOINT SHEAR STRENGTH REQUIREMENT

Instead of using horizontal and vertical joint shear forces and stresses, the principal tensile stress is used as an index in determining the joint shear capacity as shown in "Figure 40".

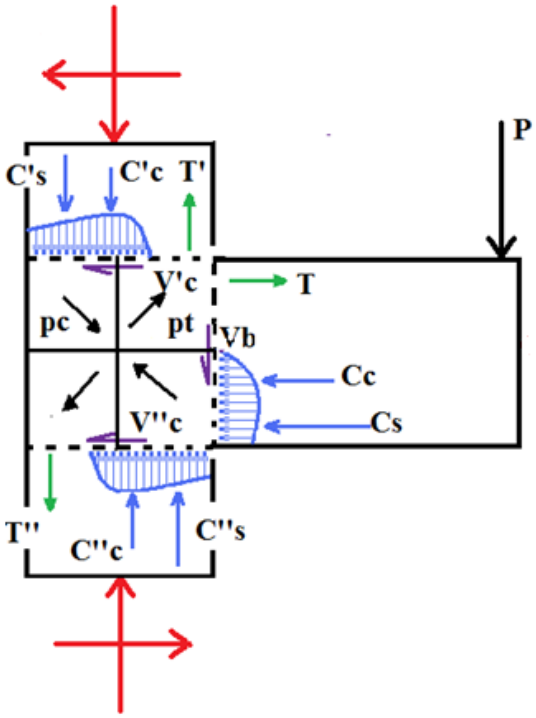

Figure 40 Principle Tensile Stresses in Beam-Column Joints

From Mohr's circle the principle tensile is expressed as

$$\sigma_{1,2} = \frac{\sigma_x+\sigma_y}{2} \pm \sqrt{\left(\frac{\sigma_x-\sigma_y}{2}\right)^2 + \tau_{xy}^2} \quad (3.5)$$

Where:

σ_x = stress on plane parallel to the longitudinal axis of the member which is equal to the axial (σ_a) on the column; σ_y = normal stress plane perpendicular to the axis of member, which is zero for the joint; and τ_{xy}= shear stress which is equal to v_{jh} , so for the exterior joints equation [3.5] can be written as

$$P_t = -\frac{\sigma_a}{2} + \sqrt{\left(\frac{\sigma_a}{2}\right)^2 + v_{jh}^2} \tag{3.6}$$

Where:

σ_a= column axial stress $\left(\frac{N}{A_g}\right)$

v_{jh}= horizontal shear stress $\left(\frac{V_{jh}}{A_j}\right)$

3.3 FAILURE MODE IN EXTERIOR BEAM-COLUMN JOINTS

If principle tensile stress of joint is less than or equal to the tensile strength of concrete which is equation [3.7]

$$\emptyset V_{nj} = 0.75\gamma\sqrt{f_c'}A_j \tag{3.7}$$

So the joint will fail in shear and the diagonal cracks will appear in the joint region and this diagonal crack will form opposite to its previous if the load is applied from the bottom of the beam as shown in “Figure 41 & 42”.

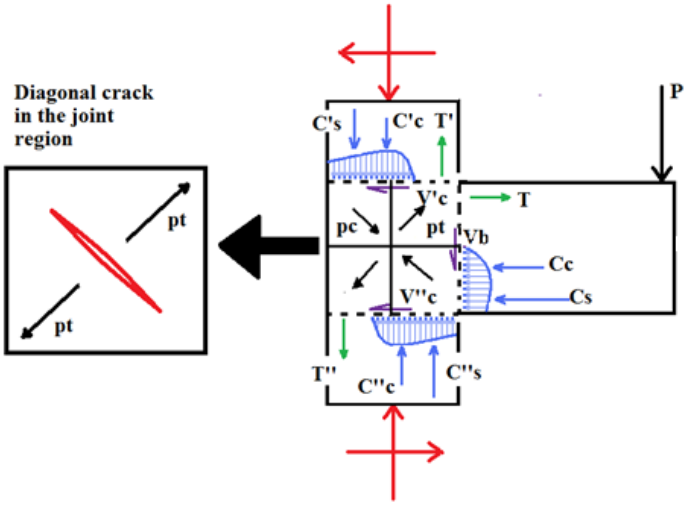

Figure 41 Diagonal Crack in Beam-Column Joints

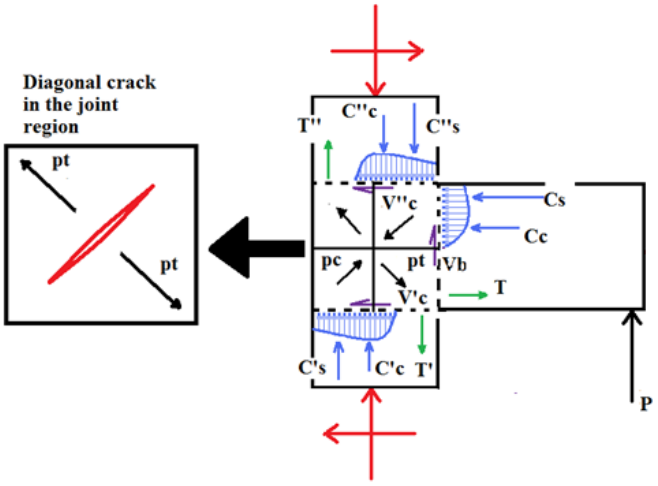

Figure 42 Diagonal Crack in Beam-Column Joints on Pulling

The shear force in the joint gives rise to diagonal cracks thus requiring reinforcement of the joint. The detailing patterns of longitudinal reinforcements of beam significantly affect joint efficiency. Some of the detailing patterns for exterior joints are shown in "Figure 43b"and "Figure 43c". The bars bent away from the joint core "Figure 43b"result in efficiencies of 25-40 % while those passing through and anchored in the joint core show 85- 100% efficiency. However, the stirrups have to be provided to confine the concrete core within the joint.

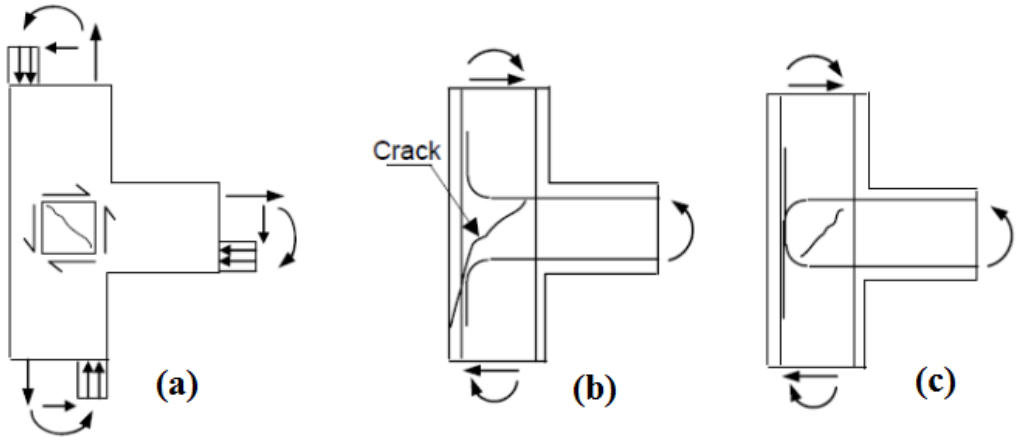

Figure 43 (a) Forces in Exterior Beam Column Joint (b) Exterior Joint with Bent up Bar (c) Exterior Joint with Bent in Bar

Some limits for the principal tensile stress and the post-cracking behaviour of reinforced concrete beam-column joints have been proposed by Priestley (1997) and extended by Pampanin (2003) for different types of joint, reinforcement and detailing. After the initial diagonal cracking occurs in the joint, the strength will reduce. The amount of the reduction depends on the joint type, reinforcement used and detailing, as shown in "Figure 44"

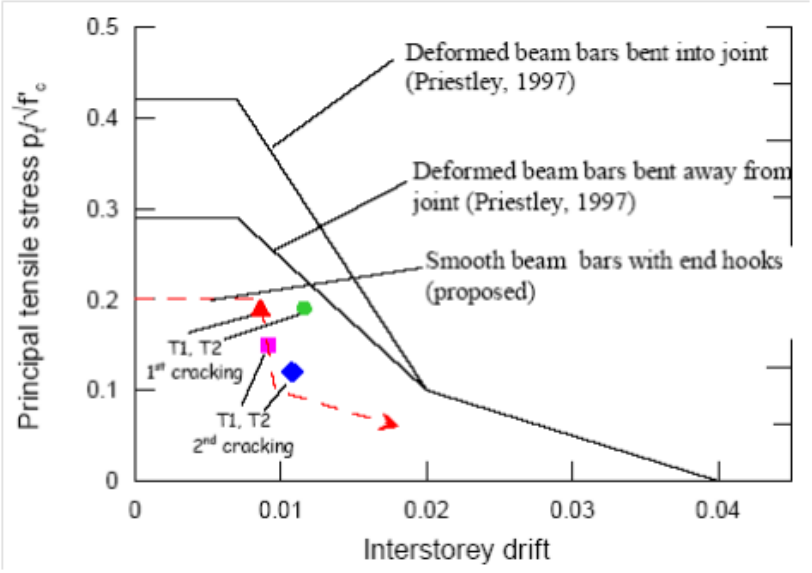

Figure 44 Proposed Principal Tensile Stress Limits, Pampanin [5]

CHAPTER 4

FINITE ELEMENT MODELING OF BEAM-COLUMN JOINTS

4.1 INTRODUCTION OF FINITE ELEMENT MODELING OF BEAM-COLUMN JOINTS

Finite element studies and their comparison with the experimental test results for the verification is becoming important day by day to idealize the real behavior of the actual tested specimens.

In recent years more studies and test have been conducted on the beam column joints due to their important role in the stability of RC structures and many researches and studies have been conducted in the last few years on the finite element modeling of beam-column joints to understand the behavior of their mode of failure using different finite element software for example ANSYS, ABAQUS, Vector 2 and DIANA as given in literature review in previous chapter 2. DIANA9.4.3 is used in this research to model the tested beam-column joints.

4.2 FINITE ELEMENT MODELING IN DIANA

DIANA, which stands for DIsplacement ANAlyzer, is general purpose finite element software based on the Displacement Method. Since its creation in 1972, DIANA has been under constant improvement at TNO Building and Construction Research in The Netherlands. DIANA's most powerful tools are in the modeling of concrete and soils behavior under basically any condition.

Standard DIANA application work includes: concrete cracking, excavations, tunneling, composites, plasticity, creep, cooling of concrete, engineering plastics, various rubbers, groundwater flow, fluid-structure interactions, temperature-dependent material behavior, heat conduction, buckling, sub structuring, etcetera. DIANA's element type ranges from the more simple (straight beams elements) to the more complex ones (spring and interface elements). DIANA also offers an outstanding variety of material models that can easily be used to describe the elastic and/or nonlinear behavior (softening) of any structure.

A large diversity of analysis can be used with this computer program. Some of these are: linear, static, nonlinear, dynamic, stability, potential flow, coupled flow-stress, phased, parameter estimation, lattice, last but not least nonlinear-dynamic analysis. Material models that are offered include: elasticity, cracking, viscoelasticity, soil specials, interface nonlinearities, and user-supplied material models. To be able to solve the system of equations that are obtained from the finite element, several solution procedures

are provided. Linear equations, nonlinear equations, eigenvalues, and sub structuring are the main solvers used by DIANA for this purpose.

Basically, there are three ways of providing the input to DIANA. The first, a Batch Interface, where the user defines the finite element model via an input data file; the second, Graphical User Interface (GUI), also call iDIANA, where the input data is created automatically from the basic model geometry; and finally, User-supplied Subroutines, where the code of various subroutines with predefined arguments may be supplied to define special material models, interface behavior, etc.

To specify how the analysis is performed, analysis commands must be provided to the program. It can be done using iDIANA, a program that transforms the command input from a graphical interface form to an MS-DOS application that internally executes the commands. Also, the results to be output from the analysis and the elements and/or nodes that these correspond has to be included within the analysis commands.

4.3 MATERIAL CONSTITUTIVE MODELS

4.3.1 Concrete Plasticity

Drucker-Prager yield criterion is used to model the stress level at which yielding of concrete is initiated. The yield surface of Drucker-Prager model is a circular cone

"Figure 45" specified through the cohesion c, the friction angle φ, and the dilatancy angle ψ. The formulation is given by

$$f(\sigma, K) = \sqrt{\frac{1}{2}\sigma^T P \sigma} + \alpha_f \pi^T \sigma - \beta \bar{C}(K) \tag{4.1}$$

with $\bar{C}$ (κ) the cohesion which is a function of the internal state variable. The projection matrix is equal to the projection matrix P defined in Equation [4.2]. The projection vector π is given by Equation [4.3].

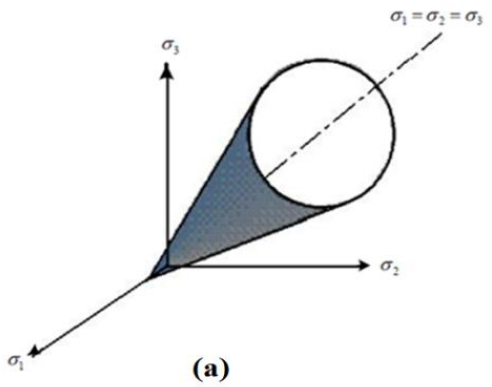

Figure 45 3D Yield Surface of Drucker-Prager [16]

$$P = \begin{bmatrix} 2 & -1 & -1 & 0 & 0 & 0 \\ -1 & 2 & -1 & 0 & 0 & 0 \\ -1 & -1 & -2 & 0 & 0 & 0 \\ 0 & 0 & 0 & 6 & 0 & 0 \\ 0 & 0 & 0 & 0 & 6 & 0 \\ 0 & 0 & 0 & 0 & 0 & 6 \end{bmatrix} \tag{4.2}$$

$$\pi = \begin{Bmatrix} 1 \\ 1 \\ 1 \\ 0 \\ 0 \\ 0 \end{Bmatrix} \tag{4.3}$$

The scalar quantities α_f and β are given by

$$\alpha_f = \frac{2\sin\emptyset(\kappa)}{3-\sin\emptyset(\kappa)} \quad \text{and} \quad \beta = \frac{6\cos\emptyset_o}{3-\sin\emptyset_o}$$

The angle of internal friction φ is also a function of the internal state variable. The initial angle of internal friction is given by φ_o. The flow rule is given by a general non-associated flow rule $g \neq f$, with the plastic potential given by

$$f(\sigma,\kappa) = \sqrt{\tfrac{1}{2}\sigma^T P\sigma} + \alpha_g \pi^T \sigma \tag{4.4}$$

with the scalar α_g defined by the dilatancy angle ψ

$$\alpha_g = \frac{2\sin\psi(\kappa)}{3-\sin\psi(\kappa)} \tag{4.5}$$

which results for the plastic strain rate vector in

$$\dot{\varepsilon}^P = \dot{\lambda}\left\{\frac{P\sigma}{2\psi} + \alpha_g\pi\right\} \tag{4.6}$$

with the scalar Ψ defined by

$$\psi = \sqrt{\tfrac{1}{2}\sigma^T P\sigma} \tag{4.7}$$

4.3.2 Hardening

The relation between the internal state variable κ and the plastic process is given by the hardening hypothesis. For the Drucker-Prager yield condition we consider only the strain hardening hypothesis.

4.3.3 Strain hardening

In the case of strain hardening the relation is given in the principal space by

$$\dot{\kappa} = \sqrt{\frac{2}{3}(\dot{\varepsilon}_1^P \dot{\varepsilon}_1^P + \dot{\varepsilon}_2^P \dot{\varepsilon}_2^P + \dot{\varepsilon}_3^P \dot{\varepsilon}_3^P)} \tag{4.8}$$

With

$$\begin{Bmatrix} \dot{\varepsilon}_1^P \\ \dot{\varepsilon}_2^P \\ \dot{\varepsilon}_3^P \end{Bmatrix} = \dot{\lambda}\left(\frac{1}{2\Psi}\begin{Bmatrix} 2\sigma_1 - \sigma_2 - \sigma_3 \\ -\sigma_1 + 2\sigma_2 - \sigma_3 \\ -\sigma_1 - \sigma_2 + 2\sigma_3 \end{Bmatrix} + \alpha_g \begin{Bmatrix} 1 \\ 1 \\ 1 \end{Bmatrix}\right) \tag{4.9}$$

Equation 4.8 can be elaborated to

$$\dot{\kappa} = \dot{\lambda}\sqrt{1 + 2\alpha_g^2} \tag{4.10}$$

The cohesion is related to the concrete strength through the relation given by Equation 3.38 DeWitte & Kikstra, [16].

$$c = f_c'[\frac{1 - sin\emptyset}{2cos\emptyset}] \tag{4.11}$$

The flow rule determines the direction of plastic straining. The flow rule is termed "associative" if the plastic strain occurs in a direction normal to the yield surface. The plasticity model is termed "associated plasticity" in the case of associative flow rule. In Drucker-Prager plasticity model, the associated plasticity is established by setting $\varphi = \psi$ and there will be a volumetric expansion of the material with plastic strains. The non-associated plasticity is established by setting $\varphi > \psi$ and there will be less volumetric expansion. Clearly, if ψ is zero, there will be no volumetric expansion (DeWitte & Kikstra, 2005). [16] Since the structural model is plain stress, the value of ψ is not essential (DeWitte & Kikstra, 2005) [16].

For a normal strength quality concrete, the ratio between the uniaxial compressive strength and the biaxial compressive strength is approximately 1:16 as shown in "Figure 46", which results in a friction angle $\varphi \approx 10^{o}$ and a cohesion c=0.42$f'c$.

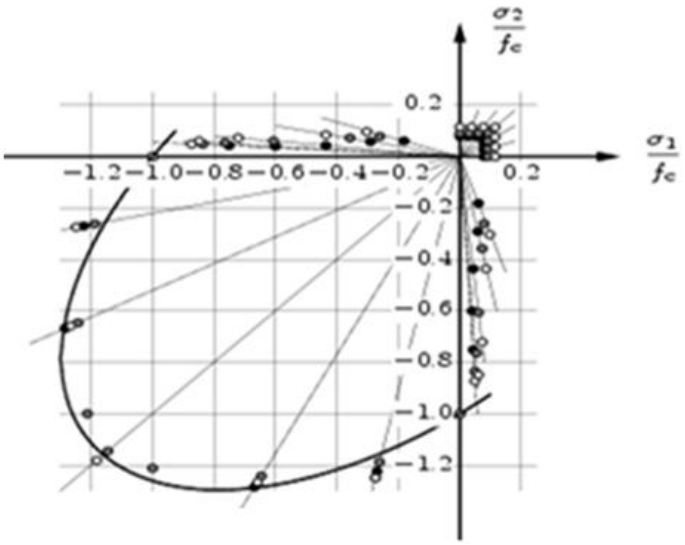

Figure 46 Uniaxial Compressive Strength and the Biaxial Compressive [16]

Thus for associated plasticity, $\varphi = \psi$. The hardening rule describes the changing of the yield surface with progressive yielding so that the stress states for subsequent yielding can be established. Hardening can either be isotropic (or work), or kinematic. In isotropic hardening, the yield surface remains centered about its initial centerline and expand in size as the plastic strains develop. In kinematic hardening, the yield surface remains constant in size and the surface translates in the stress space with progressive yielding. The concrete behavior under monotonic loading has been modeled by many (Imran & Pantazopoulou, [17]; Smith *et al.* [18] using isotropic hardening. Thus, the isotropic hardening rule was selected to describe the hardening behavior of the concrete.

4.3.4 Concrete Cracking

The cracking of the concrete was specified as a combination of constant tension cut-off, linear tension softening, and shear retention "Figure 47". Tension cut-off criterion was set to be a linear stress cut-off while tension softening criterion was set to be nonlinear tension softening with ultimate strain. The shear retention criterion was set to be constant shear retention factor with a constant β value.

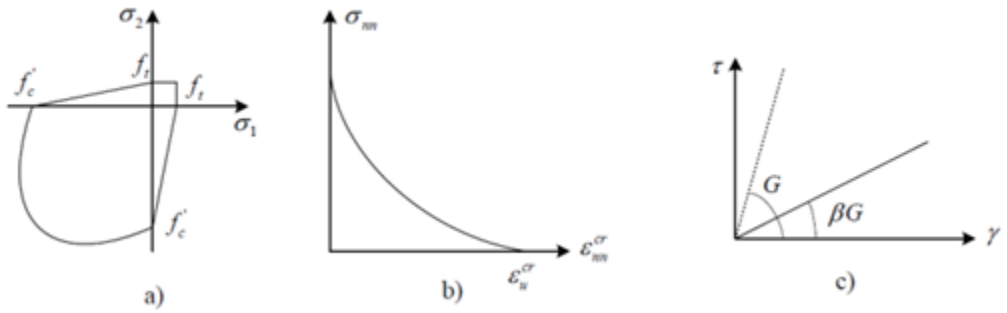

Figure 47 (a) Linear Tension Cut-off, (b) Nonlinear Tension Softening & (c) Constant Shear Retention Factor [16]

4.3.5 Reinforcement

For reinforcement Von Mises-Plasticity with work hardening is used matching the behavior determined from testing. CFRP layers are also modeled as the reinforcement but with the properties of CFRP.

4.4 FINITE ELEMENT MESHING

The concrete is modeled by eight-noded quadrilateral isoparametric plane stress element CQ16M as shown in "Figure 48a" .The rebar and stirrups are modeled as embedded reinforcement elements with perfect bond between rebar and concrete. The rebar embedded model is shown in "Figure 48b".

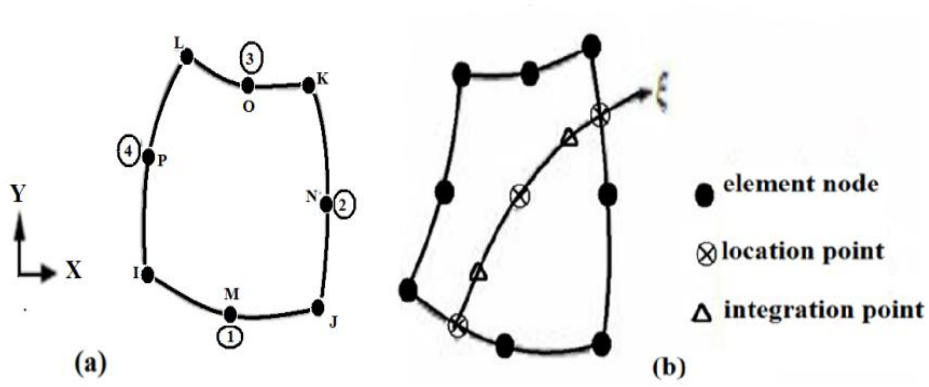

Figure 48 (a)Eight-Node Quadrilateral Isoparametric Plane Stress Element & (b) Embedded Reinforce Element [16]

4.5 GEOMETRY

The creation of the geometry in DIANA is very simple; one way of doing it is by entering the coordinates to create points and later create lines to connect the points. Another way is by creating the geometry in a CAD program and then imports it into DIANA, but this

could create problems later on when assigning properties to the geometry. The geometry of the exterior beam column joint in 2D is appearing through its length and height. The thickness in the third direction is one of the inputs for the 2D plane stress element.

CHAPTER 5

EXPERIMENTAL PROGRAM OF TEST AT KFUPM

5.1 INTRODUCTION

To investigate the behavior of non-seismically designed reinforced concrete exterior beam-column joints, test were carried out on three specimens with in adequate joint shear strength and no transverse reinforcement in the joint, the difference between three specimens were in the detailing of bent of the longitudinal reinforcement of beam in the joint as shown in "Figure 49 & 50" the difference and details of all three specimens are given in table [2], one had the bent up in the column with 12mm diameter reinforcement, second was bent in the joint with 12mm diameter reinforcement and third specimen was. Bent in detail in the joint but with 18mm diameter reinforcement to see the comparison between these three non-seismically detail exterior beam column joints specimens were tested under cyclic loading up-to failure.

Table 2 Specimens Details

S.NO	SPECIMENS	DETAILS	FIGURE NO.
1	J-BU-12	Beam bars bent up in column having 12mm diameter	6.5
2	J-BI-12	Beam bars bent in joint having 12mm diameter	6.6
3	J-BI-18	Beam bars bent in joint having 18mm diameter	6.7

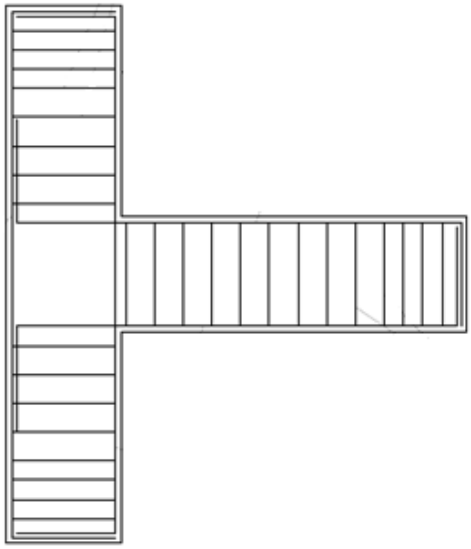

Figure 49 Bent up Details for Beam Longitudinal Reinforcement

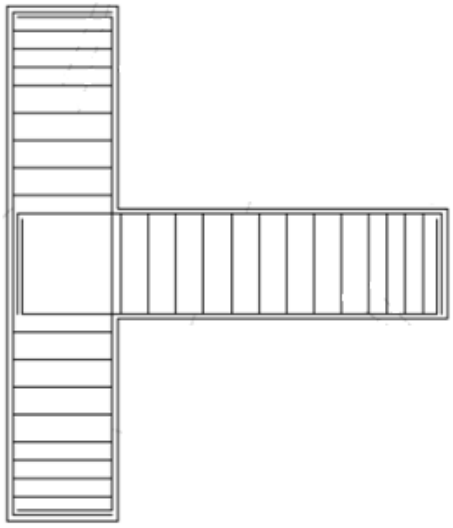

Figure 50 Bent in Details for Beam Longitudinal Reinforcement

5.2 SPECIMEN DETAILS

5.2.1 Beam-Column Size

Configuration was same for all the specimens, beams and columns of the specimens were produced with same dimensions 250mm X 300mm, the cantilever length of beam was 900mm and the height of column was 1400mm as shown in "Figure 51". Dimensions were selected to represent as approximately average sized beam-column joint, and were limited by the dimensions, maximum load and deflection capacity of existing testing frame as given in "Figure 52".

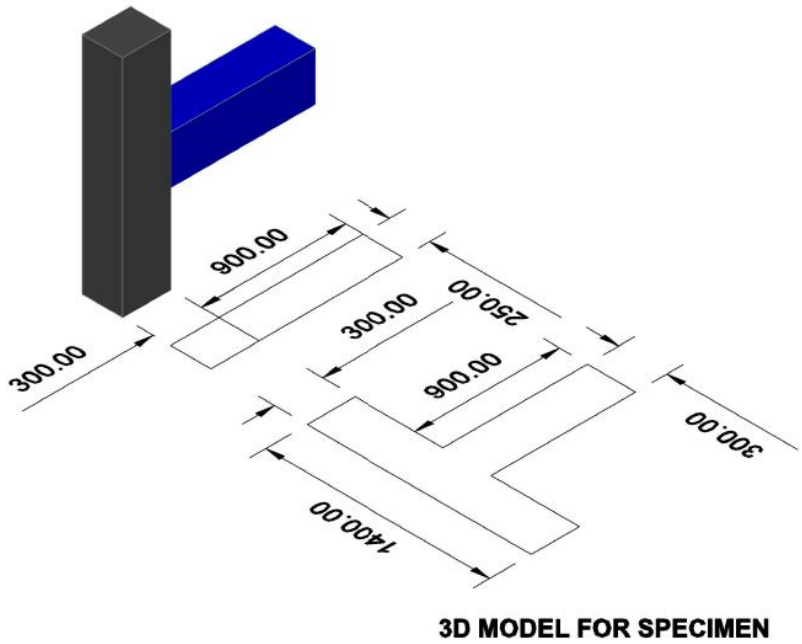

Figure 51 Geometric Size for Specimens

Figure 52 Existing Frame in KFUPM Lab

5.2.2 Beam-Column Reinforcement

Amount of longitudinal reinforcement was constant for J-BU-12 and J-BI-12 specimens as shown in "Figure 53 & 54". Six bars of 12mm diameter were used in the column for longitudinal reinforcement and 8mm diameter closed ties at a spacing of 75mm were used as transverse reinforcement. For beams three bars of 12mm diameter were used for

both the top and bottom longitudinal reinforcement and 8mm diameter closed stirrups with spacing of 75mm were used for transverse reinforcement in the beam except for J-BI-18 specimen in which all the main reinforcement used was of 18mm diameter and there was no transverse reinforcement provided in the joint region in all the specimens. This design resulted for J-BU-12 and J-BI-12 in a column and beam flexure strength of 84.61KN-m and 53.56KN-m and for J-BI-18 the designed column and beam flexure strength was 164.355KN-m and 124.00KN-m detailed calculations for column and beam flexure strength are included in appendix [A]. Details of specimen's geometry and reinforcement are given in "Figure 53, 54 and 55".

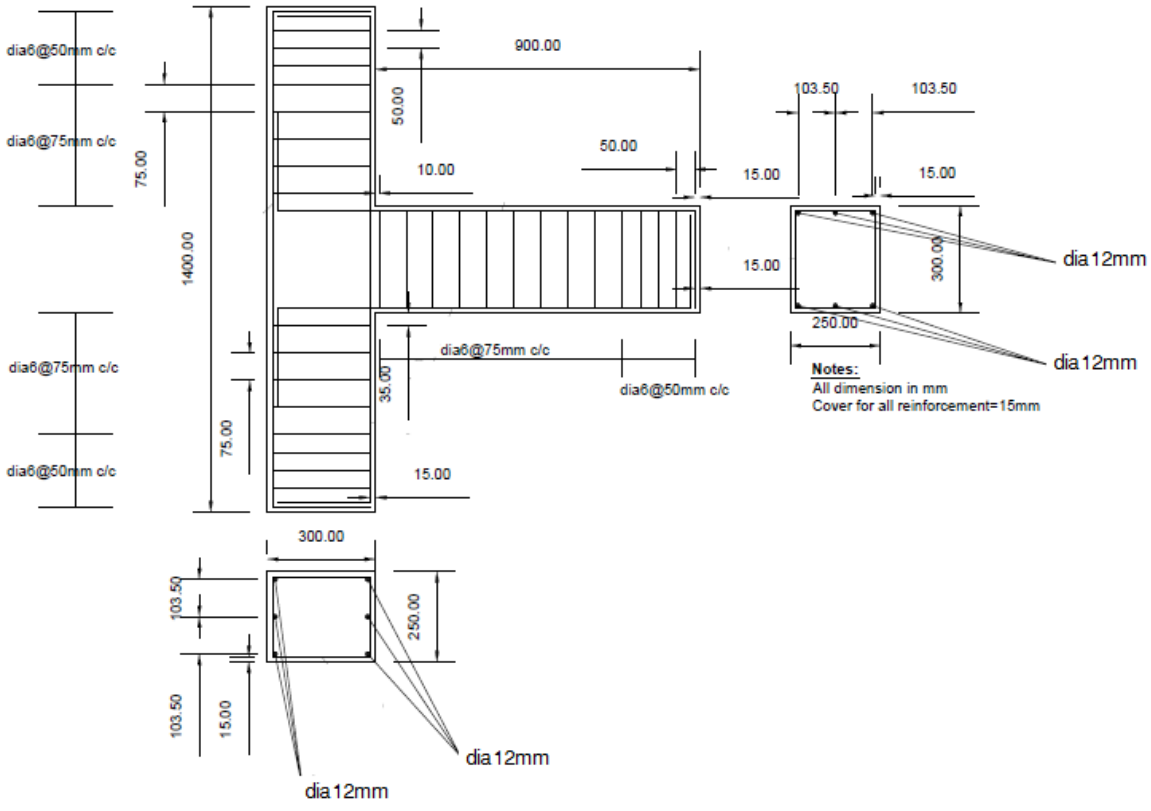

Figure 53 Geometric and Reinforcement Details for J-BU-12

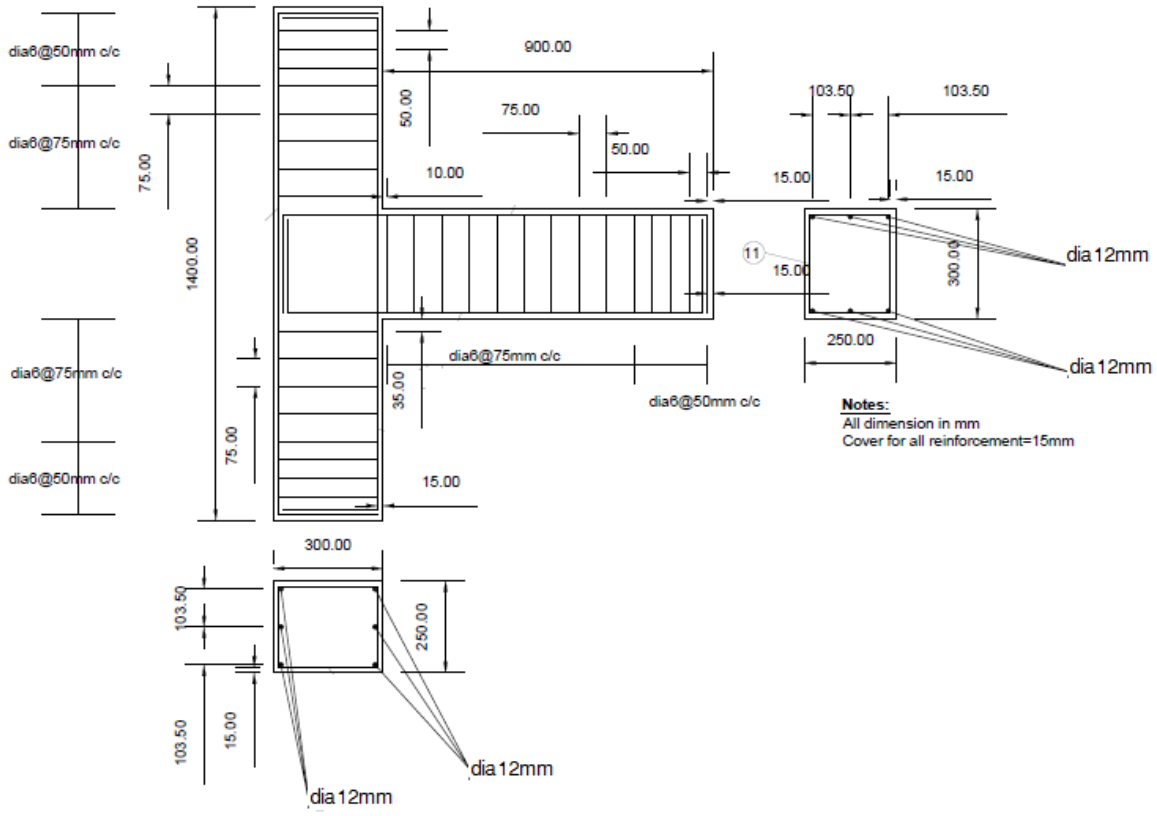

Figure 54 Geometric and Reinforcement Details for J-BI-12

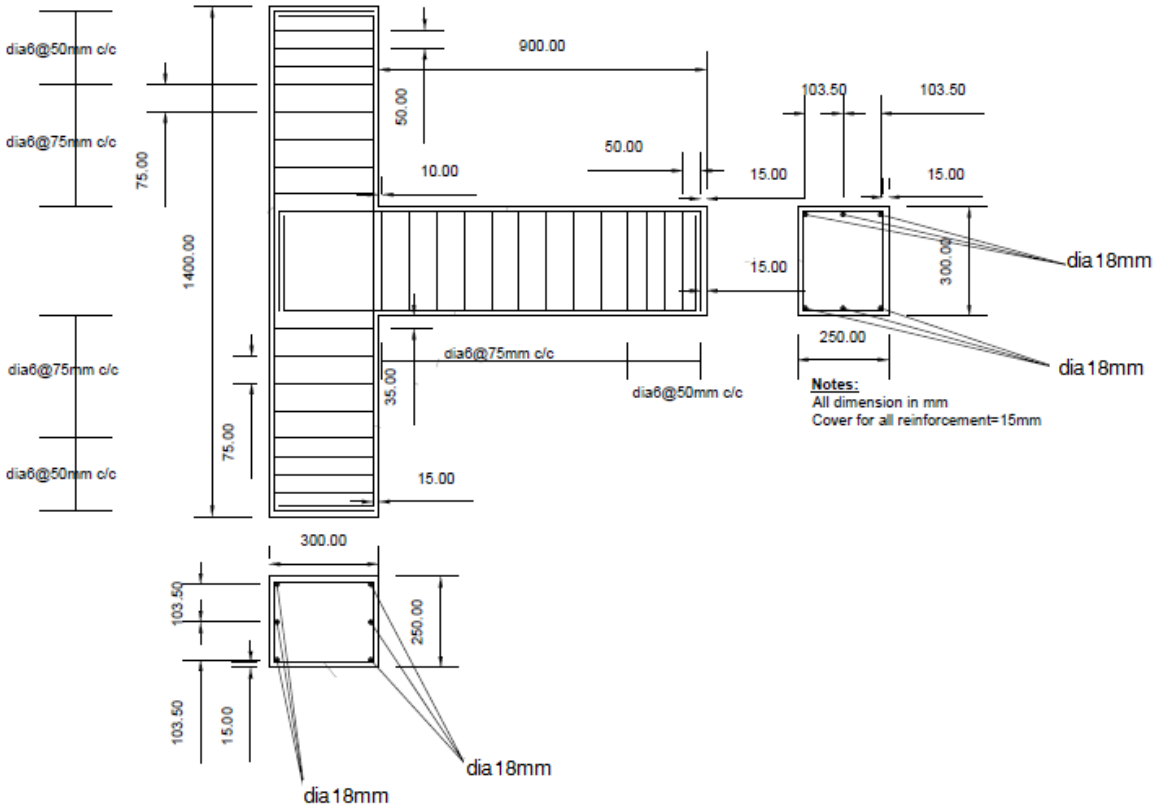

Figure 55 Geometric and Reinforcement Details for J-BI-18

5.2.3 Concrete

Concrete used in the specimens was ready mix with the required strength of 30MPa with 102mm slump and with 25mm maximum size aggregate. Specimens were casted in the lab of KFUPM. 4 cylinders of 3"x6" were casted and compression tests were performed in the lab to determine the concrete strength at the time of testing of specimens as shown in "Figure 56". Table [3] shows the test results at required days.

-

Figure 56 Cylinder Test for Concrete Compressive Strength

Table 3 Compressive Strength of Concrete

CYLINDER NO.	COMPRESSIVE STRENGTH (MPa)	AVERAGE COMPRESSIVE STRENGTH
1	24.517	30 MPa
2	31.7	
3	35.504	
4	28.42	

5.2.4 Steel Reinforcement

In all three specimens longitudinal and transverse reinforcement were 12mm, 18mm diameter and 6mm diameter were used. Tensile test were carried out to determine the actual tensile strength of reinforcement. The properties of the reinforcements are summarized in table [4].and stress strain curves are given in "Figure 57, 58 & 59". The

actual tensile strength f_y of the reinforcement was used in the calculation of nominal moment capacity M_n of the beam for each specimens.

Table 4 Mechanical Properties of Reinforcement

Reinforcements	Diameter (mm)	Fy (MPa)
Φ8	8	480
Φ12	12	610
Φ18	18	660

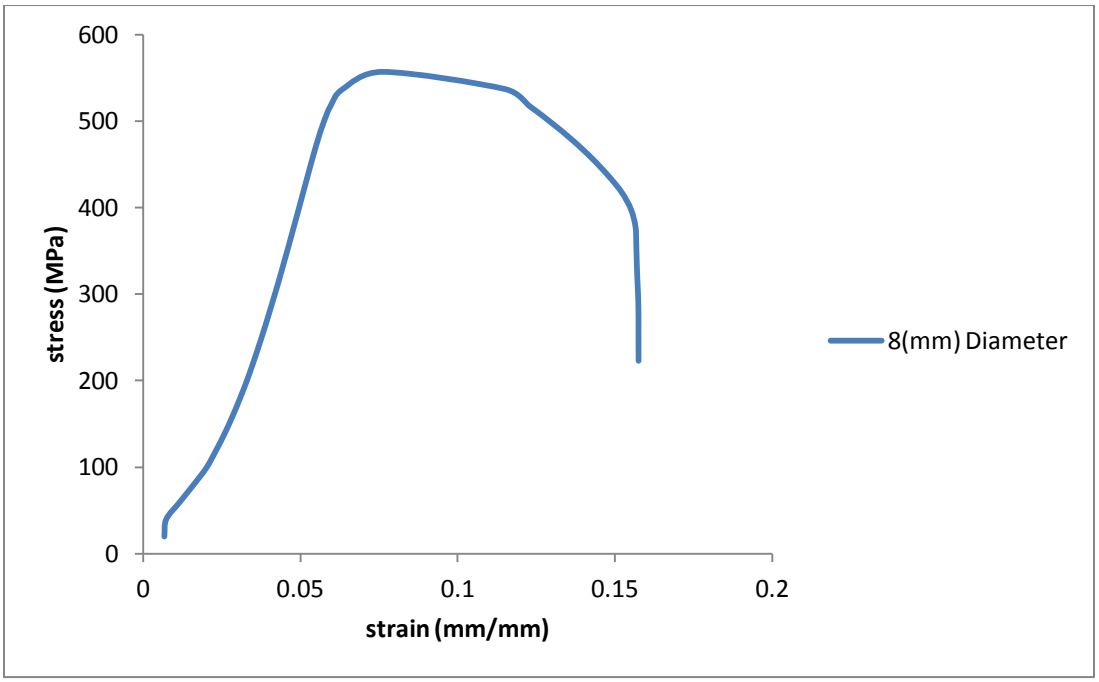

Figure 57 Stress Strain Graph for 8mm Diameter Reinforcement

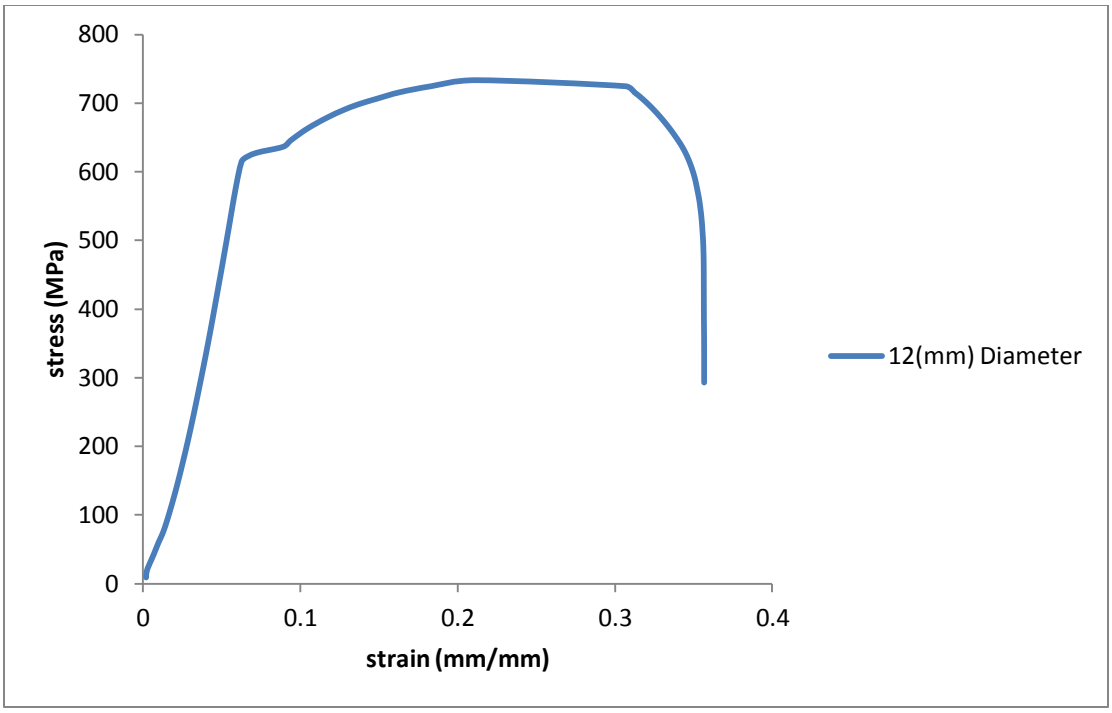

Figure 58 Stress Strain Graph for 12mm Diameter Reinforcement

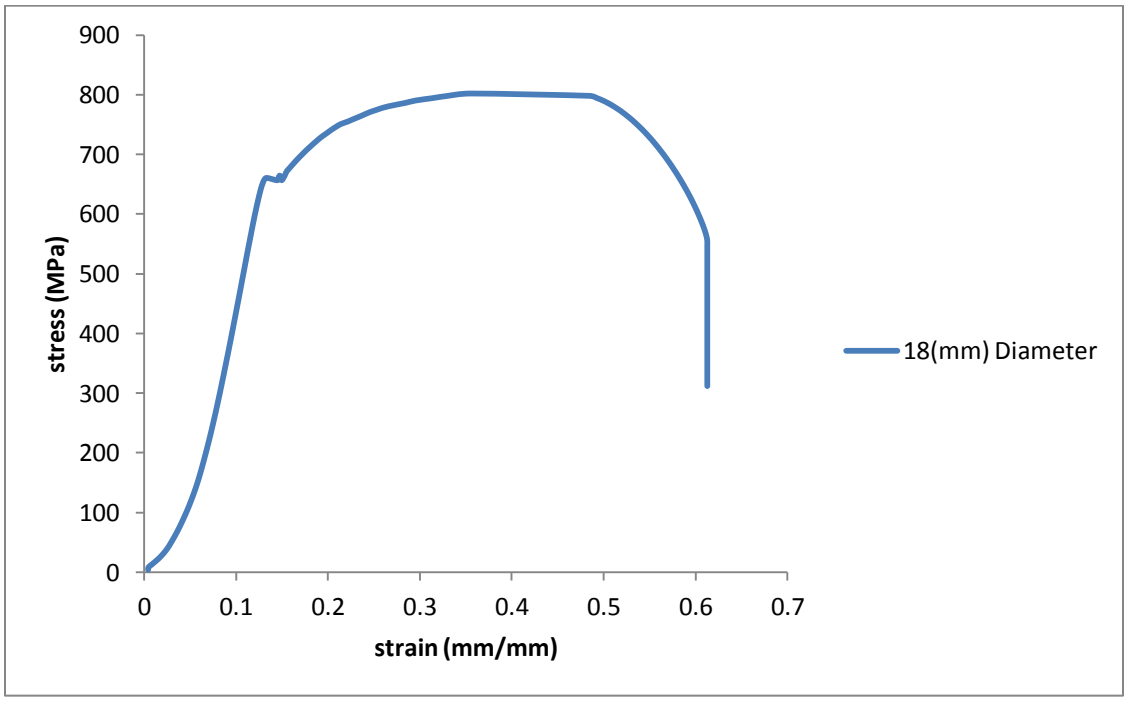

Figure 59 Stress Strain Graph for 18mm Diameter Reinforcement

5.3 STRAIN GAUGES

Total numbers of 12 strain gauges were installed in each specimen in the selected position in the beam column and joint reinforcement as shown in "Figure 60". Two gauges were placed on front face of the center reinforcement above and below the joint region and one gauge was placed on each lateral tie just above and below the joint region, and two gauges were placed on the center beam reinforcement top and bottom one in joint and on just after joint interface. Before the bonding of strain gauges surface was prepared on the reinforcement as shown in "Figure 61" and the adhesive were used to paste the gauges on the reinforcement surface and then wrapped with the tape as shown in "Figure 62".

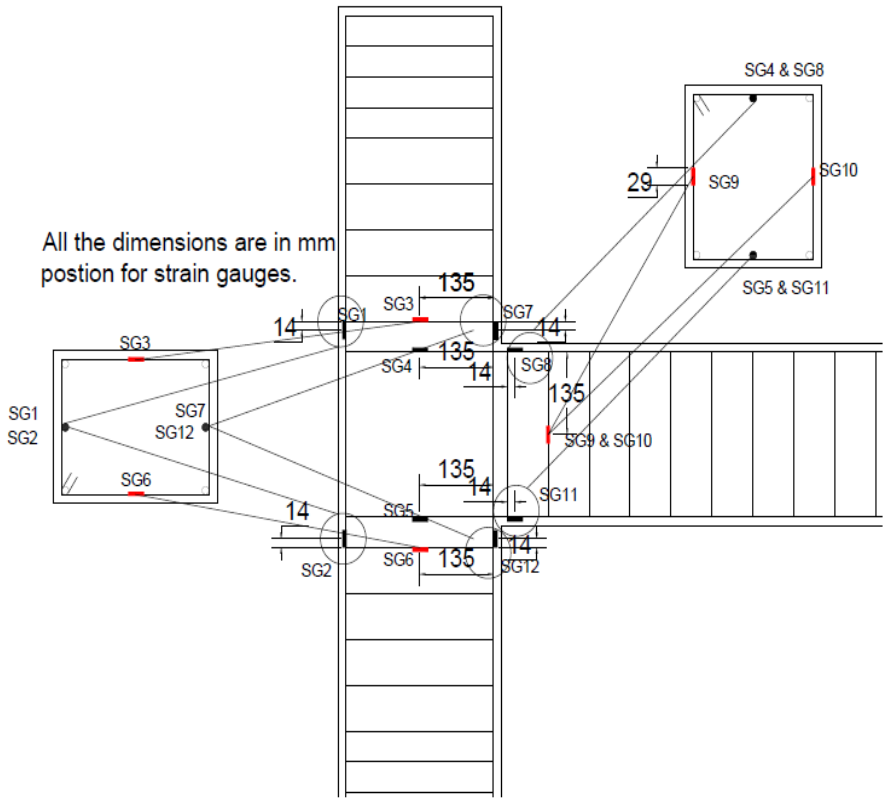

Figure 60 Locations for Strain Gauges for Reinforcement

Figure 61 Surface Preparation for Installation of Strain Gauges

Figure 62 Installation of Reinforcement Stain Gauges

5.4 CASTING OF BEAM COLUMN JOINTS

For the casting of beam-column joints wooden form work was used and the reinforcing cage was set into the form work as shown in “Figure 63”, the joints of the form work was sealed to prevent water seeping out and after the installation of strain gauges on the reinforcement the specimens casted and for casting the concrete mix was batched and delivered in the mixer truck to KFUPM lab. All the concrete was placed in the wheel barrow and then shoved in the form work. After concreting the trowel was used to make the smooth surface of the specimens then specimens were covered with the wetted burlap for curing and then covered by plastic tarp to maintain the moisture level as shown in “Figure 64 & 65”

Figure 63 Specimen Form Work And Reinforcement Cage

Figure 64 Casting of Specimens

Figure 65 Specimens Covered with Wet Burlap for Curing

5.5 TESTING ARRANGEMENTS

Specimens were tested in a self-reaction steel loading, additional clamping system was provided to the frame to hold the specimen at the top and bottom of column and at the tip of beam to apply the load from hydraulic jack as given in “Figure 66”. Two hydraulic jacks were used for application of loads. One hydraulic jack (A) of 30 ton at the top of the column for constant axial load and one hydraulic jack (B) of 10 ton at the tip of the beam for cyclic loading on the beam as shown in “Figure 67”.

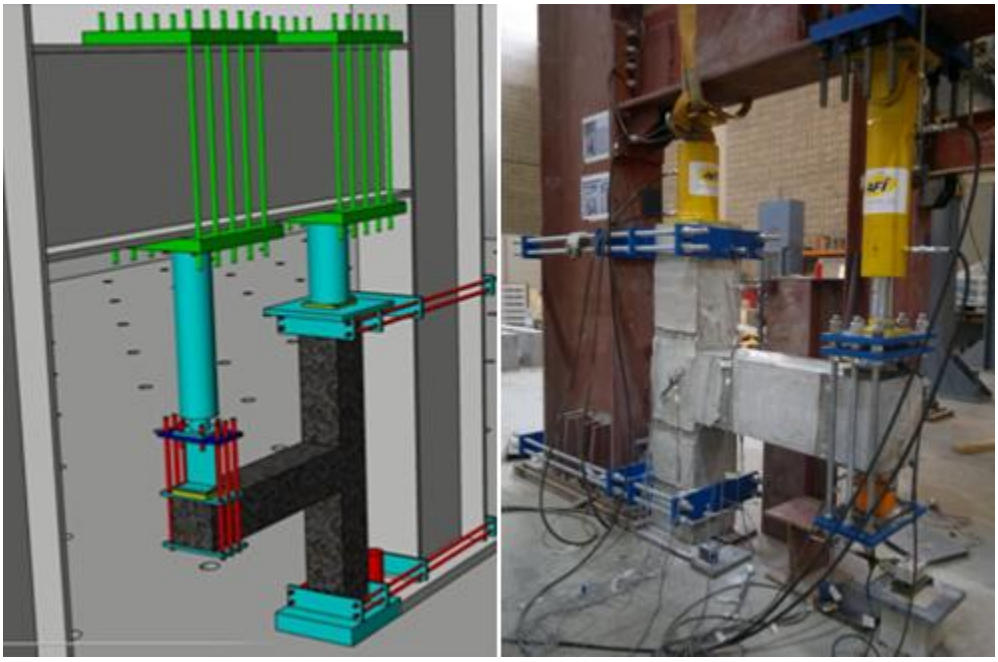

Figure 66 Additional Clamping System to Hold the Specimens During the Test

Figure 67 Hydraulic Jacks Used For Testing Of Beam Column Joints

5.5.1 Instruments for Monitoring Test

Load cells, LVDT's and concrete surface stain gauges were also installed to the specimens during the test of all specimens to monitor the loads stresses and deflections.

Load cells. One Load cell (LC3) of 20ton capacity was installed at the top of column and two load cells (LC1 and LC2) of 100ton capacity were installed at the top and bottom of tip of beam as shown in "Figure 68 & 69"

Figure "Figure 70 & 71" shows LVDT's (J1 and J2) were installed at the joint region to observe the diagonal crack openings, two LVDT's (C1 and C2) were also installed at top and bottom of column to see the movements and one string type LVDT (patriot B2) was installed at the tip of beam to measure the deflections during the tests of specimens.

Concrete surface strain gauges were pasted on the compression and tension side of beam and column to observe the strains on the surface of concrete, as given in “Figure 72”.

Figure 68 Load Cells Used For Testing

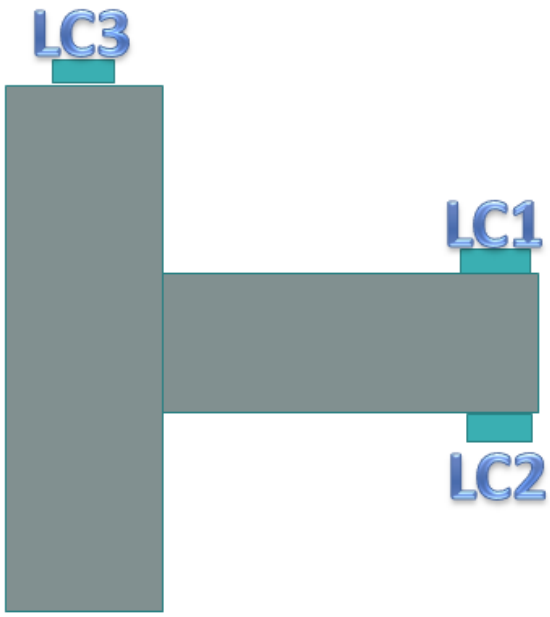

Figure 69 Positions of Load Cell during the Test

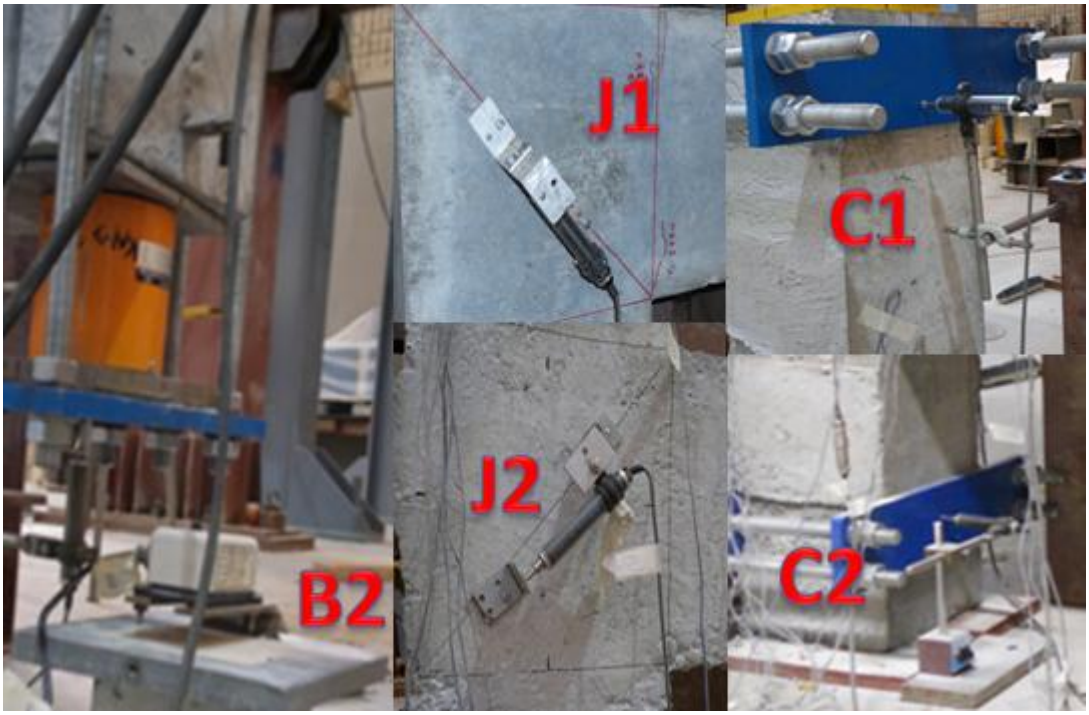

Figure 70 LVDT's used during the Test

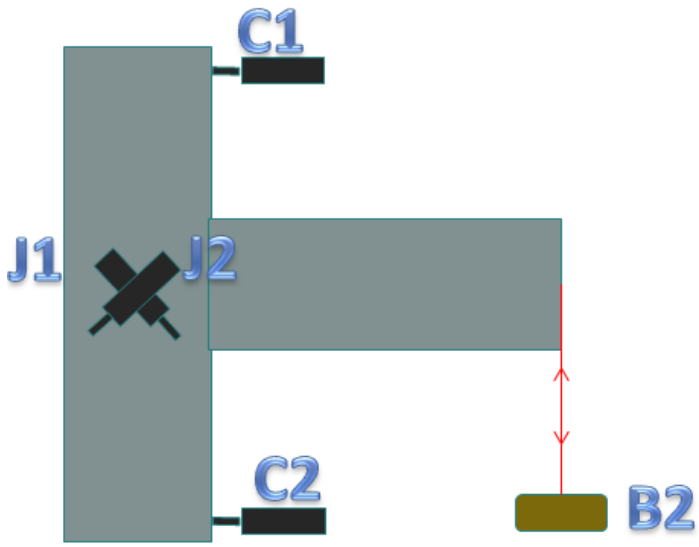

Figure 71 Positions for LVDT's Attached to the Specimens during the Test

Figure 72 Concrete Surface Strain Gauges

5.6 TESTING PROCEDURE

Exterior beam-column joints were tested under deflection control method. Two types of loading were applied to the specimens as shown in "Figure 73" a constant axial load on column (150KN) and increasing displacement at the tip of the beam on both push and pull side up-to the failure of specimens. Photo graphs of the specimens were taken throughout the testing process and the cracks that were developed during the test were noted. Three types of data were collected in the experiments. They were the loads and displacement at the beam tip and the strain values at the selected location of reinforcement in each specimens.

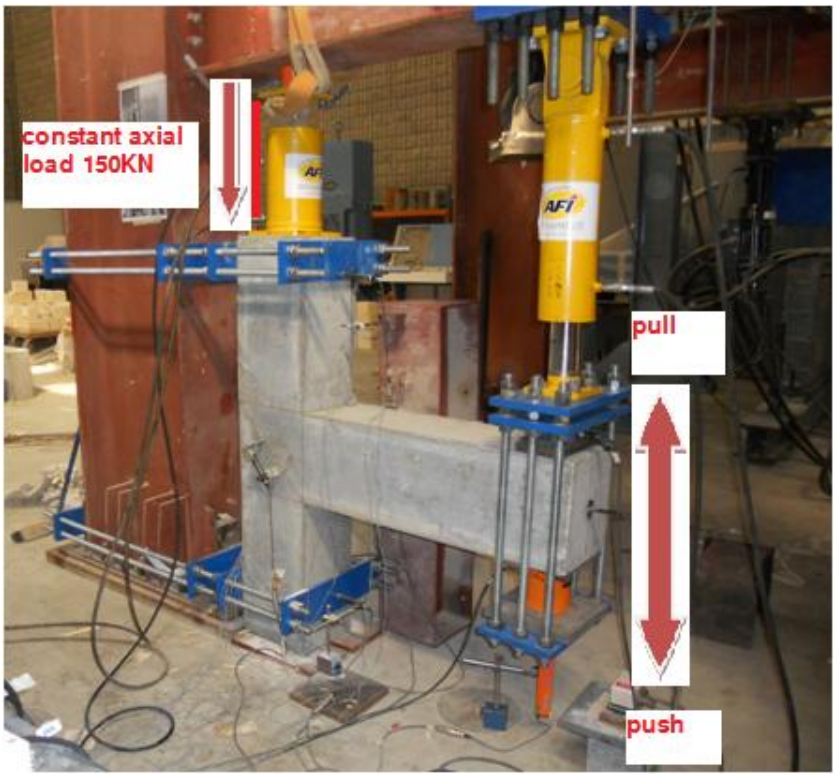

Figure 73 Testing Procedure for Beam-Column Joints

CHAPTER 6

EXPERIMENTAL TEST RESULTS KFUPM SPECIMENS

6.1 CYCLIC TEST RESULTS FORTYPE J-BU-12

Type J-BU-12 specimen has the bent up detailing in the joint region with 12mm diameter flexural reinforcement for beam and column. “Figure 74” shows the load and displacement relationships for J-BU-12 specimen for both push and pull directions.

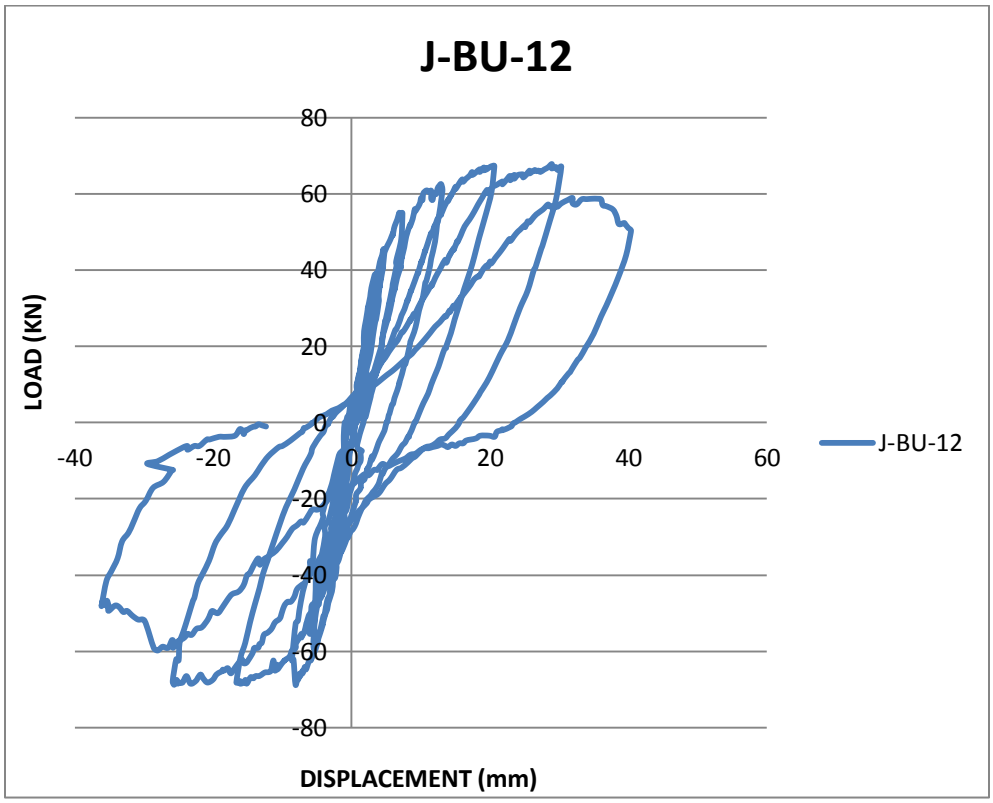

Figure 74 Load Verses Displacement Graph for Specimen J-BU-12

In type J-BU-12 specimen during the testing the first crack was found in the first cycle in the push direction on two places one at the beam column joint interface and second little away from the joint in the beam and both of the cracks were flexural cracks at the load of 25KN and the displacement of 2.2mm, the first diagonal crack found in the joint at third cycle in push direction at load of 53KN and at the displacement of 6.844mm as shown in "Figure 75".

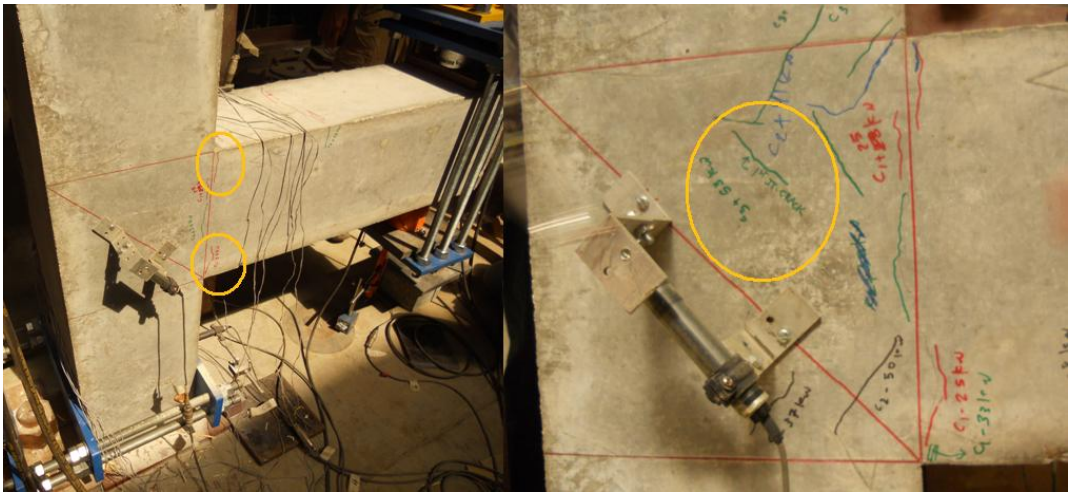

Figure 75 Location of First Crack at Beam Column Interface and In Joint for Specimen J-BU-12

During the cyclic load test the cracks starts from the beam column joint interface and reached towards the joint as the load cycle increased, in all the load cycling process it was observed that the cracks were opened and closed opposite to their loading directions and the diagonal cracks were widen up to 3mm at the sixth cycle in push direction at 66KN, in this specimen same diagonal cracks were found in both push and pull direction as it was found in the type J-BI-12 specimen but the difference was that these diagonal

cracks reached to the columns and sever shear X cracks were formed as shown in “Figure 76, 77 & 78”.

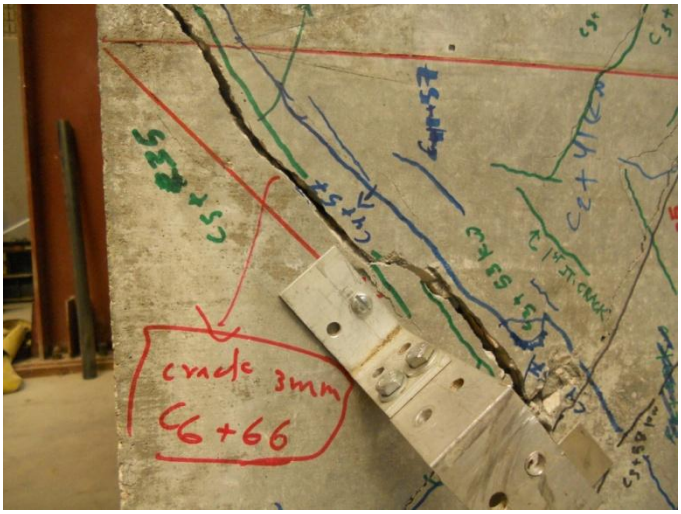

Figure 76 Widening Up of Shear Diagonal Crack in Joint for Specimen J-BU-12

Figure 77 Formation of Crack in Joint during Cyclic Load Test in Specimen J-BU-12

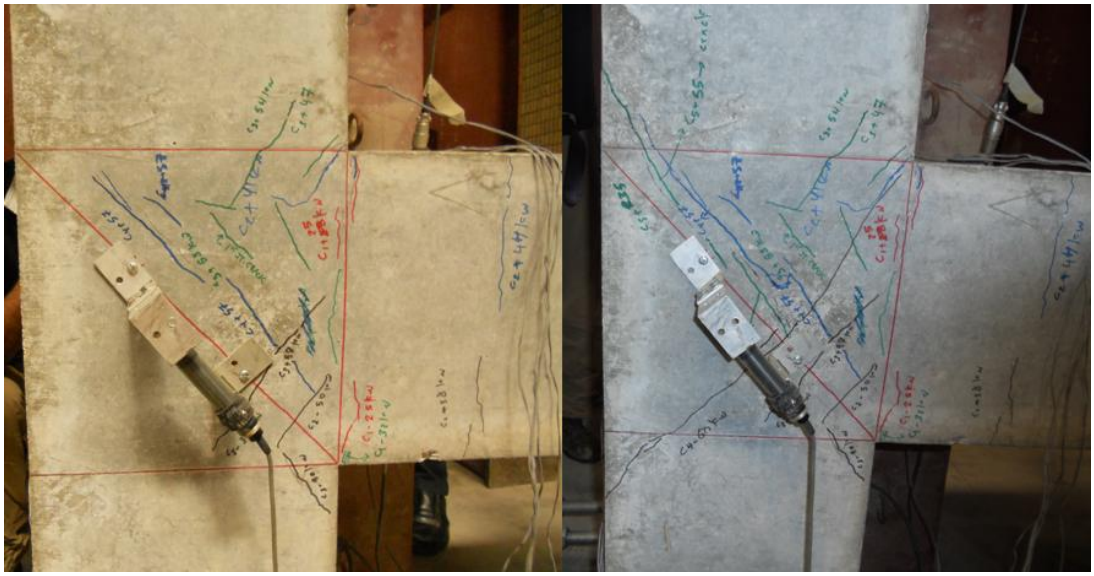

Figure 78 Formation of Crack in Joint during Cyclic Load Test in Specimen J-BU-12

The failure of the specimens were totally in shear in the joints, the concrete of the joint were spilled off from the surface and there were sever damages at the back side of the joint, at the failure joint was totally crushed and the reinforcements were totally visible and the residual displacement remains in the beam which were visible to the naked eye as shown in “Figure 79 & 80”.

Figure 79 Failure of Specimen J-BU-12

Figure 80 Crushing Of Joint and Residual Displacement in Beam of Specimen J-BU-12

To observe the opening in the joints LVDTs were installed diagonally to the joint on both the sides opposite to each other as shown in “Figure 81”.

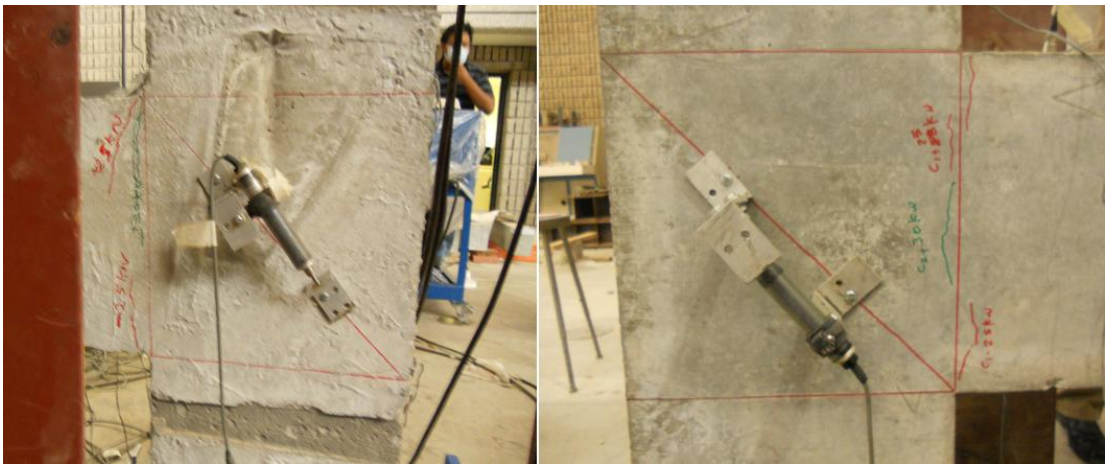

Figure 81 Position of LVDT's in Joint to Observe Diagonal Cracks

the graphs are plotted for both side joint crack openings as given in "Figure 82 & 83" both the LVDTs shows that when the displacements starts in the push direction the cracks starts to increase and reduces as the displacement reduce, this condition was same for the pull side displacement but the behavior was vice versa as it was in push direction tension side converts into compression and compression side converts into tension

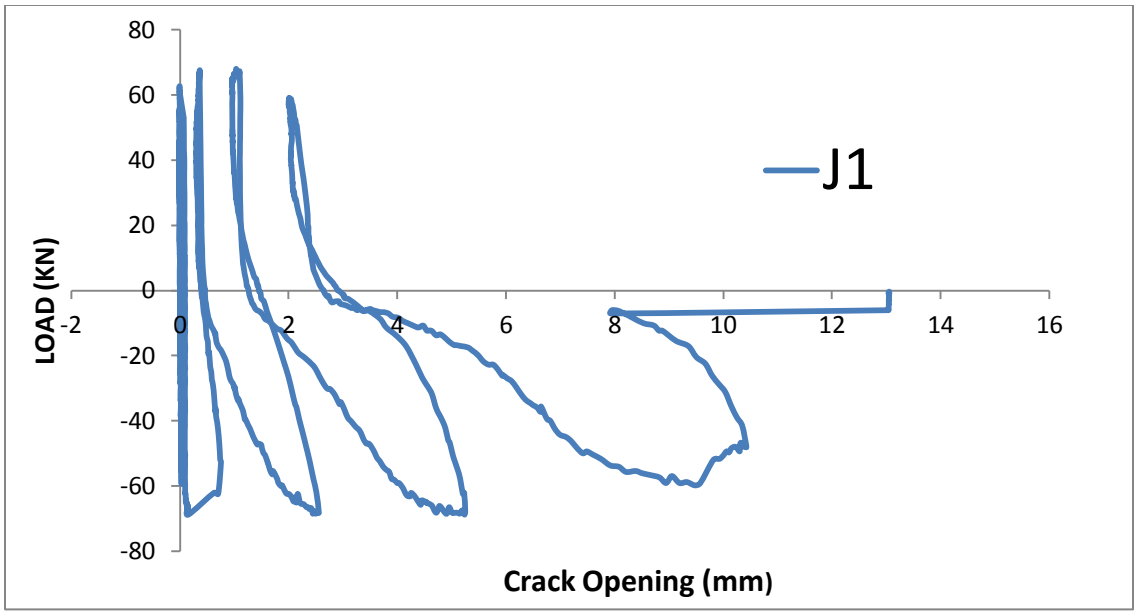

Figure 82 Load Verses Crack Opening Graph for LVDT J1

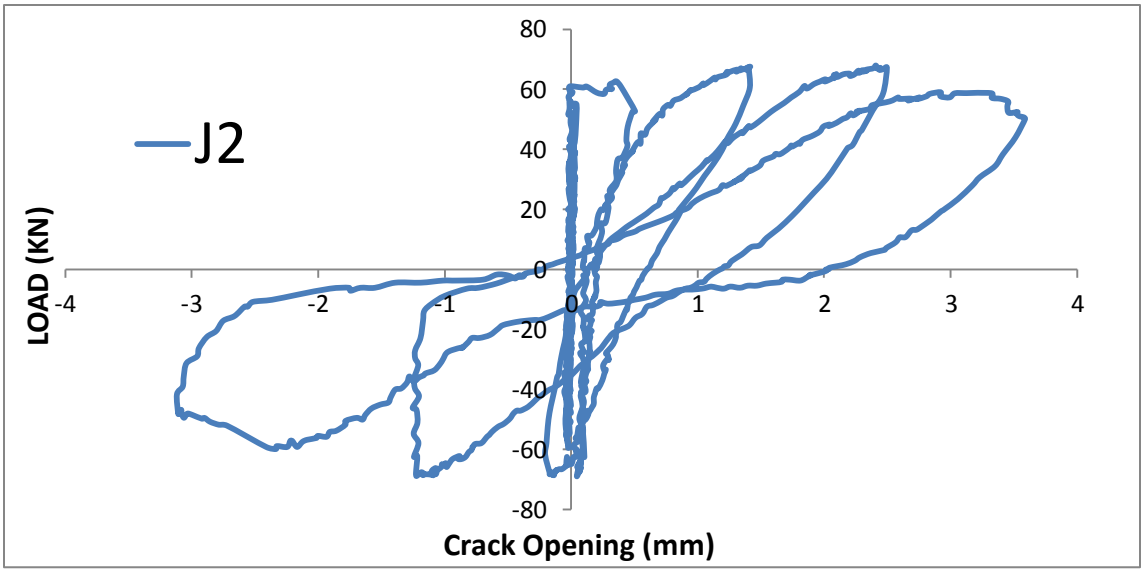

Figure 83 Load Verses Crack Opening Graph for LVDT J2

Strain gauges were installed to monitor the strains in the reinforcement; “Figure 84 & 85” shows the graphs between load and strains in the steel for top and bottom reinforcement

of beam in the specimen which shows the cyclic behavior according to the cyclic test of beam-column joints

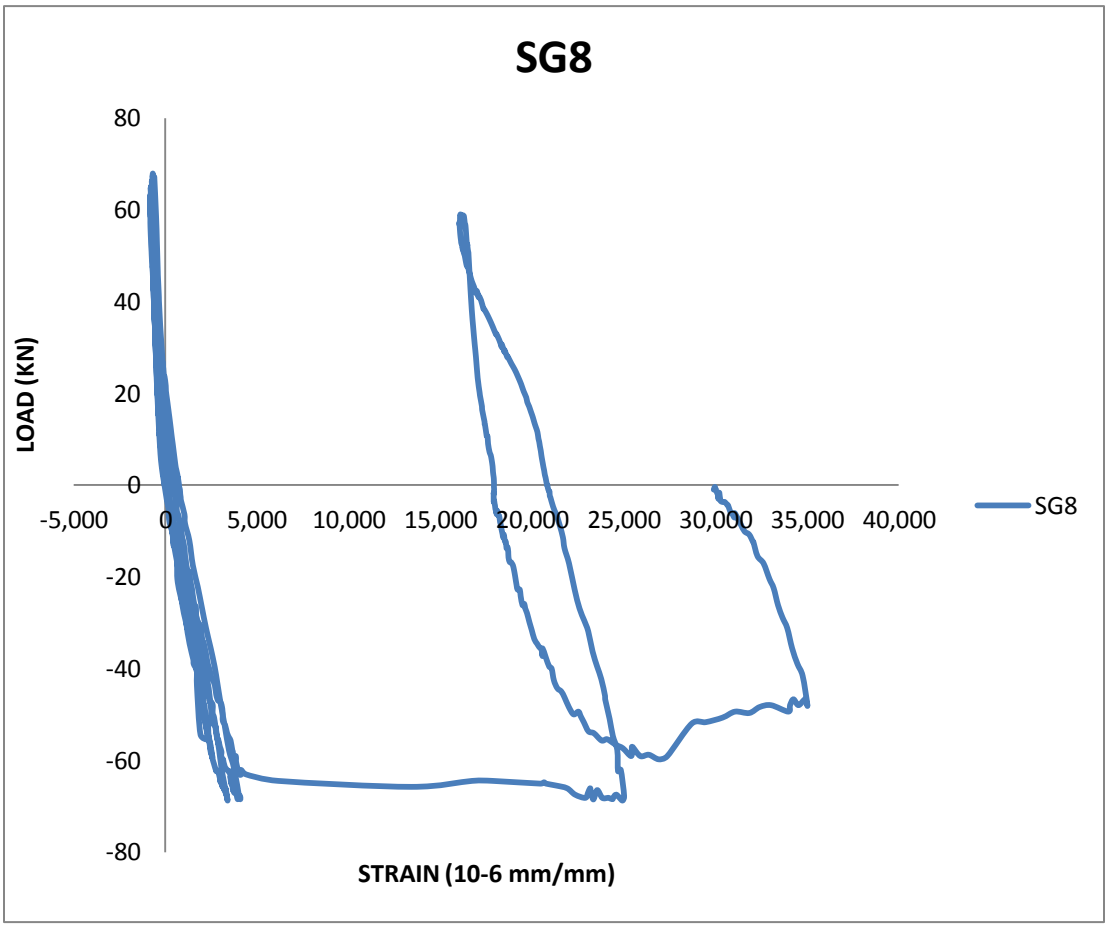

Figure 84 Load Verses Strain Graph for Top Beam Reinforcement

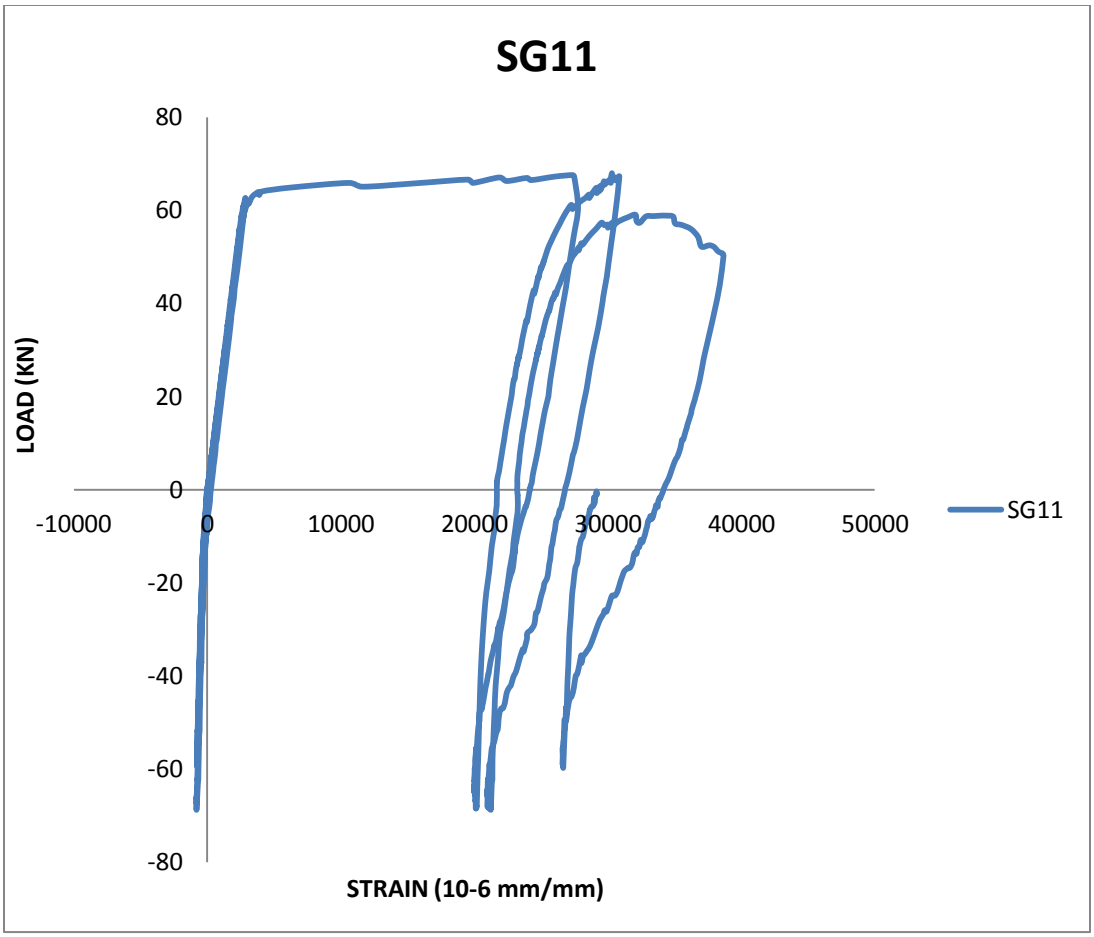

Figure 85 Load Verses Strain Graph for Bottom Beam Reinforcement

All the strain gauges were monitored and the graphs were plot between load and strains for cyclic load test of beam-column joints as shown in “Figure 86 and 87”.

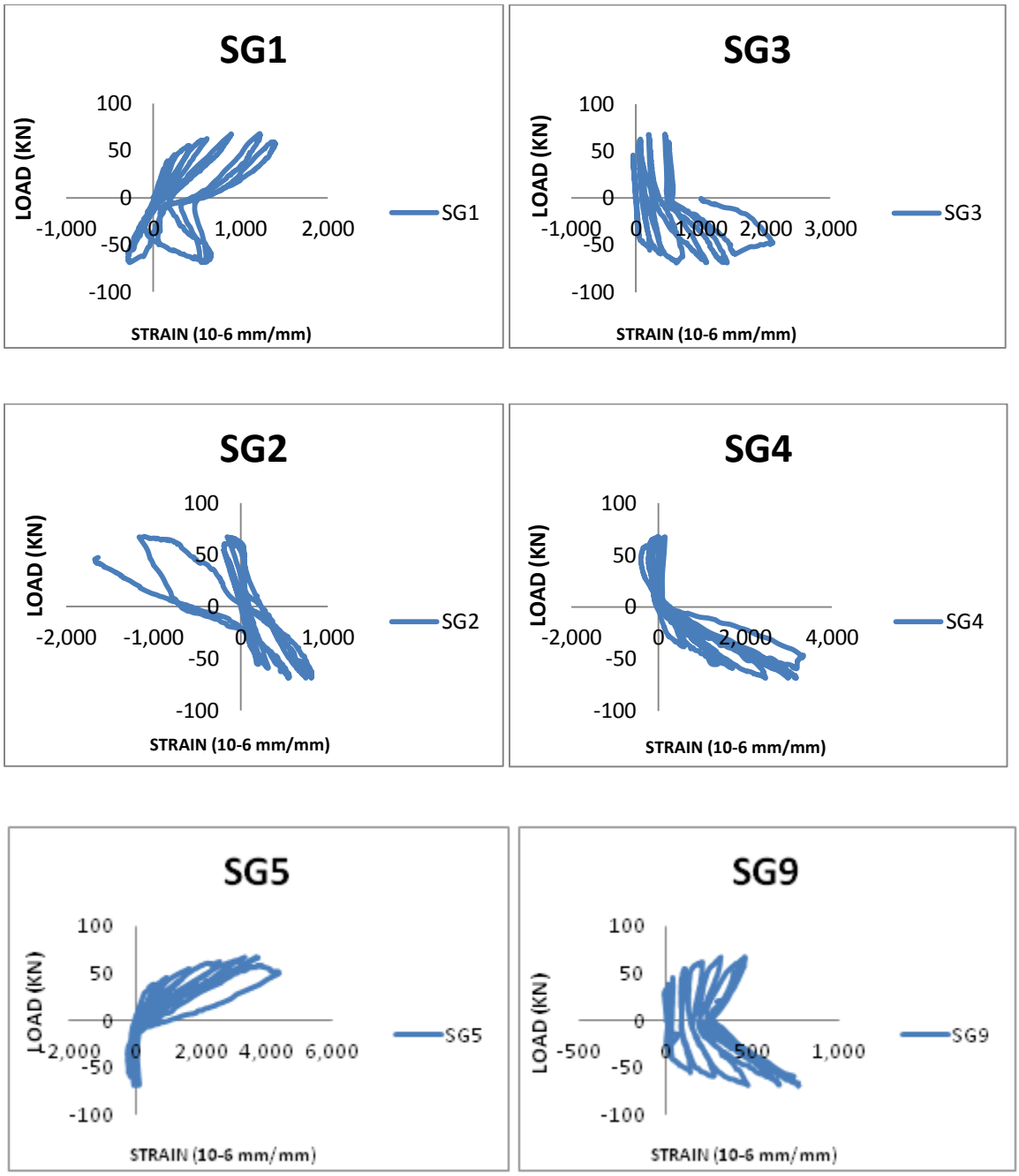

Figure 86 Load Verses Strain Graph for Reinforcement at Selected Positions

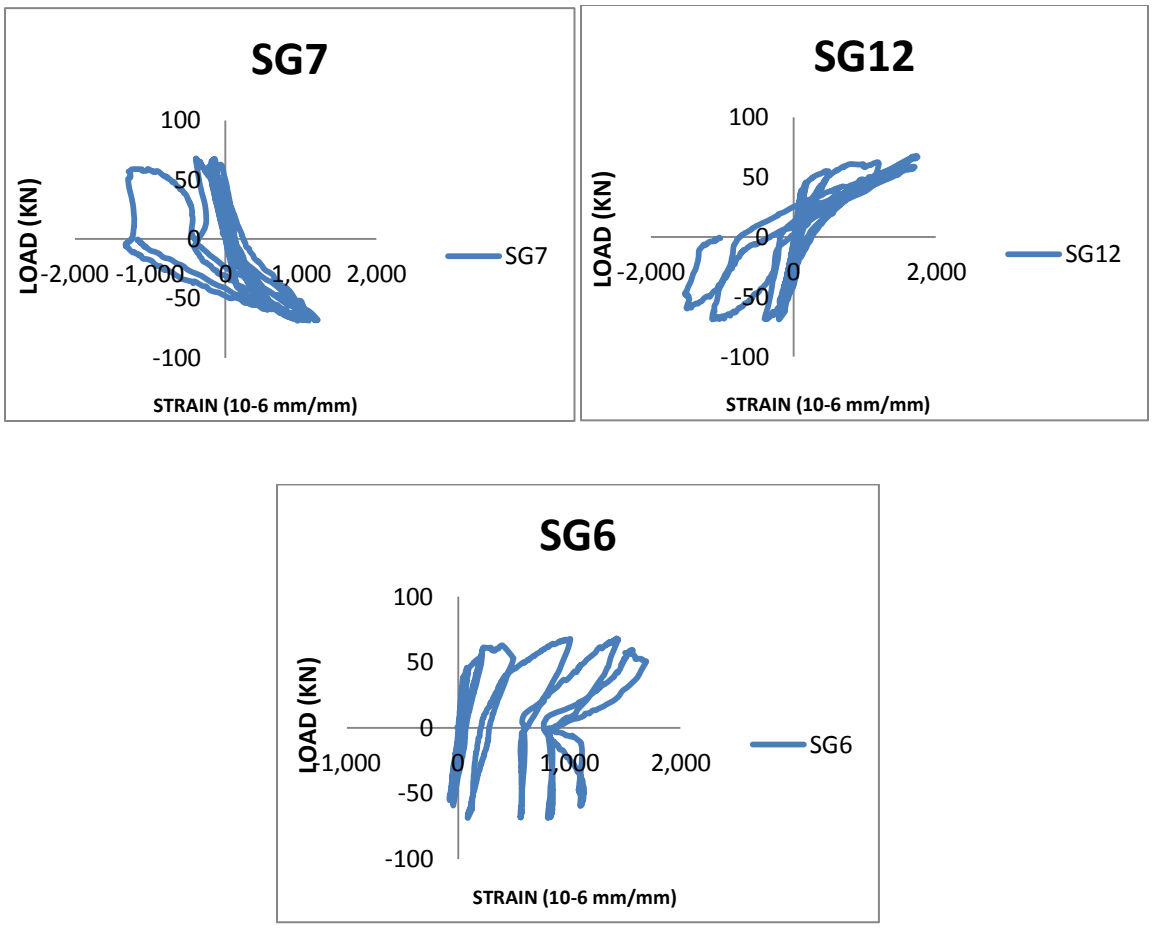

Figure 87 Load Verses Strain Graph for Reinforcement at Selected Positions

6.2 CYCLIC TEST RESULTS FORTYPE J-BI-12

Type J-BI-12 specimen has the bent in joint detailing of beam main reinforcement, all the main reinforcements were 12mm diameter used in this specimen, “Figure 88” shows the load verses displacement graph for cyclic load test of J-BI-12

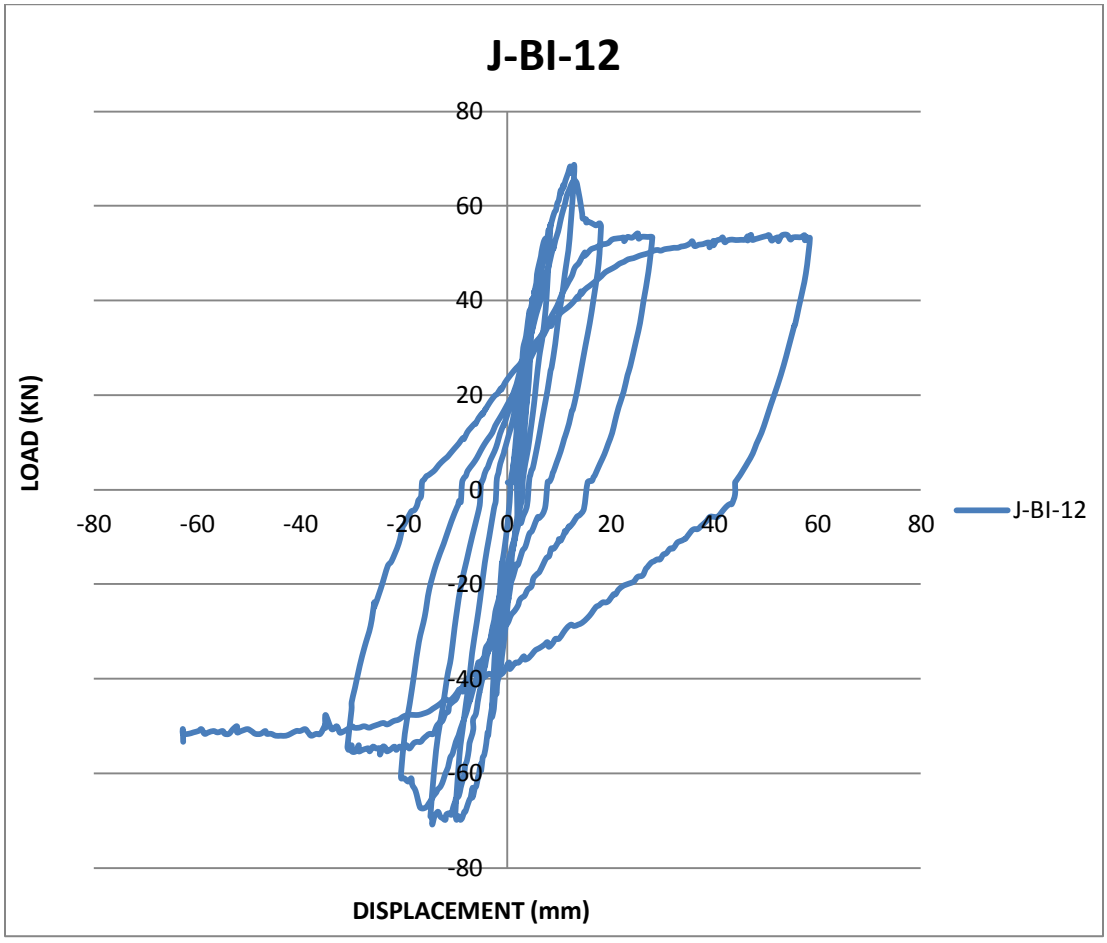

Figure 88 Load Verses Displacement Graph for Specimen J-BI-12

Load verses displacement graph shows that the maximum load and displacement reached in push direction was 68.77KN and 58.67mm and the maximum load and displacement in pull direction was 70.80KN and 63.38mm.The first crack formed in the specimen was flexural crack near the beam column interface during the first cycle both on push and pull displacement at the load of 25KN (push) and 20KN (pull) as shown in "Figure 89"

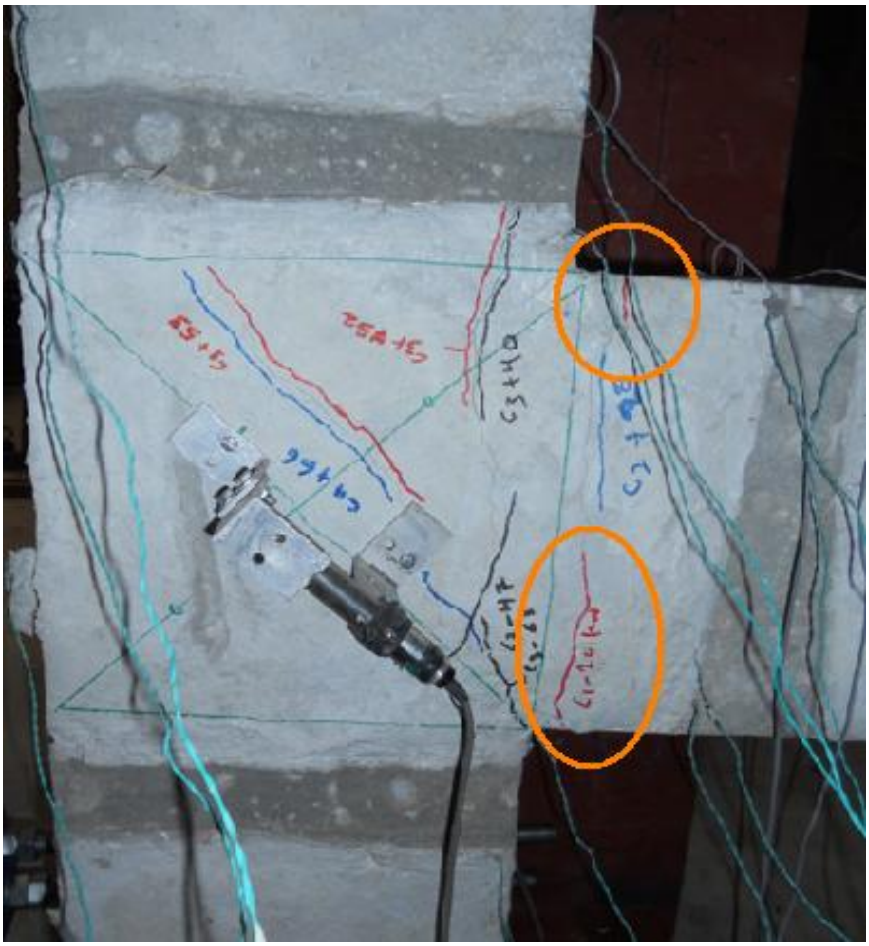

Figure 89 First Flexural Crack for Specimen J-BI-12

The first diagonal crack at the joint region was formed in the third cycle at the push side at the load of 53KN and the diagonal crack extended at load of 66 KN in fourth cycle in when displaced in push direction as shown in “Figure 90”

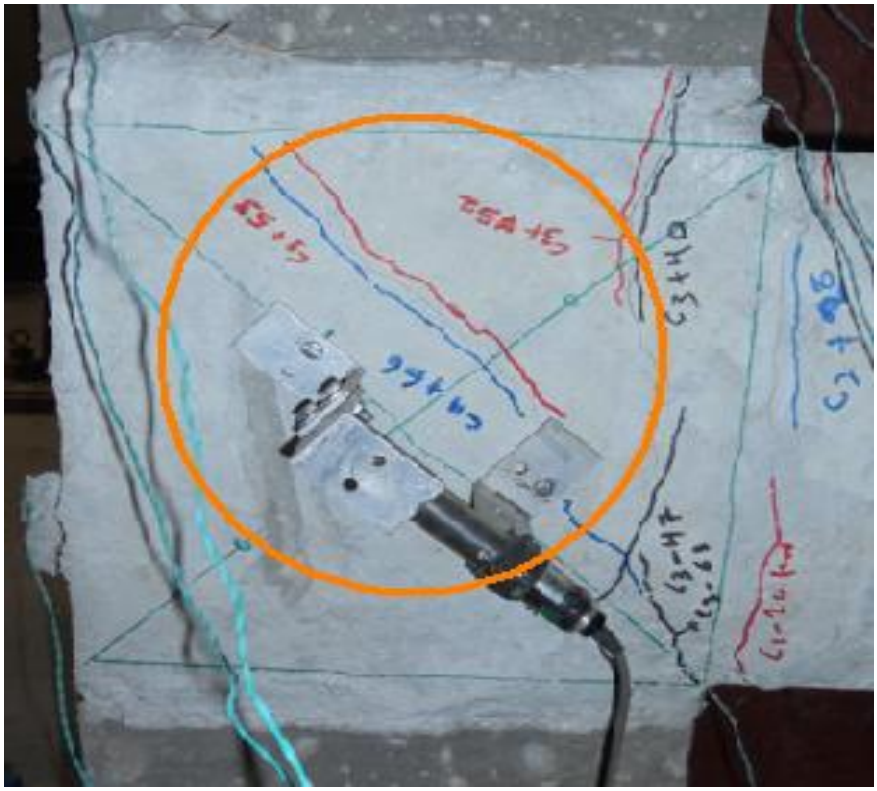

Figure 90 First Diagonal Crack In Joint for Specimen J-BI-12

In the last two cycle the beam column interface of the specimen was totally damaged and crushed, concrete cover spall off from one side of the joint, the reinforcement was totally visible to the naked eye the failure in this specimen was totally flexural and the residual displacement of the beam can been scene clearly as shown in “Figure 91, 92 and 93”

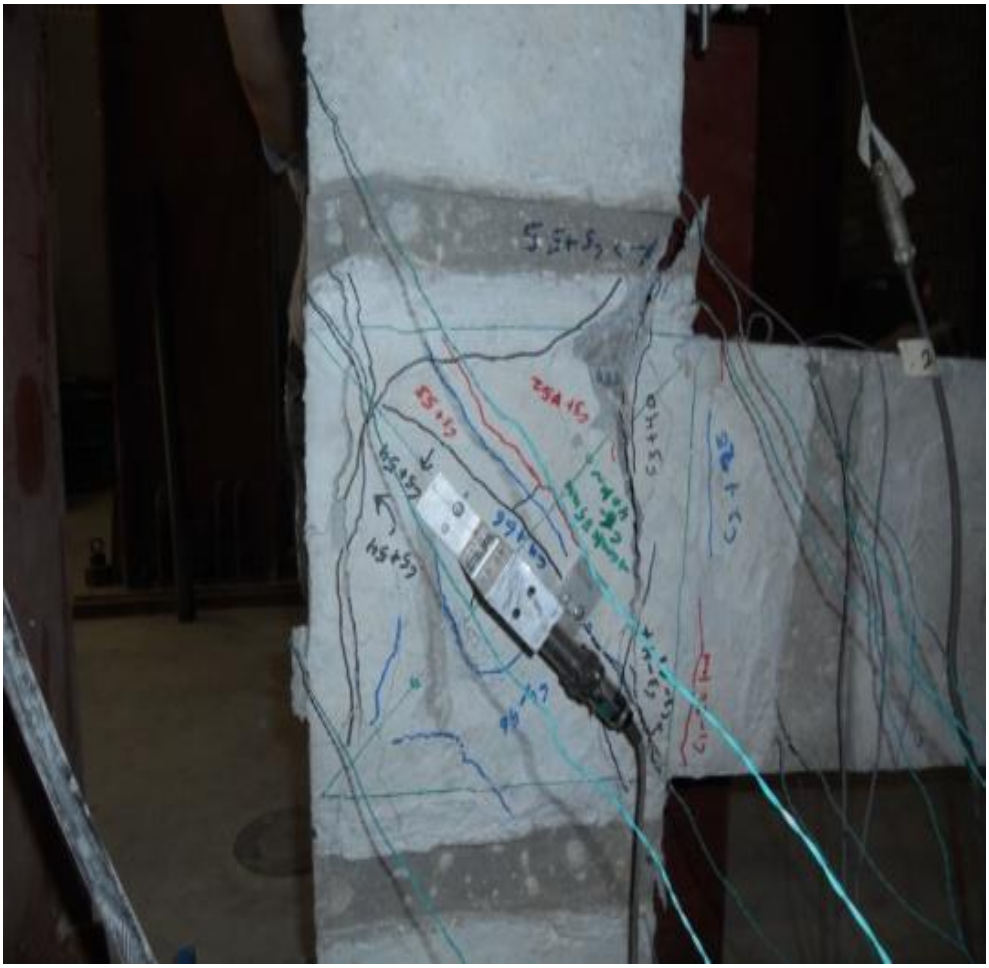

Figure 91 Crushing of Concrete near Beam Column Interface for Specimen J-BU-12

Figure 92 Spilling Of Concrete in Joint Region for Specimen J-BU-12

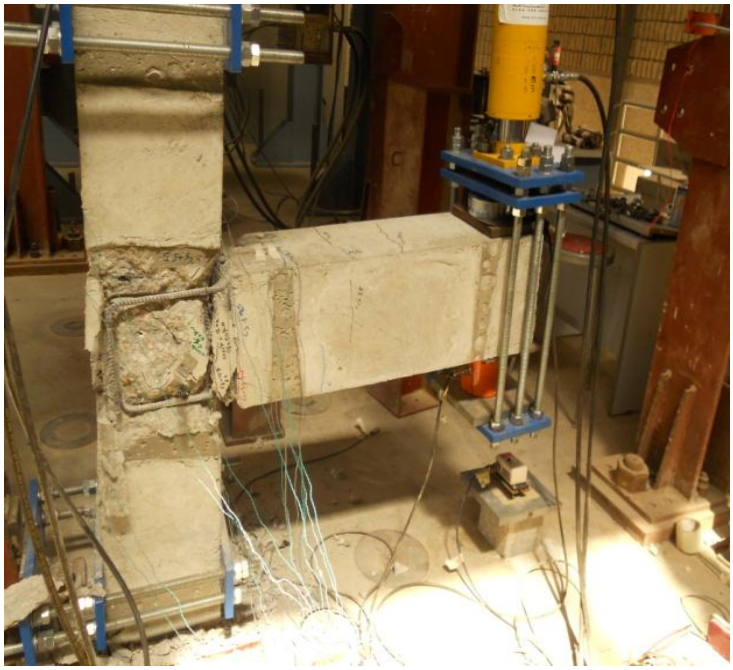

Figure 93 Residual Displacement in Beam for Specimen J-BU-12

LVDT's were installed at the joint region diagonally on both side to observe the crack opening during the push and pull loading as shown in "Figure 94 & 95", the graphs were plotted between the load and diagonal crack opening in the joint as given in "Figure 96 & 97 ".

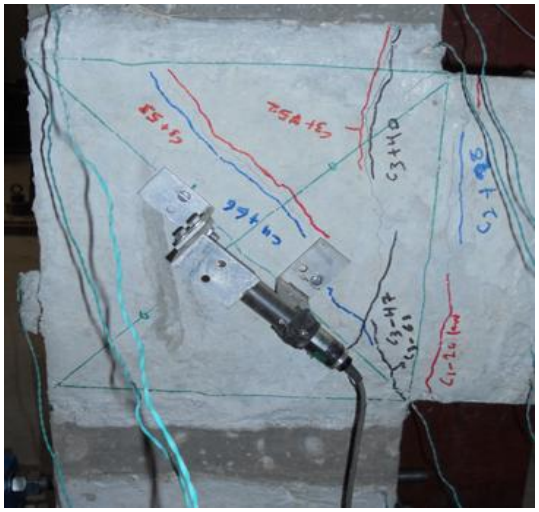

Figure 94 Position of LVDT J1 in Joint to Observe Diagonal Crack

Figure 95 Position of LVDT J2 in Joint to Observe Diagonal Crack

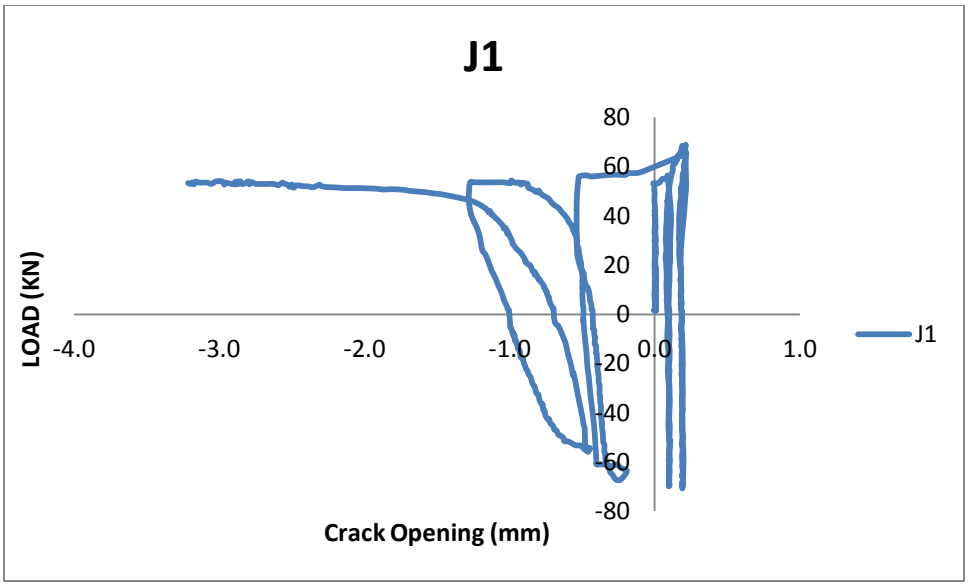

Figure 96 Load Verses Crack Opening Graph for LVDT J1

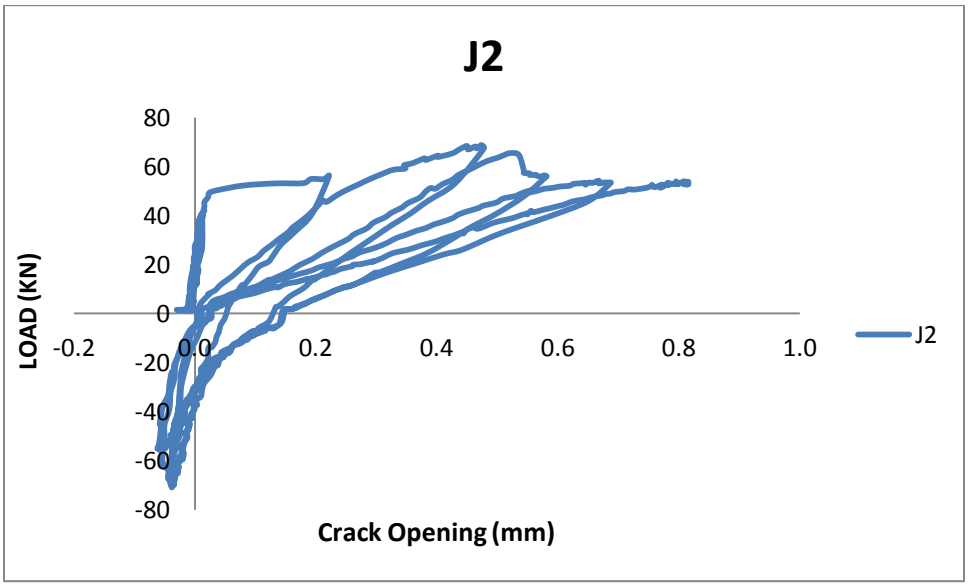

Figure 97 Load Verses Crack Opening Graph for LVDT J2

Strain gauges were installed to observe the strains in the reinforcement on the selected positions and the graphs were plotted between the load and strains in the reinforcements

as shown in “Figure 98 & 99”, graphs for SG8 and SG11 shows the strains for the beam top and bottom reinforcements and the “Figure 100 & 101” clearly shows the compression and tension behavior of steel during the push and pull cyclic displacement of beam.

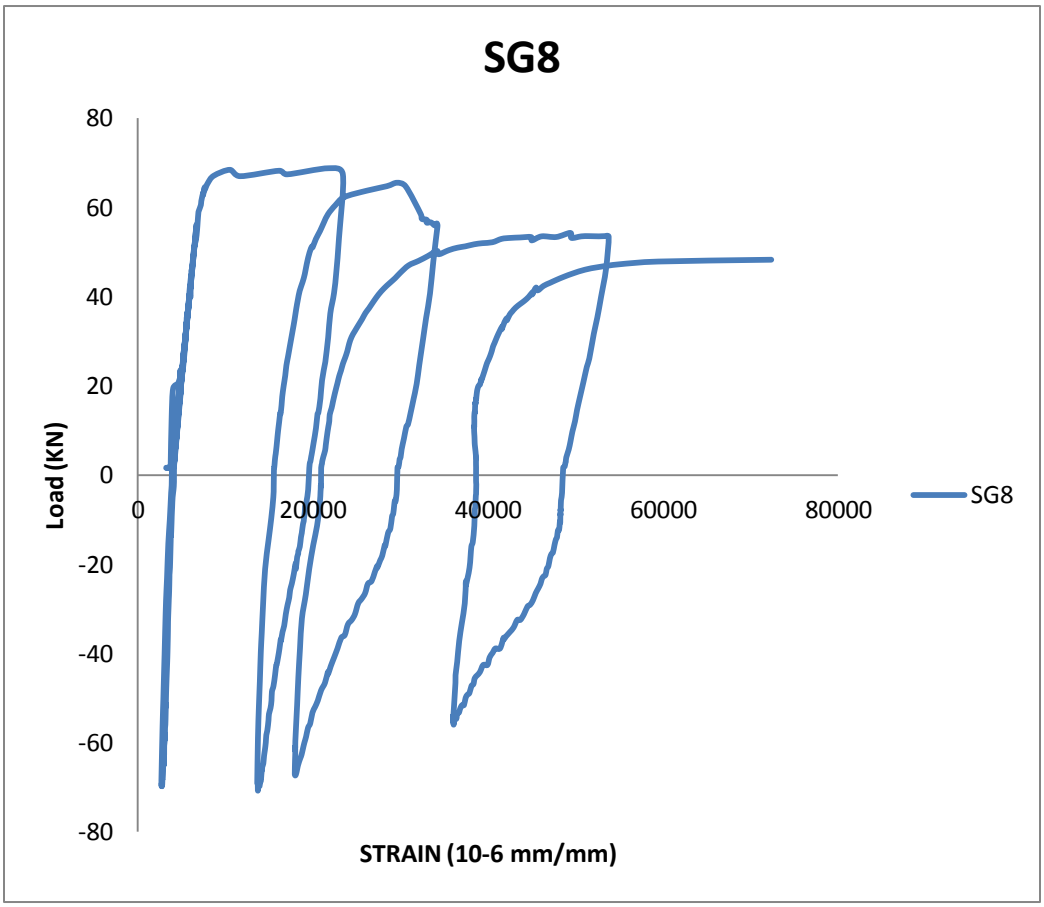

Figure 98 Load Verses Strain Graph for Top Beam Reinforcement

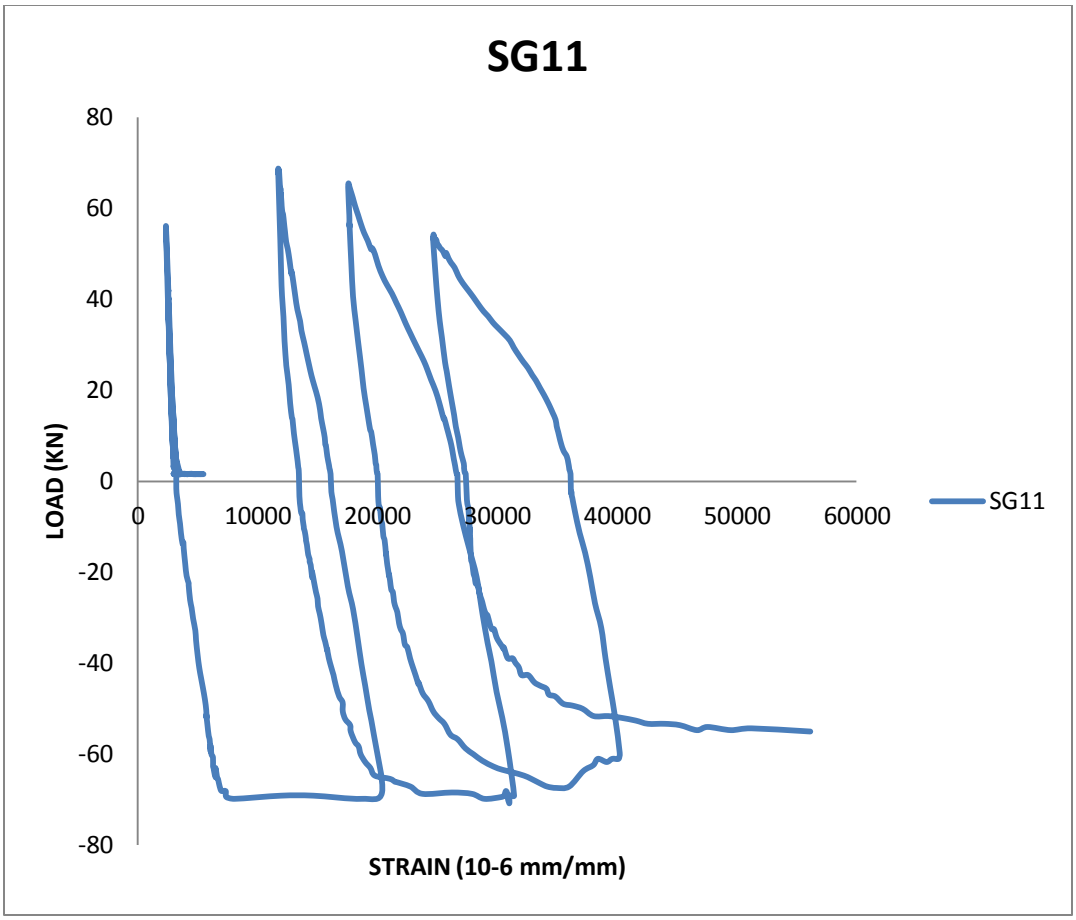

Figure 99 Load Verses Strain Graph for Bottom Beam Reinforcement

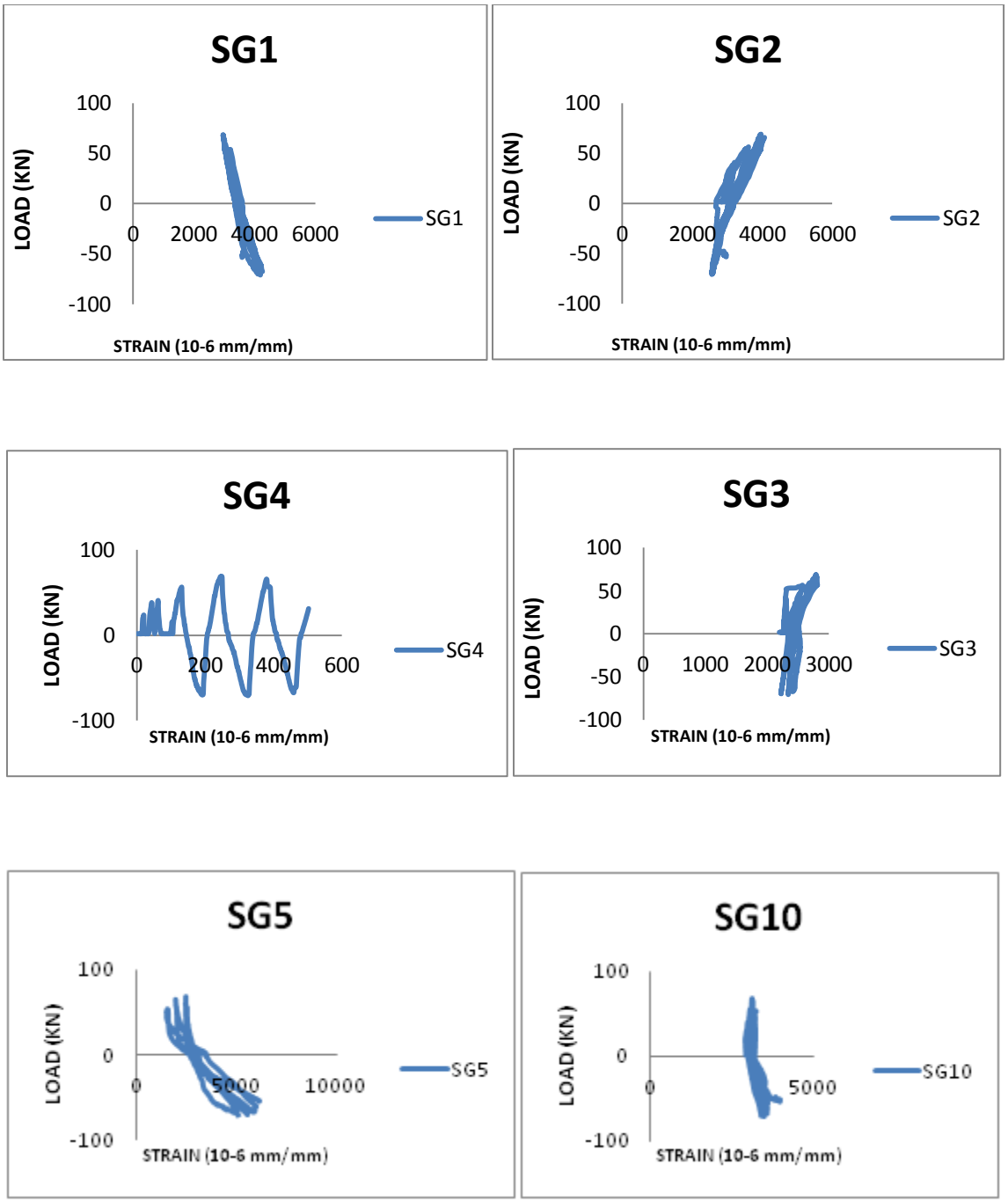

Figure 100 Load Verses Strain Graph for Reinforcement at Selected Positions

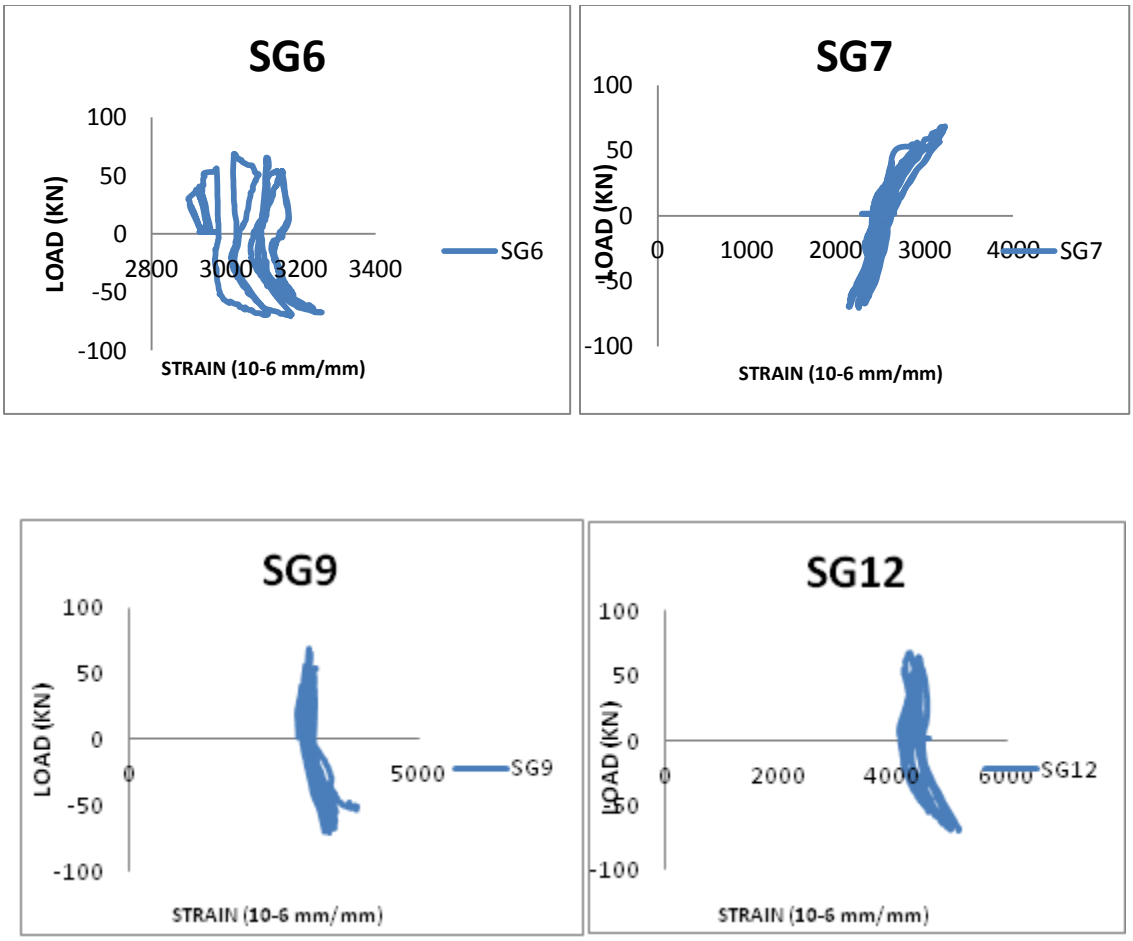

Figure 101 Load Verses Strain Graph for Reinforcement at Selected Positions

6.3 CYCLIC TEST RESULTS FORTYPE J-BI-18

TYPE J-BI-18 specimen has the bent in joint details with 18mm diameter flexural reinforcement for beam and column. “Figure 102” shows the load and displacement relationships for J-BI-18 specimen for both push and pull directions

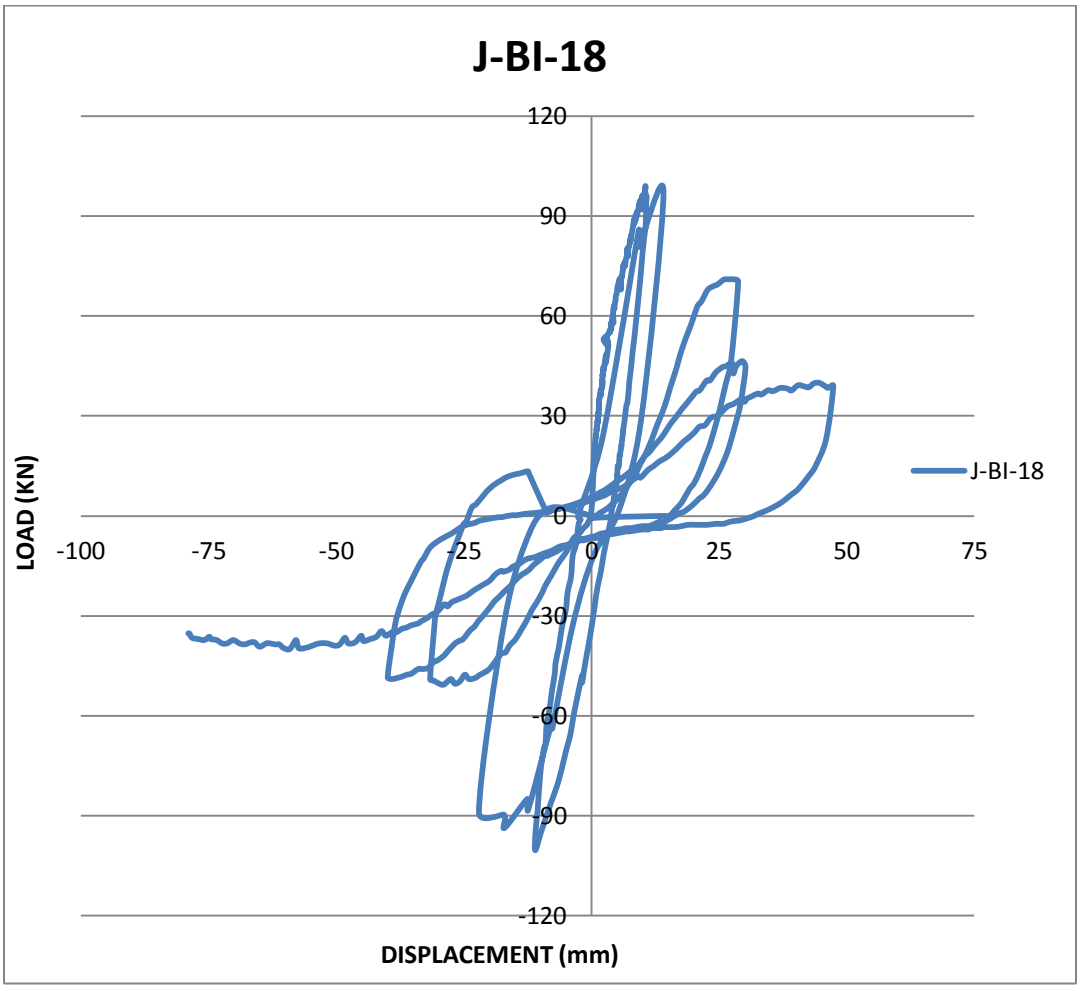

Figure 102 load Verses Displacement Graph for Specimen J-BI-18

The first flexural crack was found in the first cycle in the push down direction near the beam column interface at 45KN and displacement of 3.3mm and the when the load and displacement reached to 60KN and 5.59mm the diagonal crack in the joint appeared as shown in “Figure 103” and diagonal cracks in the joint moves towards the center with the increasing load and displacements, the maximum load reached in the push direction was 96.98KN.

Figure 103 First Flexural Crack for Specimen J-BI-18

When the specimen was displaced in pulling direction cracks were formed in the bottom of the beam at 58KN load, diagonal joint cracks were also formed in the opposite direction to the previous joint cracks as shown in “Figure 104”.

Figure 104 First Diagonal Crack in Joint for Specimen J-BI-18

The cracks were also formed on the back side of the column and all the cracks were widen up during the pull push loading process because of these wide cracks the stiffness of the specimen reduces as shown in load and displacement relationship plot. During the last two cyclic concrete on the beam column interface was crushed and joint surfaces starts to spall off on the both sides of the joint and the reinforcements were visible to the necked eye as shown in figure “Figure 105 & 106”. In the end the reinforcements were yielded, joint was completely failed and the residual displacement was observed.

Figure 105 Formation of Crack in Joint during Cyclic Load Test in Specimen J-BI-18

Figure 106 Spilling Of Concrete in Joint Region for Specimen J-BI-18

LVDTS were placed diagonally in the joint region to observe the tension crack openings in the joints and the graph was plotted for load and opening as given in "Figure 107 & 108", it can be seen from the graph when the displacement starts in the push direction the cracks starts to increase and reduces as the displacement reduce, this condition was same for the pull side displacement but the behavior was vice versa as it was in push direction tension side converts into compression and compression side converts into tension and the cracks were seen on both direction in the joint in the form of X as shown in "Figure 109" and this X crack was also observed in the core of concrete joint.

Figure 107 Position of LVDT J1 in Joint to Observe Diagonal Crack

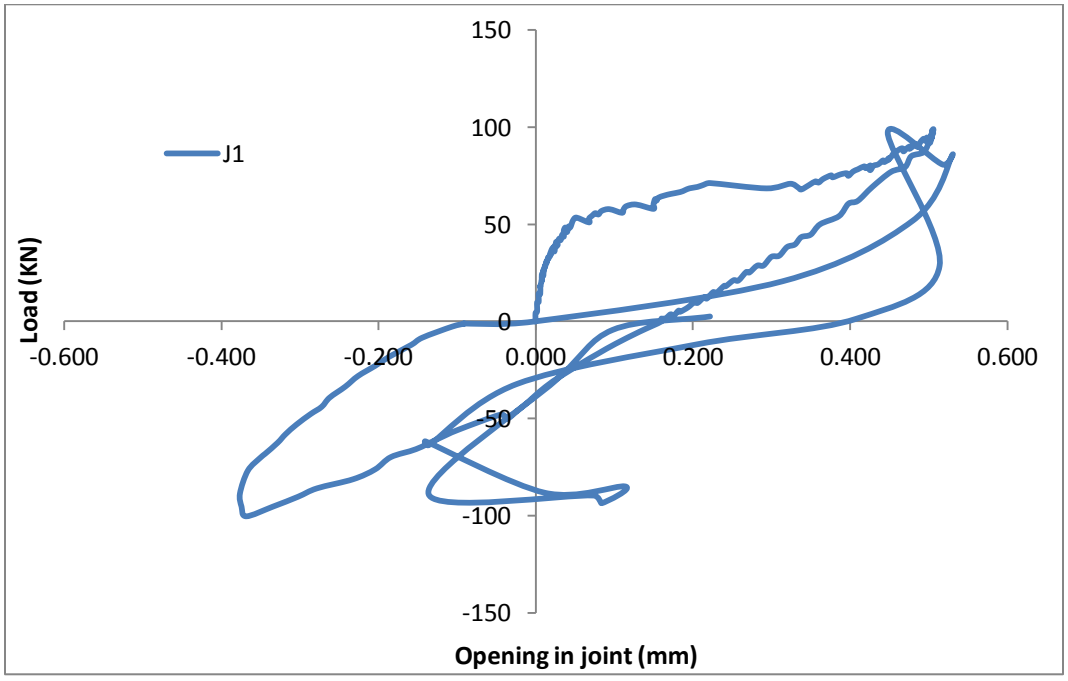

Figure 108 Load Verses Crack Opening Graph for LVDT J1

Figure 109 Diagonal X Crack Failure in Joint Core

Strain gauges were installed in the reinforcement to observe the strain in the steel during the test, strain gauge SG8 and SG11 were located at the top and bottom reinforcement of beam near the beam column interface, it is clear from "Figure 110 & 111" when the displacement was applied in the push direction to the specimen, the top reinforcements of the beam face the tension while the bottom reinforcements were facing compression and the opposite conditions were observed when the specimen was displaced in pull direction.

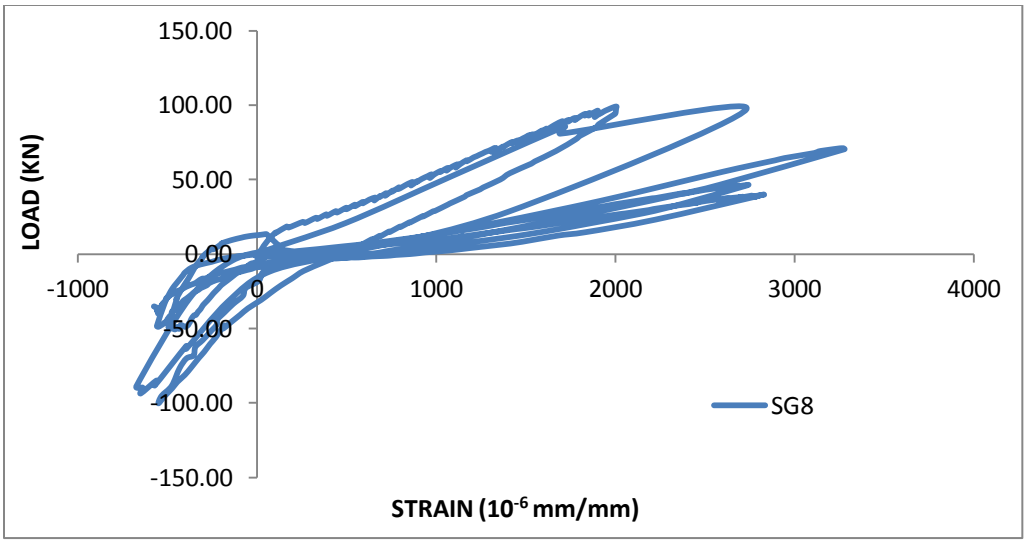

Figure 110 Load Verses Strain Graph for Top Beam Reinforcement

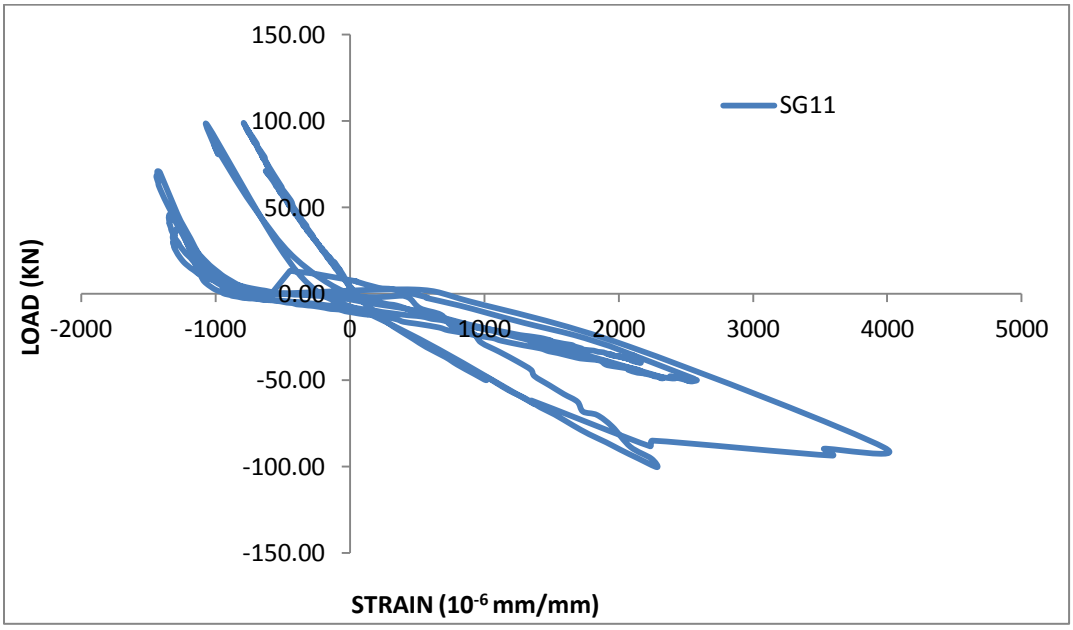

Figure 111 Load Verses Strain Graph for Bottom Beam Reinforcement

All the strain gauges were monitored and the graphs were plot between load and strains for cyclic load test of beam-column joints as shown in “Figure 112 & 113”.

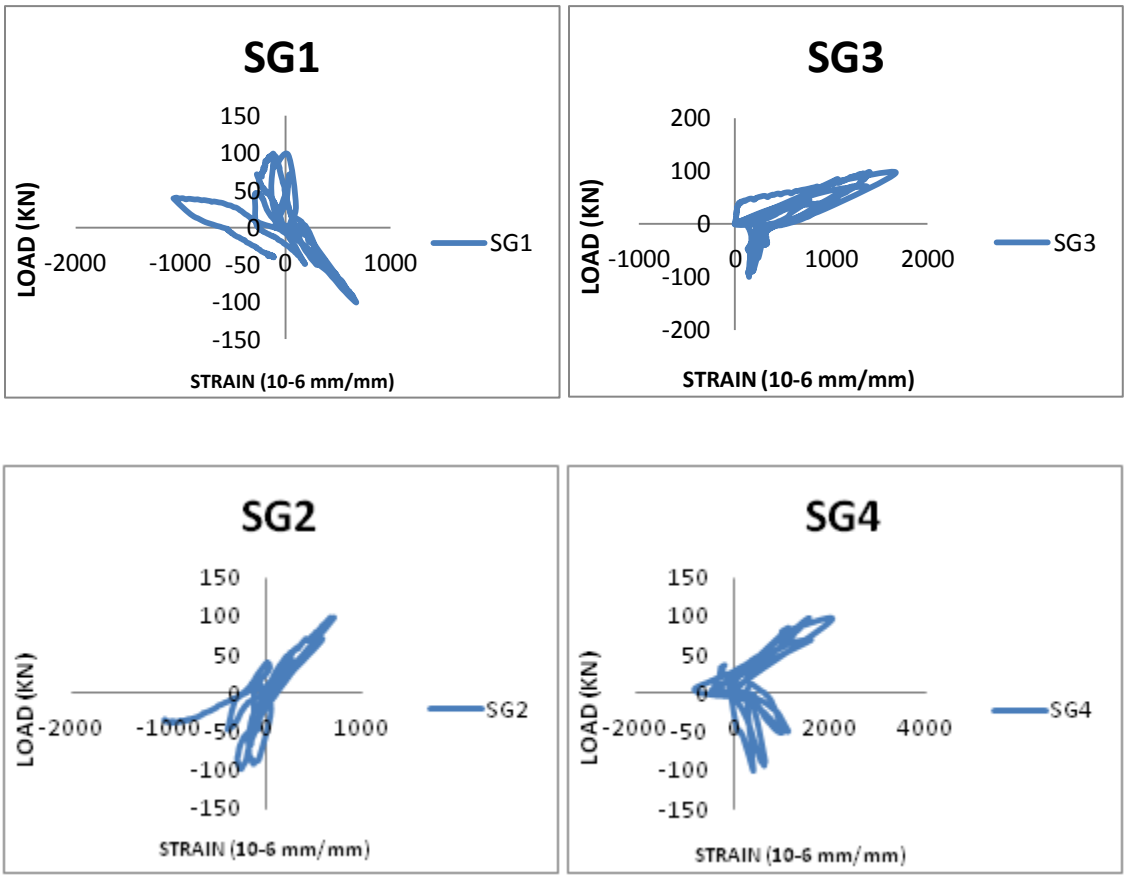

Figure 112 Load Verses Strain Graph for Reinforcement at Selected Positions

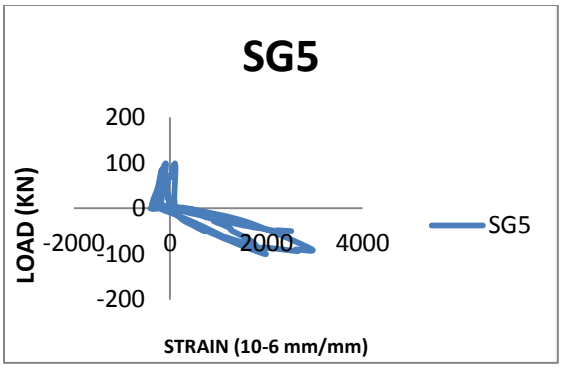

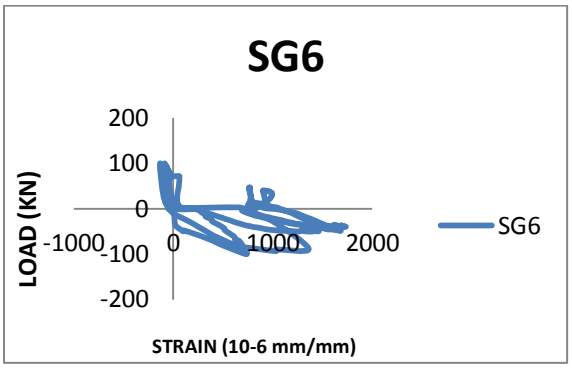

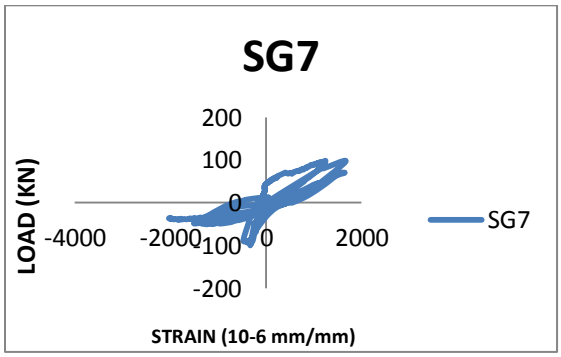

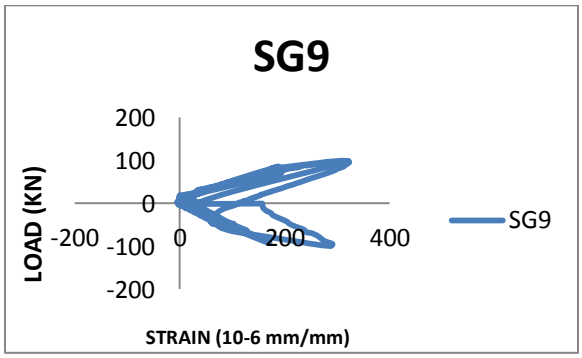

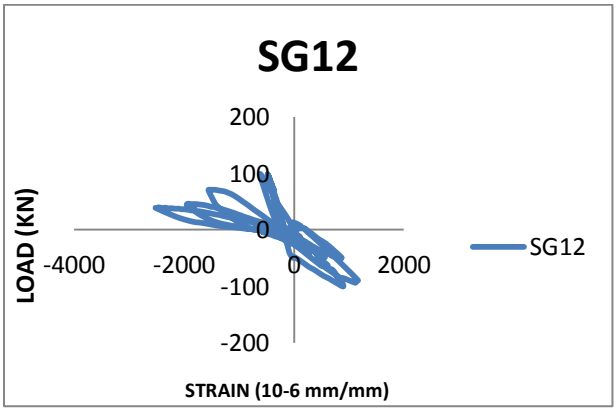

Figure 113 Load Verses Strain Graph for Reinforcement at Selected Positions

6.4 DISCUSSIONS OF RESULTS USING MECHANISTIC MODEL WITH EXPERIMENTAL RESULTS

To understand the failure of each specimen the predicted theoretical crack load in the joint and the joint shear capacity of specimen in calculated as given below.

For each specimen, loads in the joint at first crack in joint and at steel yielding load were calculated by using the strain values of top and bottom steel for the beam from experimental tests.

6.4.1 Theoretical Joint Load in Joint

When the principle tensile stress of joint becomes equal to the tensile strength of concrete the joint cracks so;

$$f_t = 0.625\sqrt{f_c'} \tag{6.1}$$

$$f_t = 0.625\sqrt{30} = 3.4MPa$$

$$f_t = -\frac{\sigma_a}{2} + \sqrt{\left(\frac{\sigma_a}{2}\right)^2 + v_{jh}^2} \tag{6.2}$$

Where:

σ_a= column axial stress $\left(\frac{N}{A_g}\right) = \frac{150000}{300\times250} = 2MPa$

From equation [6.1 & 6.2]

$$3.4 = -\frac{2}{2} + \sqrt{\left(\frac{2}{2}\right)^2 + v_{jh}^2}$$

$$1.5 \times v_{jh} = 2.28MPa$$

$$v_{jh} = 1.52MPa$$

Predicted V for crack in the joint is given by equation [6.3]

$$V_{cracking} = v_{jh} \times A_j \qquad (6.3)$$

$$V_{cracking} = 115.648KN$$

6.4.2 Joint Shear Capacity from ACI

The empirical equation [6.4] is given by ACI to calculate the maximum joint shear strength capacity for properly detailed exterior reinforced concrete beam column joints with the γ=15

$$\emptyset V_{nj} = 0.75\gamma\sqrt{f_c'}A_j \tag{6.4}$$

$$\emptyset V_{nj} = 383.86KN$$

6.4.3 Mechanistic Model with Experimental Results J-BU-12

At P=39KN, (before the cracking in the joint)

$\varepsilon_s = 0.001751 < \varepsilon_y$

$\varepsilon_s' = 0.000595 < \varepsilon_y$

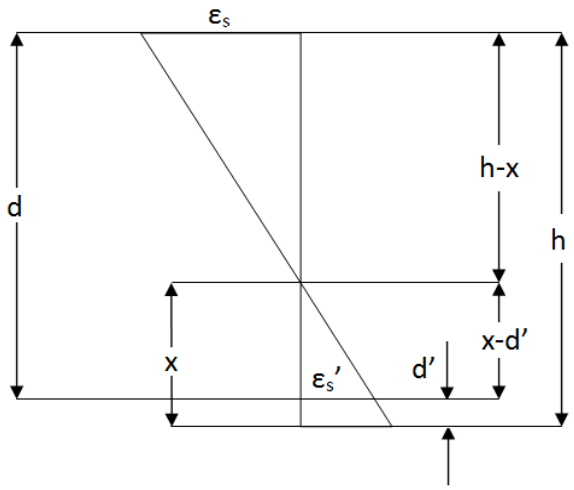

Figure 114 Details of Beam Section

$T = \varepsilon_s \times E_s \times A_s$

$T = 0.001751 \times 200 \times 335.48 = 117.48KN$

$C_s = \varepsilon_s' \times E_s \times A_s'$

$C_s = 0.000595 \times 200 \times 335.48 = 39.92KN$

$C_c = T - C_s$

$C_c = 117.48 - 39.92 = 77.56KN$

$C_c = \frac{1}{2} \times f_c' \times x \times b$, from "Figure 114 "(x=88.64mm)

$$f_c = \frac{2 \times 77.56}{250 \times 88.64} = 7MPa$$

$$V_j = T - V_c$$

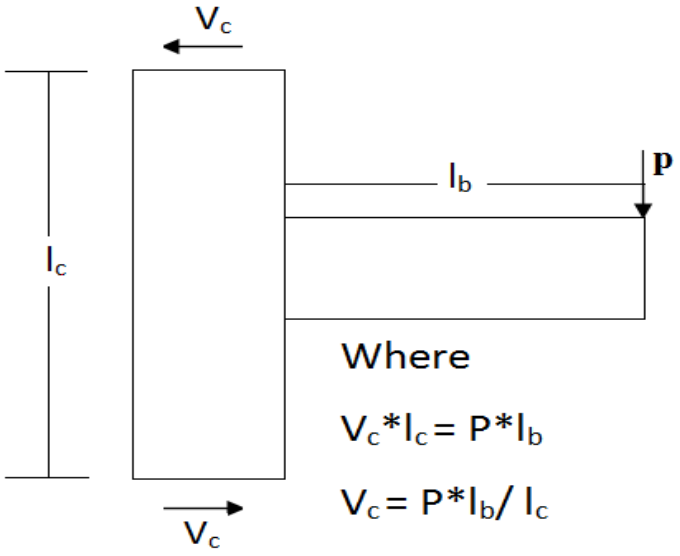

Figure 115 Shear in Column

$$V_j = 117.48 - \frac{39 \times 900}{1400} = 92.40KN$$

$$V_j = 92.40 < V_{cracking}(115.64KN)$$

At P=53KN, (at cracking of joint)

$\varepsilon_s = 0.002350 < \varepsilon_y$

$\varepsilon_s' = 0.000708 < \varepsilon_y$

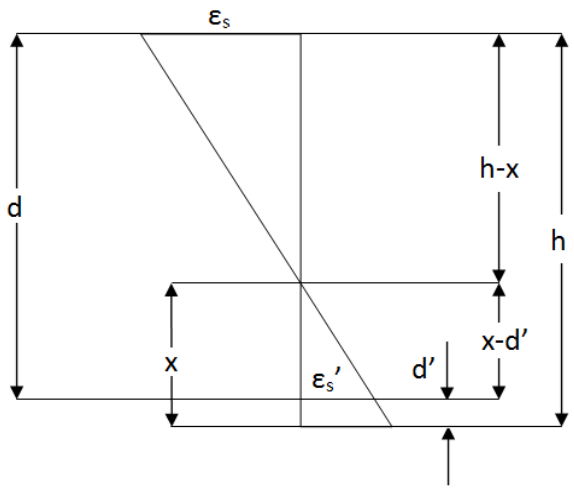

Figure 116 Details of Beam Section

$T = \varepsilon_s \times E_s \times A_s$

$T = 0.002350 \times 200 \times 335.48 = 157.45KN$

$C_s = \varepsilon_s' \times E_s \times A_s'$

$C_s = 0.000708 \times 200 \times 335.48 = 47.59KN$

$C_c = T - C_s$

$C_c = 157.45 - 47.59 = 123.20KN$

$C_c = \frac{1}{2} \times f_c' \times x \times b$, from "Figure 116"(x=83.05mm)

$$f_c = \frac{2 \times 123.20}{250 \times 83.05} = 10.34MPa$$

$$V_j = T - V_c$$

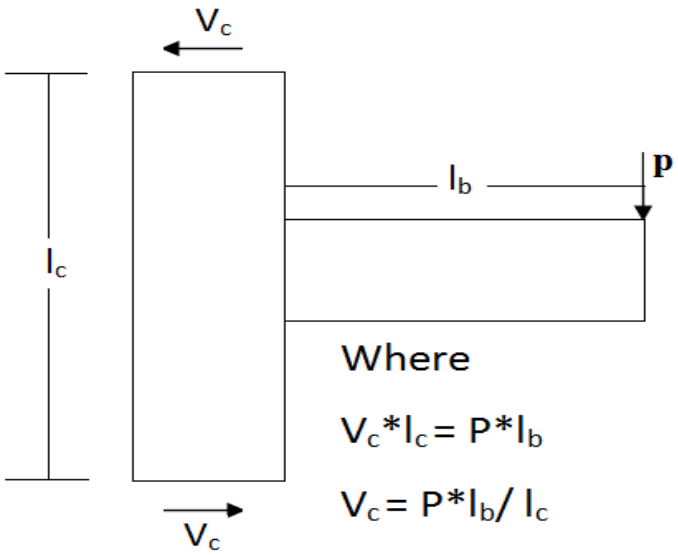

Figure 117 Shear in Column

$$V_j = 157.45 - \frac{53 \times 900}{1400} = 123.65KN$$

$$V_j = 123.65KN > V_{cracking}(115.64KN)$$

At P=62.88KN, (at steel yielding)

$\varepsilon_s = 0.003400 < \varepsilon_y$

$\varepsilon_s' = 0.000605 < \varepsilon_y$

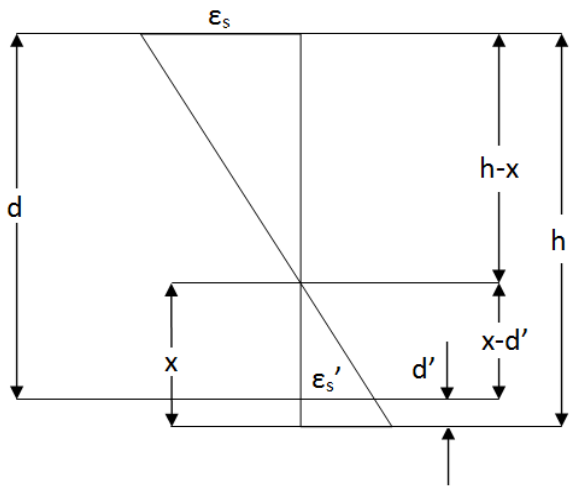

Figure 118 Details of Beam Section

$T = \varepsilon_s \times E_s \times A_s$

$T = 0.003400 \times 200 \times 335.48 = 288.18KN$

$C_s = \varepsilon_s' \times E_s \times A_s'$

$C_s = 0.000605 \times 200 \times 335.48 = 40.58KN$

$C_c = T - C_s$

$C_c = 288.18 - 4.58 = 187.70KN$

$$V_j = T - V_c$$

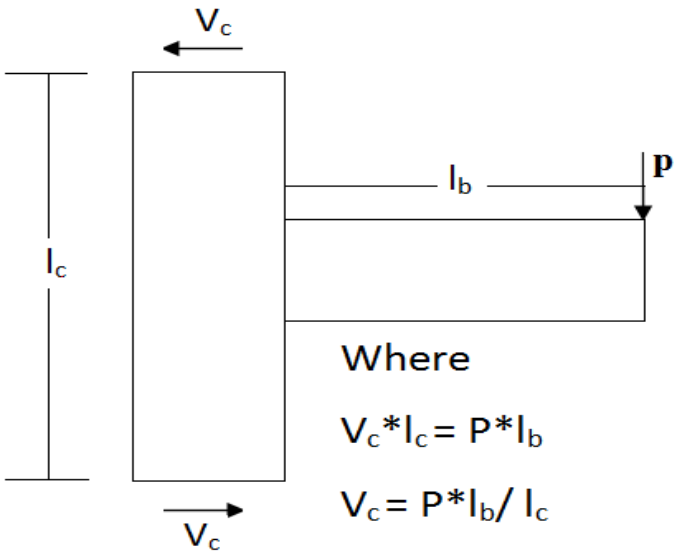

Figure 119 Shear in Column

$$V_j = 288.18 - \frac{62.88 \times 900}{1400} = 187.78KN$$

$$V_j = 187.78KN > V_{cracking}(115.64KN)$$

But less than the joint shear capacity (383.86KN)

6.4.3 Mechanistic Model with Experimental Results J-BI-12

At P=40KN, (at cracking of joint)

$\varepsilon_s = 0.002168 < \varepsilon_y$

$\varepsilon_s' = 0.000420 < \varepsilon_y$

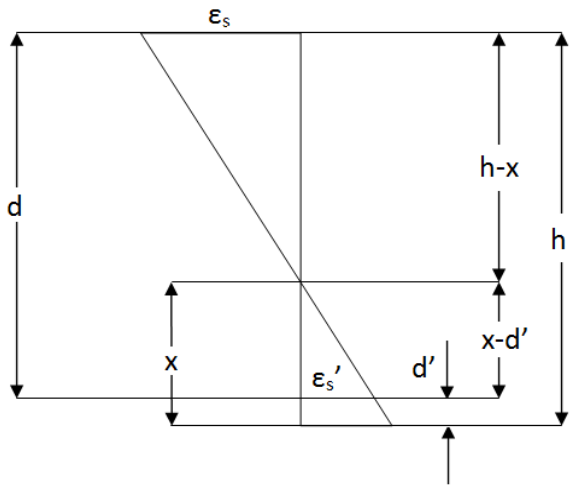

Figure 120 Details of Beam Section

$T = \varepsilon_s \times E_s \times A_s$

$T = 0.002168 \times 200 \times 335.48 = 145.40KN$

$C_s = \varepsilon_s' \times E_s \times A_s'$

$C_s = 0.000420 \times 200 \times 335.48 = 28.15KN$

$C_c = T - C_s$

$C_c = 145.40 - 28.15 = 117.20KN$

$C_c = \frac{1}{2} \times f_c' \times x \times b$, from "Figure 120" x=65.78mm)

$$f_c = \frac{2 \times 123.20}{250 \times 65.78} = 14.206MPa$$

$$V_j = T - V_c$$

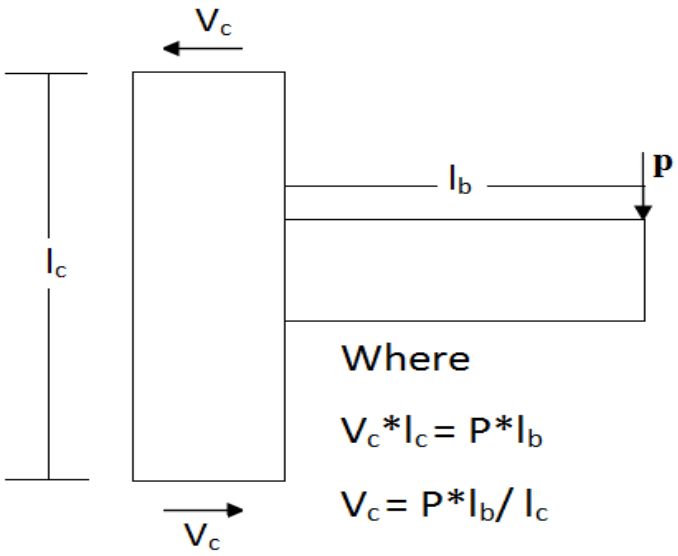

Figure 121 Shear in Column

$$V_j = 145.40 - \frac{40 \times 900}{1400} = 119.47KN$$

$$V_j = 119.47KN > V_{cracking}(115.64KN)$$

At P=56.15KN, (at steel yielding)

$\varepsilon_s = 0.002951 < \varepsilon_y$

$\varepsilon_s' = 0.000647 < \varepsilon_y$

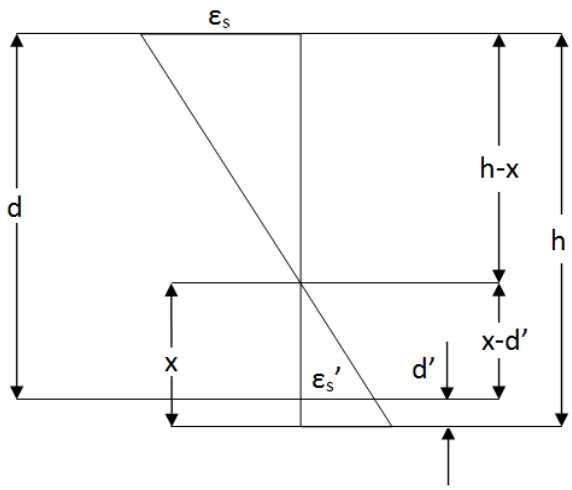

Figure 122 Details of Beam Section

$T = \varepsilon_s \times E_s \times A_s$

$T = 0.002951 \times 200 \times 335.48 = 197.93KN$

$C_s = \varepsilon_s' \times E_s \times A_s'$

$C_s = 0.000647 \times 200 \times 335.48 = 43.36KN$

$C_c = T - C_s$

$C_c = 197.93 - 43.36 = 154.52KN$

$$V_j = T - V_c$$

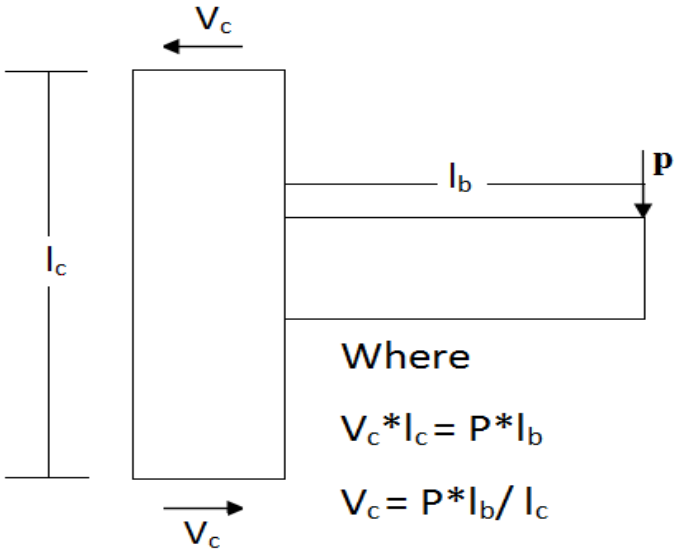

Figure 123 Shear in Column

$$V_j = 197.93 - \frac{56.15 \times 900}{1400} = 161.86KN$$

$$V_j = 161.86KN > V_{cracking}(115.64KN)$$

But less than the joint shear capacity (383.86KN)

6.4.3 Mechanistic Model with Experimental Results J-BI-18

At P=60KN, (at cracking of joint)

$\varepsilon_s = 0.001100 < \varepsilon_y$

$\varepsilon_s' = 0.000523 < \varepsilon_y$

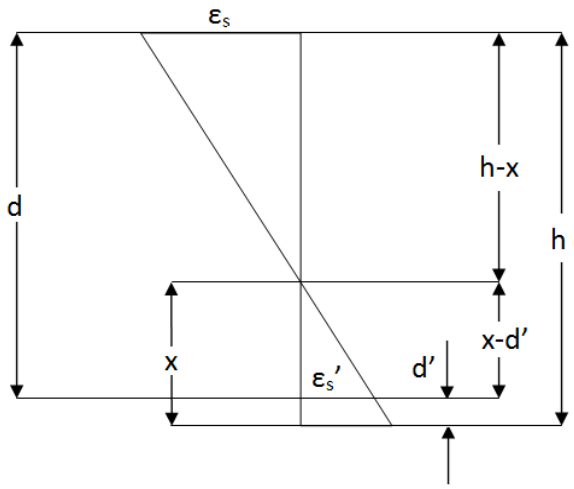

Figure 124 Details of Beam Section

$T = \varepsilon_s \times E_s \times A_s$

$T = 0.001100 \times 200 \times 761.288 = 167.43KN$

$C_s = \varepsilon_s' \times E_s \times A_s'$

$C_s = 0.000523 \times 200 \times 761.288 = 79.57KN$

$C_c = T - C_s$

$C_c = 167.43 - 79.57 = 87.80KN$

$C_c = \frac{1}{2} \times f_c' \times x \times b$, from "Figure 124"(x=105.41mm)

$$f_c = \frac{2 \times 87.80}{250 \times 105.41} = 6.65MPa$$

$$V_j = T - V_c$$

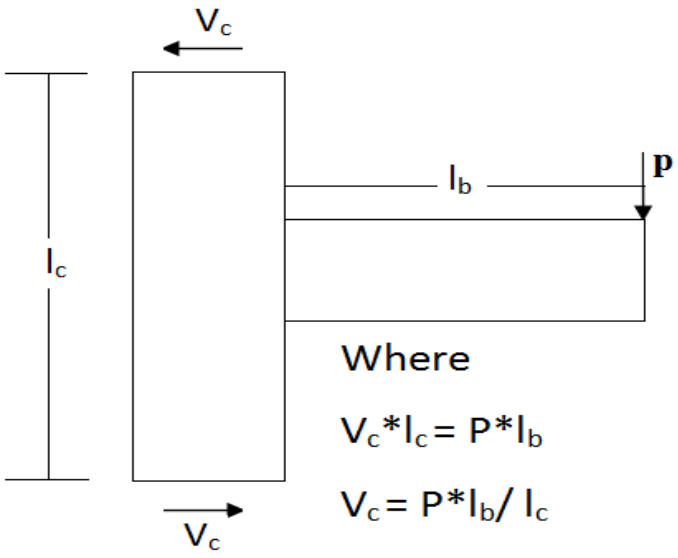

Figure 125 Shear in Column

$$V_j = 167.43 - \frac{60 \times 900}{1400} = 129.16KN$$

$$V_j = 129.16KN > V_{cracking}(115.64KN)$$

At P=99.2KN, (collapse load of specimen)

$\varepsilon_s = 0.002003 < \varepsilon_y$

$\varepsilon_s' = 0.000795 < \varepsilon_y$

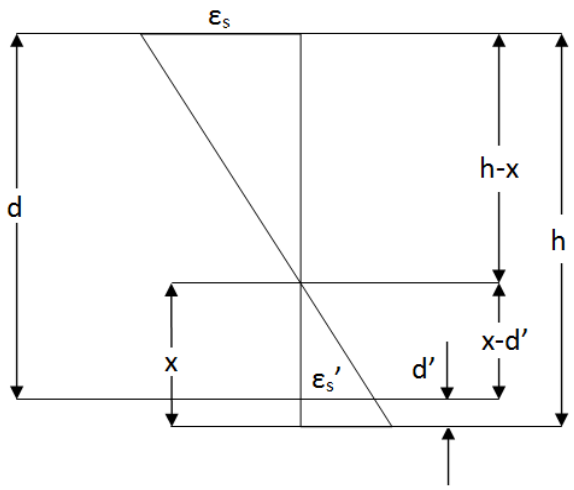

Figure 126 Details of Beam Section

$T = \varepsilon_s \times E_s \times A_s$

$T = 0.002003 \times 200 \times 761.288 = 304.24KN$

$C_s = \varepsilon_s' \times E_s \times A_s'$

$C_s = 0.000795 \times 200 \times 761.288 = 120.54KN$

$C_c = T - C_s$

$C_c = 304.24 - 120.54 = 183.70KN$

$$V_j = T - V_c$$

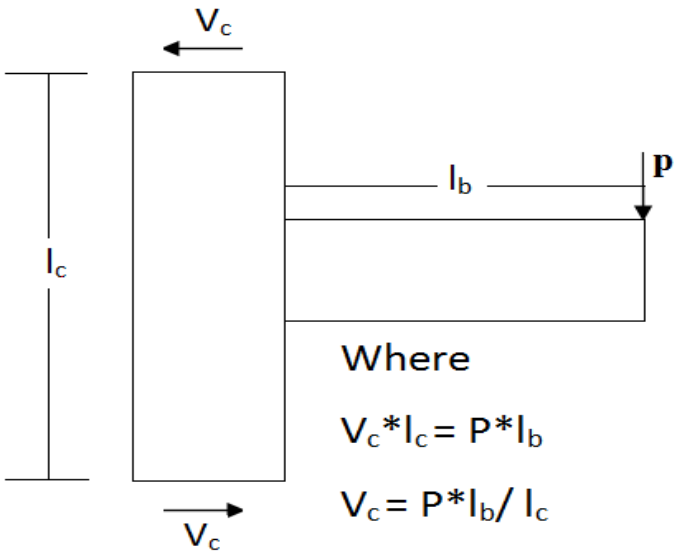

Figure 127 Shear in Column

$$V_j = 304.24 - \frac{99.2 \times 900}{1400} = 240.19KN$$

$$V_j = 240.19 > V_{cracking}(115.64KN)$$

But less than the joint shear capacity (383.86KN)

But J-BI-18 did not reach its flexural capacity this shows that the specimen collapse due to failure in the joint so we have to calculate the "γ" for poorly detailed joints

6.4.3 New "γ" for Poorly Detailed Joints

We need to back calculate the value of new "γ" from the ACI empirical equation

So,

$$\gamma = \frac{240.19}{0.75\gamma\sqrt{f_c'}A_j}$$

$\gamma = 9$ For exterior beam column joints

Shear capacity of joint, $\emptyset V_{nj} = 0.75\gamma\sqrt{f_c'}A_j = 237.62KN$

6.5 COMPARISON OF HYSTERESIS ENVELOPE OF ALL SPECIMENS

Envelop of the hysteresis for all the specimens were plotted in "Figure 128" which shows the difference of behavior for each specimen, specimen J-BI-18 has more flexural capacity than J-BU-12 and J-BI-12 where as J-BI-12 has approximate same flexural capacity as J-BU-12 but it shows the stiffer behavior both in push and pull directions.

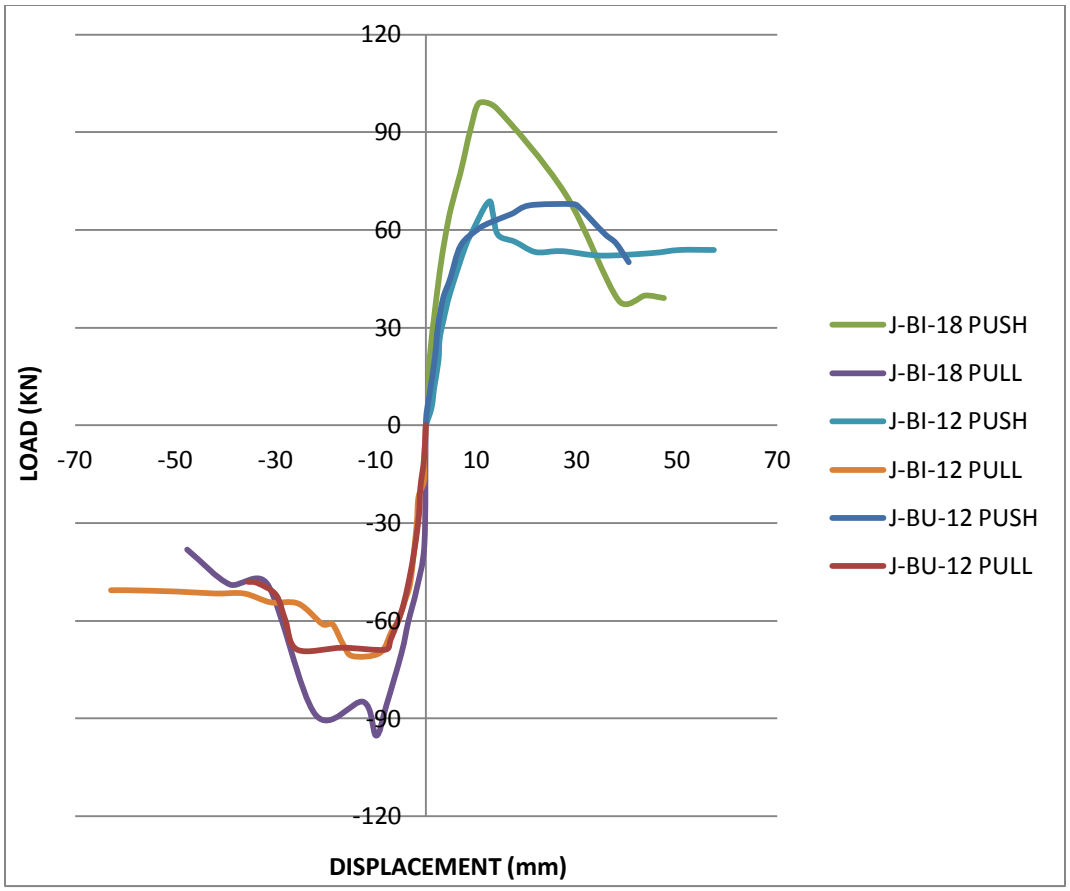

Figure 128 Comparison of Hysteresis Envelope of All Specimens

CHAPTER 7

FINITE ELEMENT ANALYSIS OF KFUPM SPECIMENS

7.1 INPUT PARAMETERS

The finite element analysis was performed using DIANA Software package. Based on the literature, Drucker Prager model with associated Plasticity was selected to model the concrete material. To satisfy the associative plasticity requirements, the values of Φ and ψ were taken to be the same and equal to 10^o but by using the 10 degree associated theory the DIANA model was giving premature failure for all specimens J-BU-12, J-BI-12 and J-BI-18, so to get the correct results Drucker Prager model with non-associative theory with the value of $\Phi=35^o$ and $\psi=2^o$ were used for specimen J-BU-12 and J-BI-12 and special condition was considered for specimen J-BI-18 by using $\Phi=30^o$ and $\psi=10^o$ in beam column and $\Phi=10^o$ and $\psi=4^o$ were used in joint because specimen J-BI-18 was failed because of joint shear failure and it did not reach its flexural capacity. In a nonlinear reinforced concrete analysis, the shear retention factor must be assumed. For closed cracks conditions the coefficient is assumed to be 1.0. A nonlinear tension softening was selected to describe the relation between the tensile stress and tensile strain at the cracked elements.

7.2 BOUNDARY CONDITIONS AND LOADING DETAILS

Boundary conditions were kept same as it was in the actual test of beam-column joints, “Figure 129” shows that bottom end of the column surface is constrained in X and Y direction, Top end of the column is constrained in X axis and free in Y direction due to downward axial force (150KN), near the tip of beam point is constrained in y direction because loading method is displacement control.

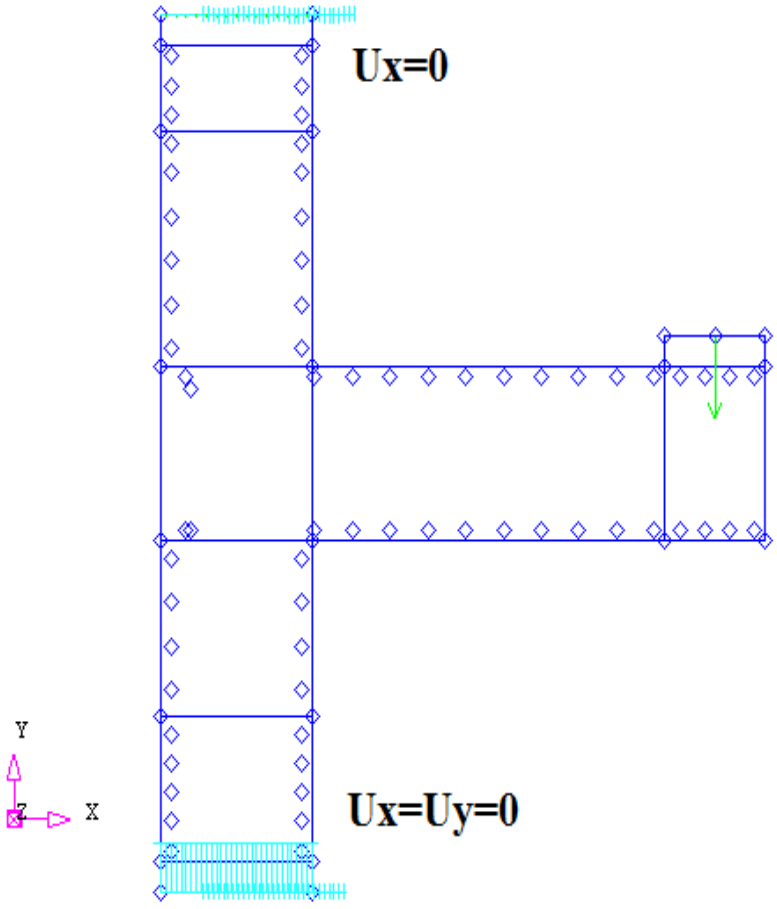

Figure 129 Boundary Conditions and Loading Details of Specimens

7.3 SPECIMEN WITH MESH

All the specimens were modeled with eight-noded quadrilateral isoparametric plane stress element CQ16M as shown in “Figure 130”

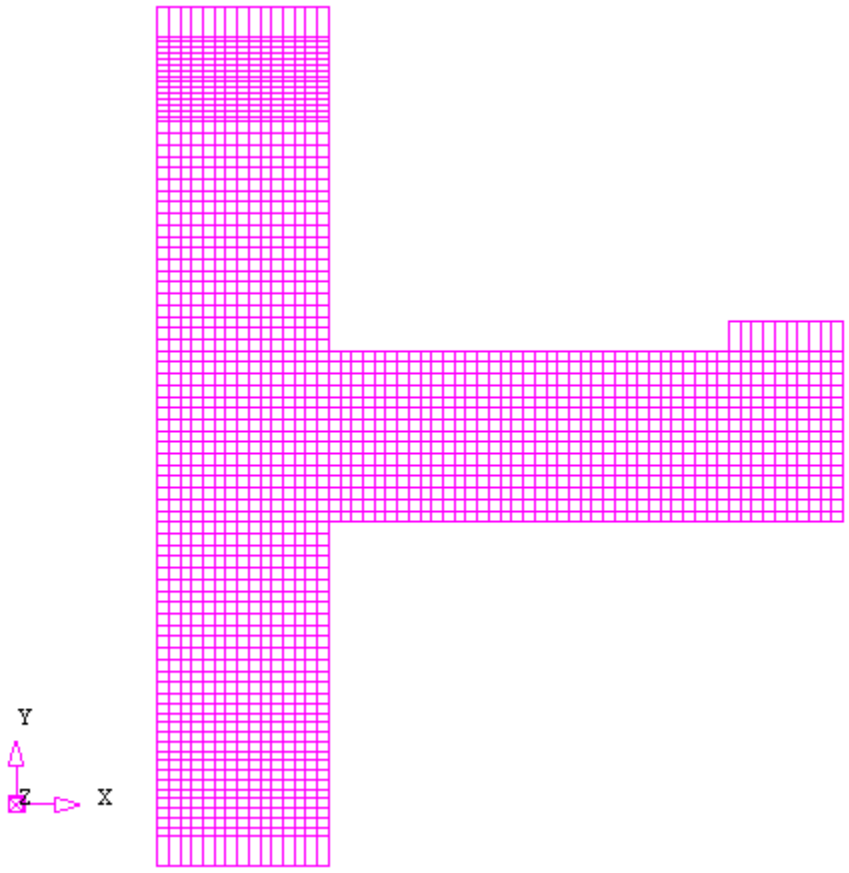

Figure 130 Specimen with Mesh

7.4 FINITE ELEMENT ANALYSIS FOR J-BU-12

Model was made in DIANA and the load displacement graphs were plotted to compare the results of experiment and finite element results as shown in “Figure 131, 132 & 133”

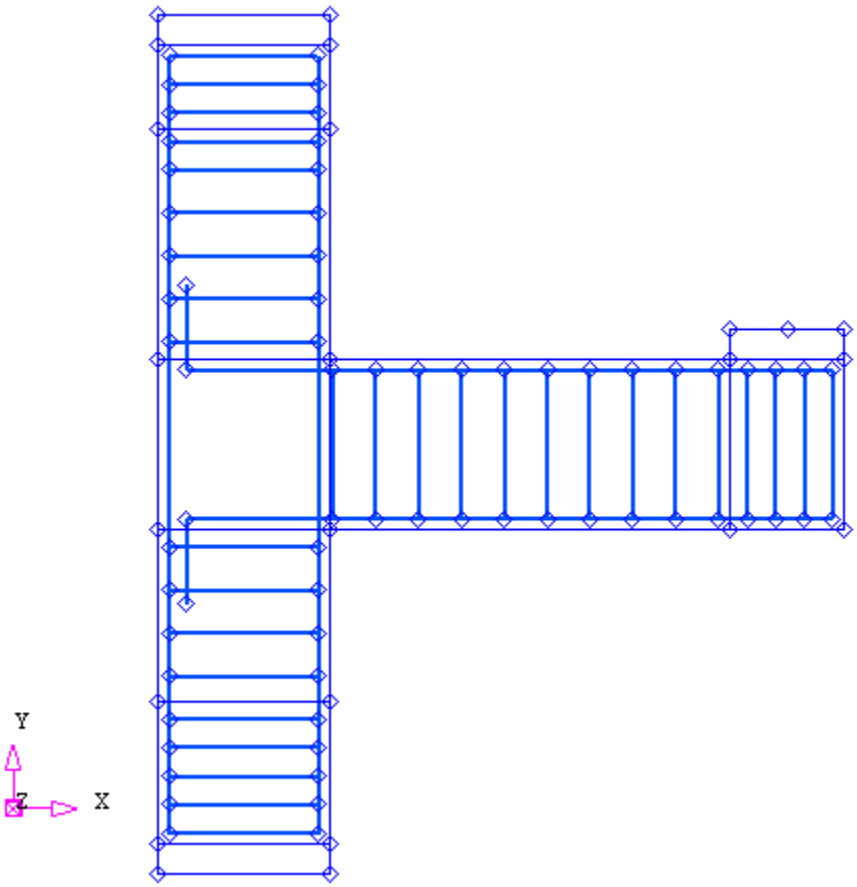

Figure 131 DIANA Model of Specimen J-Bu-12

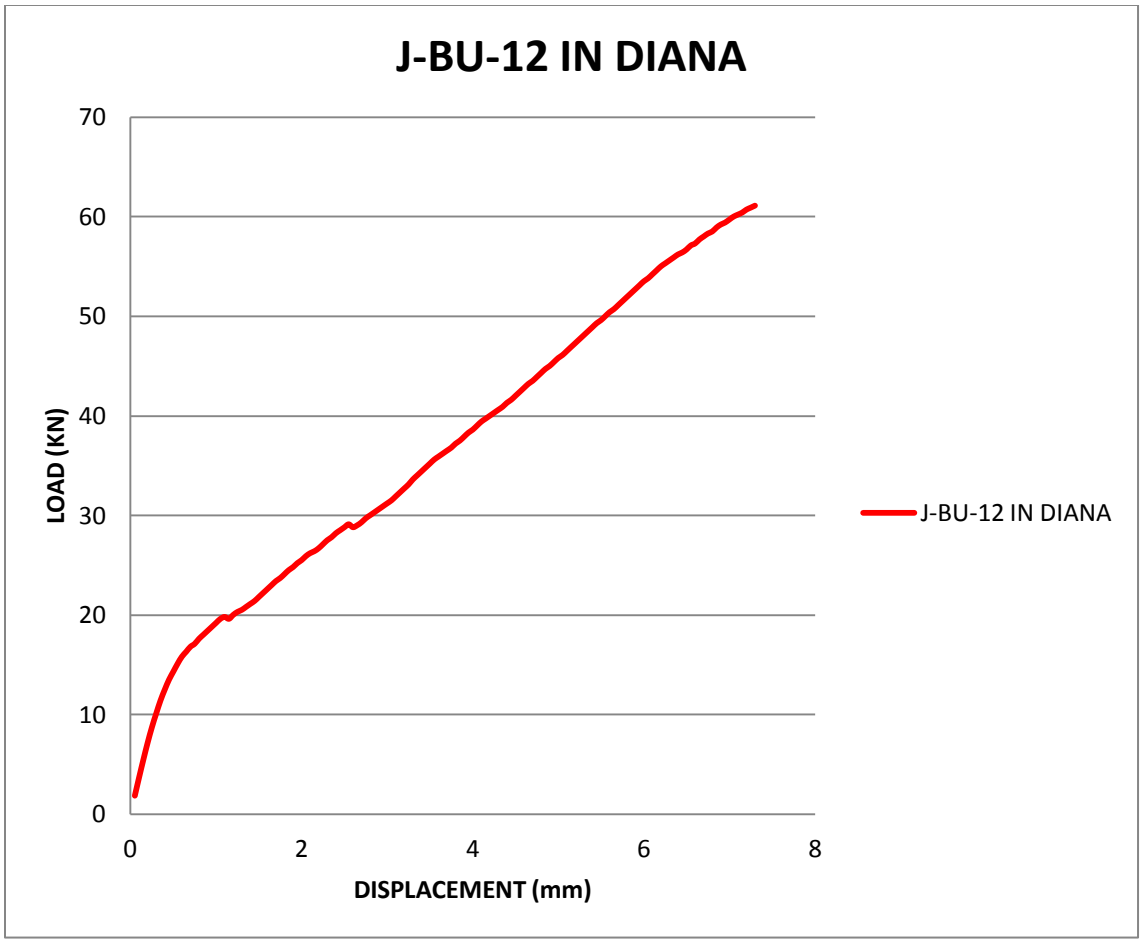

Figure 132 Load Vs Displacement Graph for Specimen J-Bu-12 in DIANA

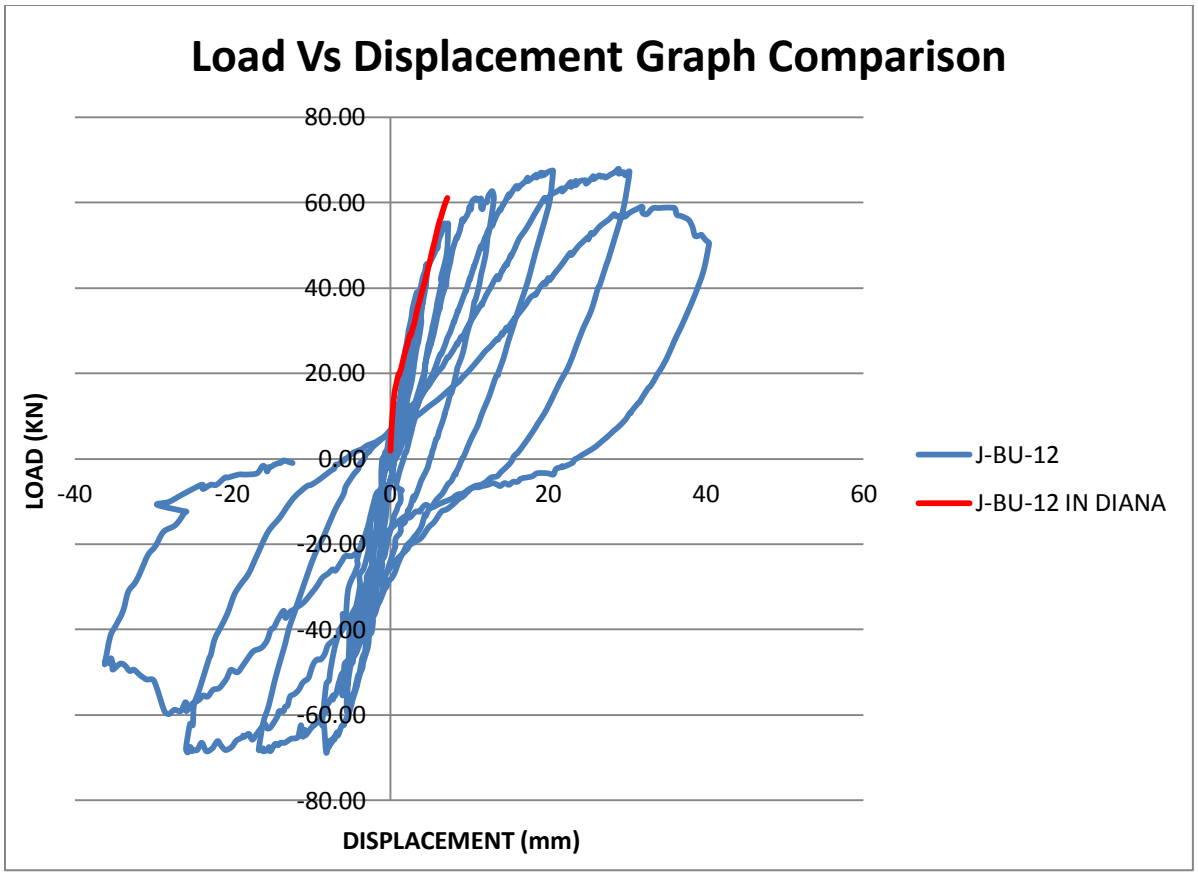

Figure 133 Load Vs Displacement Graph Comparison

The experimental results of cyclic load test on the beam-column joint carried at KFUPM are shown “Figure 133”. For numerical simulation the envelope of the load displacement curve is considered. The result of finite element simulation matches closely with experimental results as shown in Figure “Figure 133”. Diana is not able to capture the softening as reported by Bindhu et al [14] & Mitra et al [15].

The stresses in steel in x and y directions at steel yielding load that is 46.5KN and at ultimate load that is 61.1KN is shown in “Figure 134”. The stresses in top steel of the beam at steel yielding load and at ultimate load are 612MPa and 788MPa. The stresses in steel in column on tension side at steel yielding load and at ultimate load are 324MPa and 430MPa.

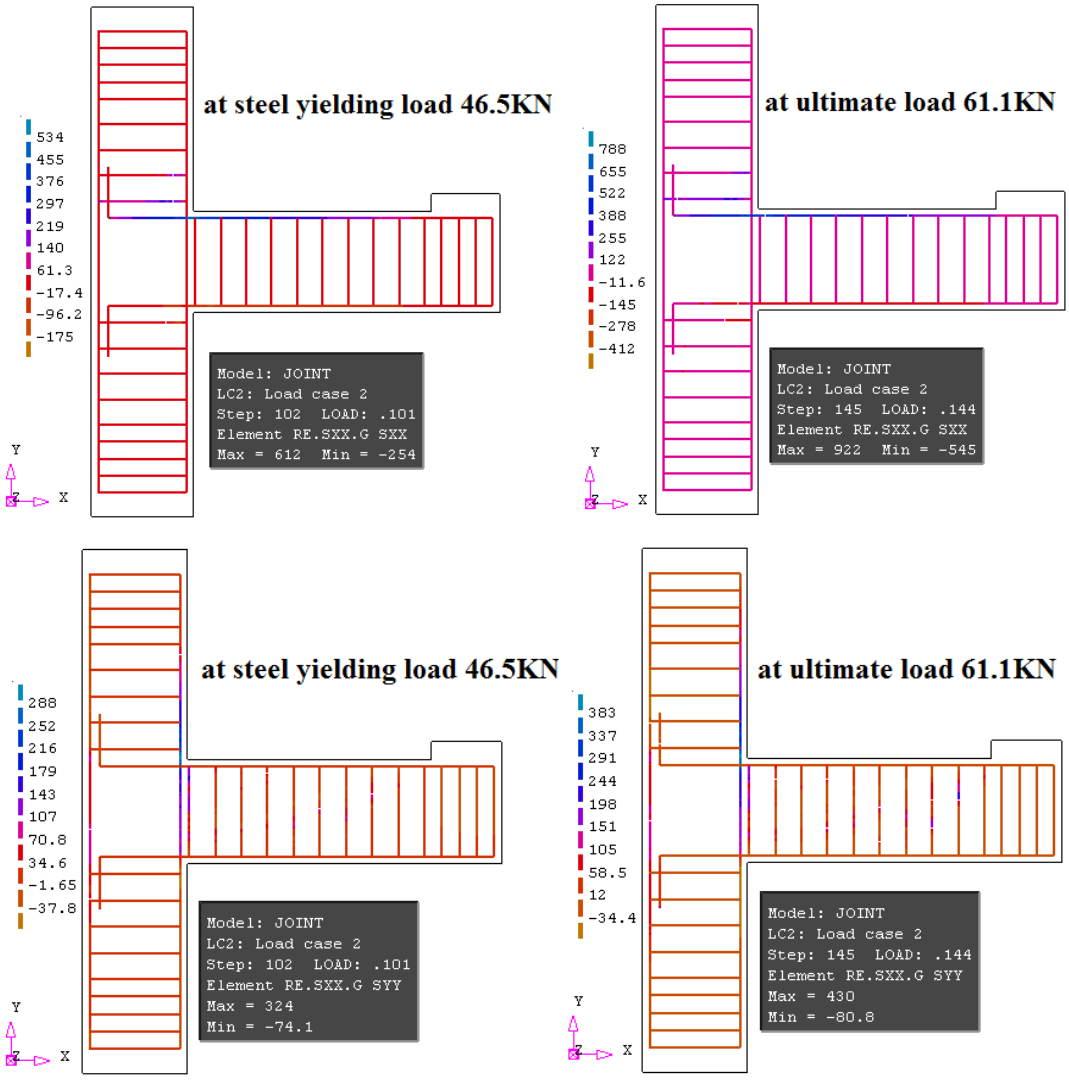

Figure 134 Stress in Steel Sxx & Syy for J-BU-12 in Diana

The stresses σx, σy and σxy in concrete at steel yielding load (46.5KN) and at ultimate load (61.1KN) are shown in "Figure 135 & 136". The stresses in concrete shows the similar behavior of stresses formed in concrete as it was observed in experimental test and the joint region of beam-column joint is found to be more critical as it was in actual test. The diagonal crack pattern at the joint closely resembles the crack pattern observed in experimental program as shown in "Figure 137".

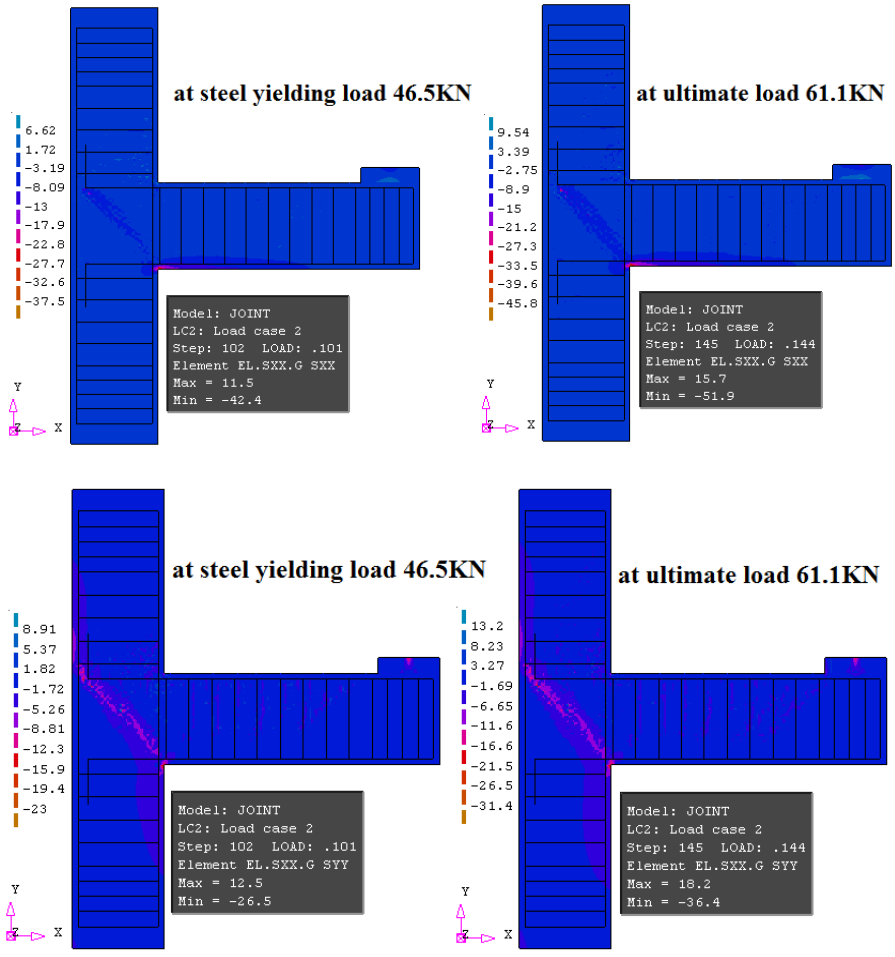

Figure 135 Tress in Concrete Sxx & Syy for J-BU-12 in Diana

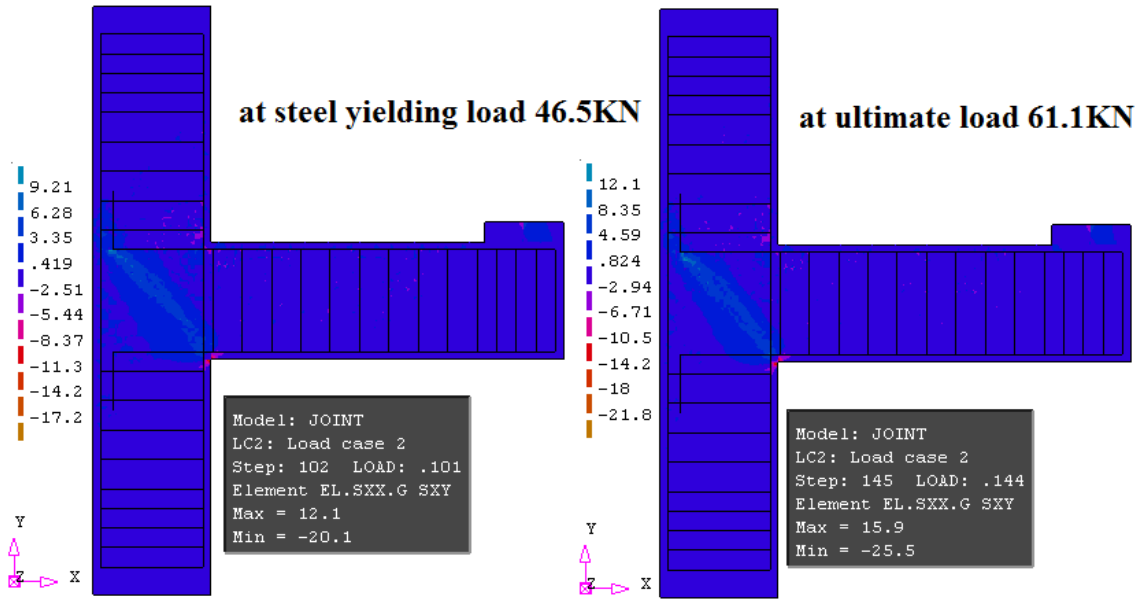

Figure 136 Stress in Concrete Sxy For J-BU-12 in Diana

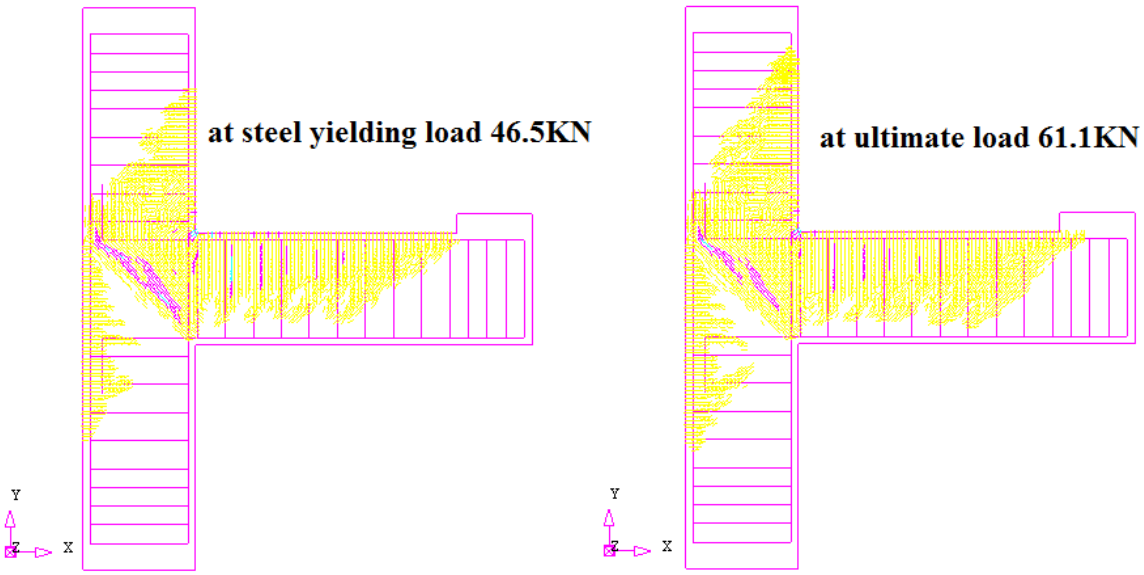

Figure 137 Crack Patterns for J-BI-12 in Diana

7.5 FINITE ELEMENT ANALYSIS FOR J-BI-12

Model was made in DIANA and the load displacement graphs were plotted to compare the results of experiment and finite element results as shown in “Figure 138, 139 & 140”

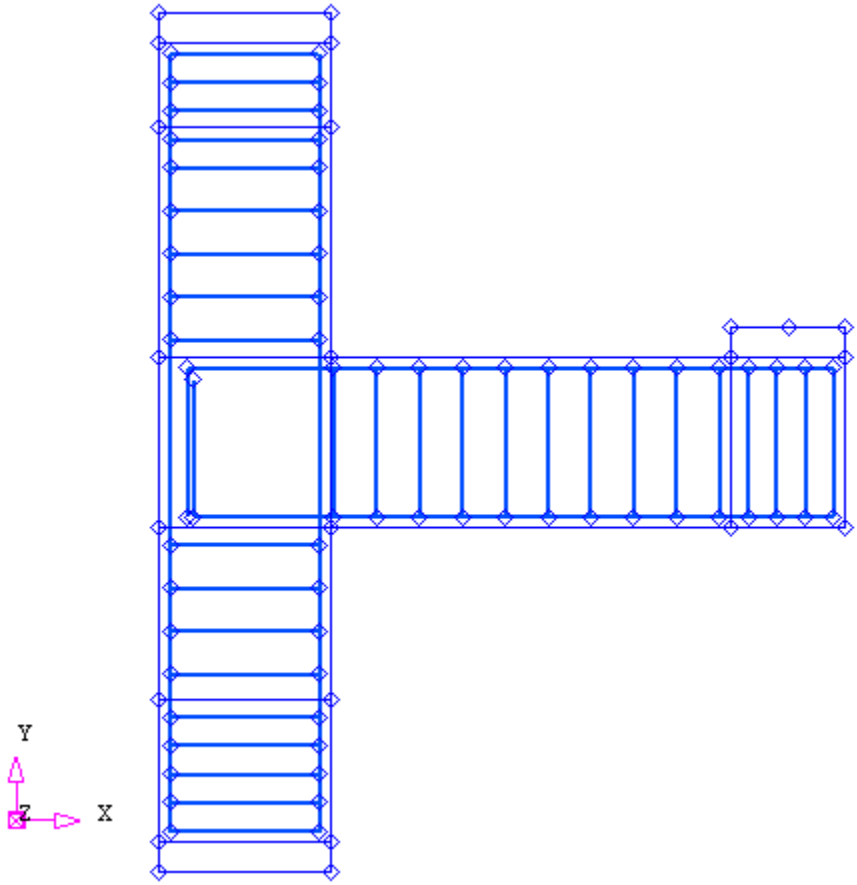

Figure 138 Diana Model of Specimen J-Bi-12

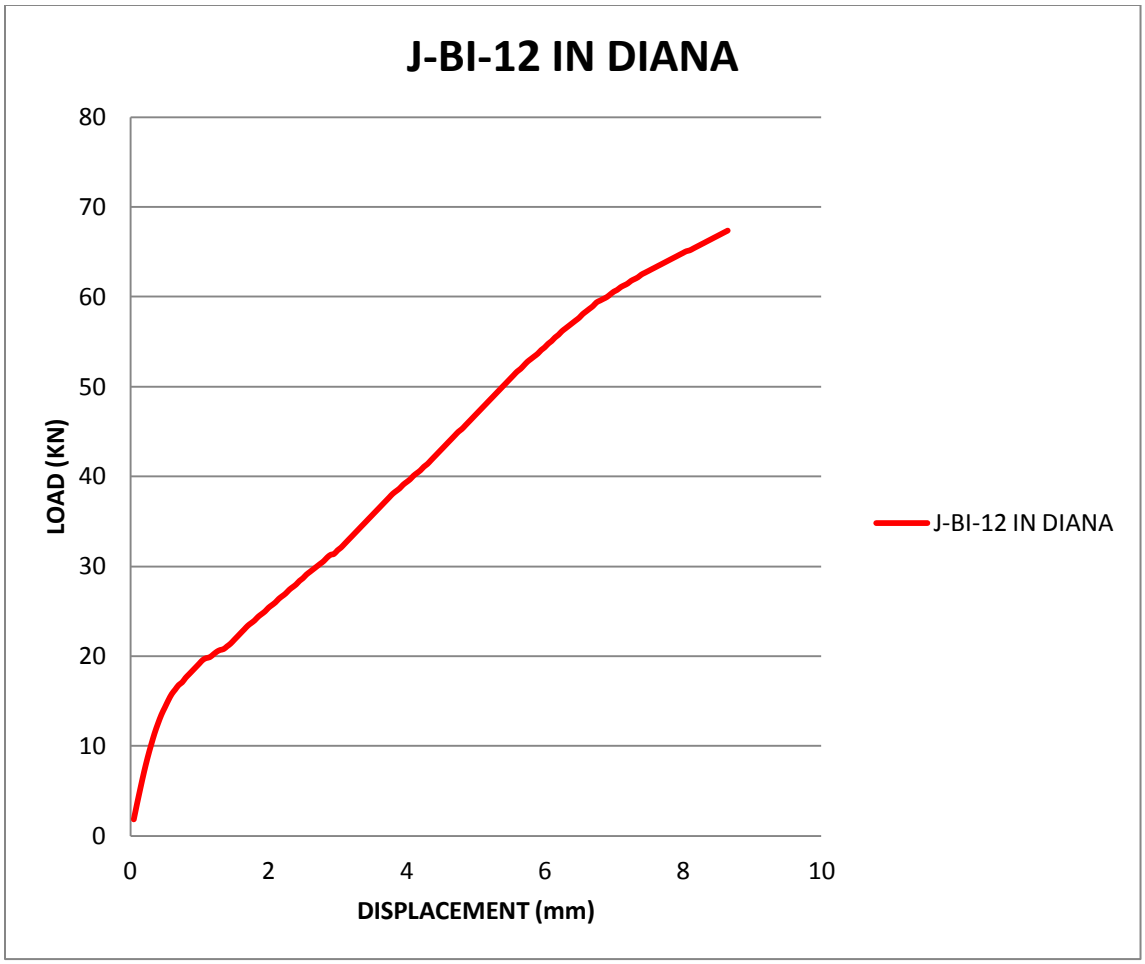

Figure 139 Load Vs Displacement Graph for Specimen J-Bi-12 in Diana

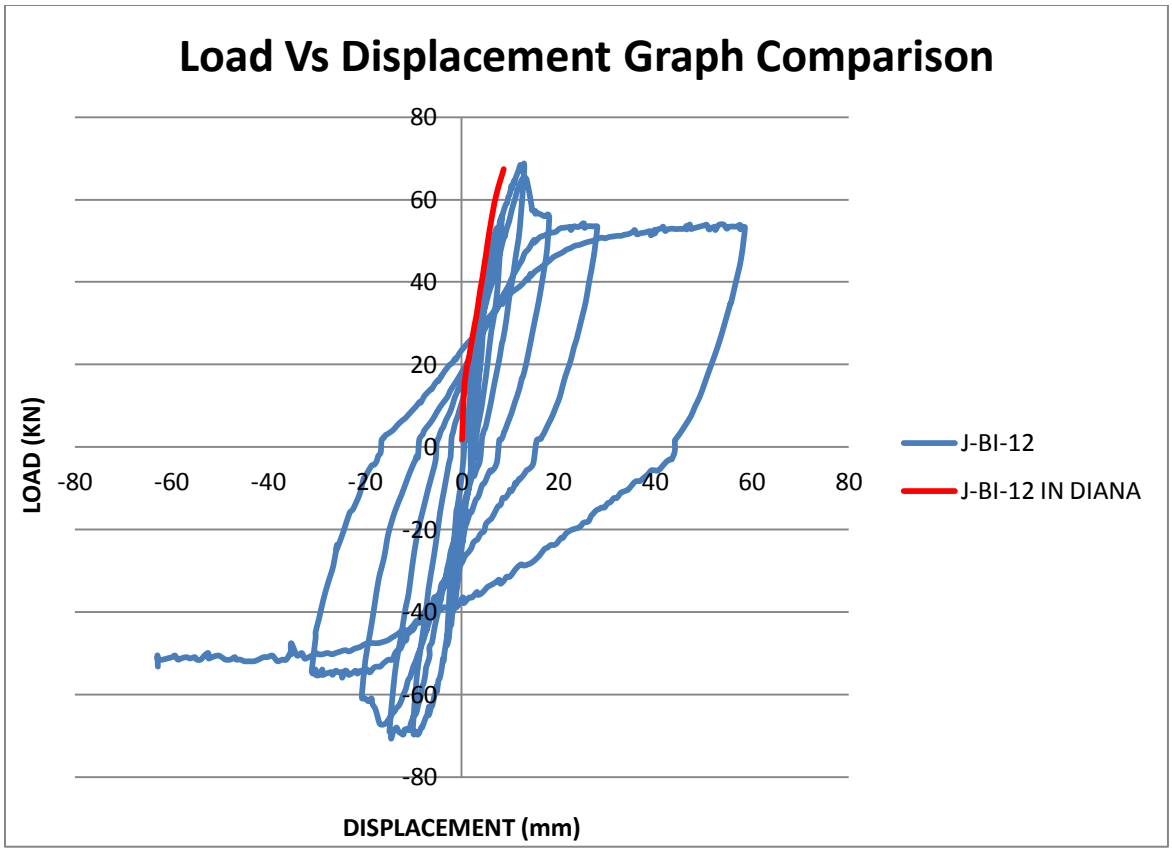

Figure 140 Load Vs Displacement Graph Comparison

The experimental results of cyclic load test on the beam-column joint carried at KFUPM are shown “Figure 140”. For numerical simulation the envelope of the load displacement curve is considered. The result of finite element simulation matches closely with experimental results as shown in “Figure 140”. Diana is not able to capture the softening as reported by Bindhu et al [14] & Mitra et al [15]

The stresses in steel in x and y directions at steel yielding load that is 57.7KN and at ultimate load that is 67.4KN is shown in “Figure 141”. The stresses in top steel of the beam at steel yielding load and at ultimate load are 605MPa and 635MPa. The stresses in steel in column on tension side at steel yielding load and at ultimate load are 385MPa and 445MPa.

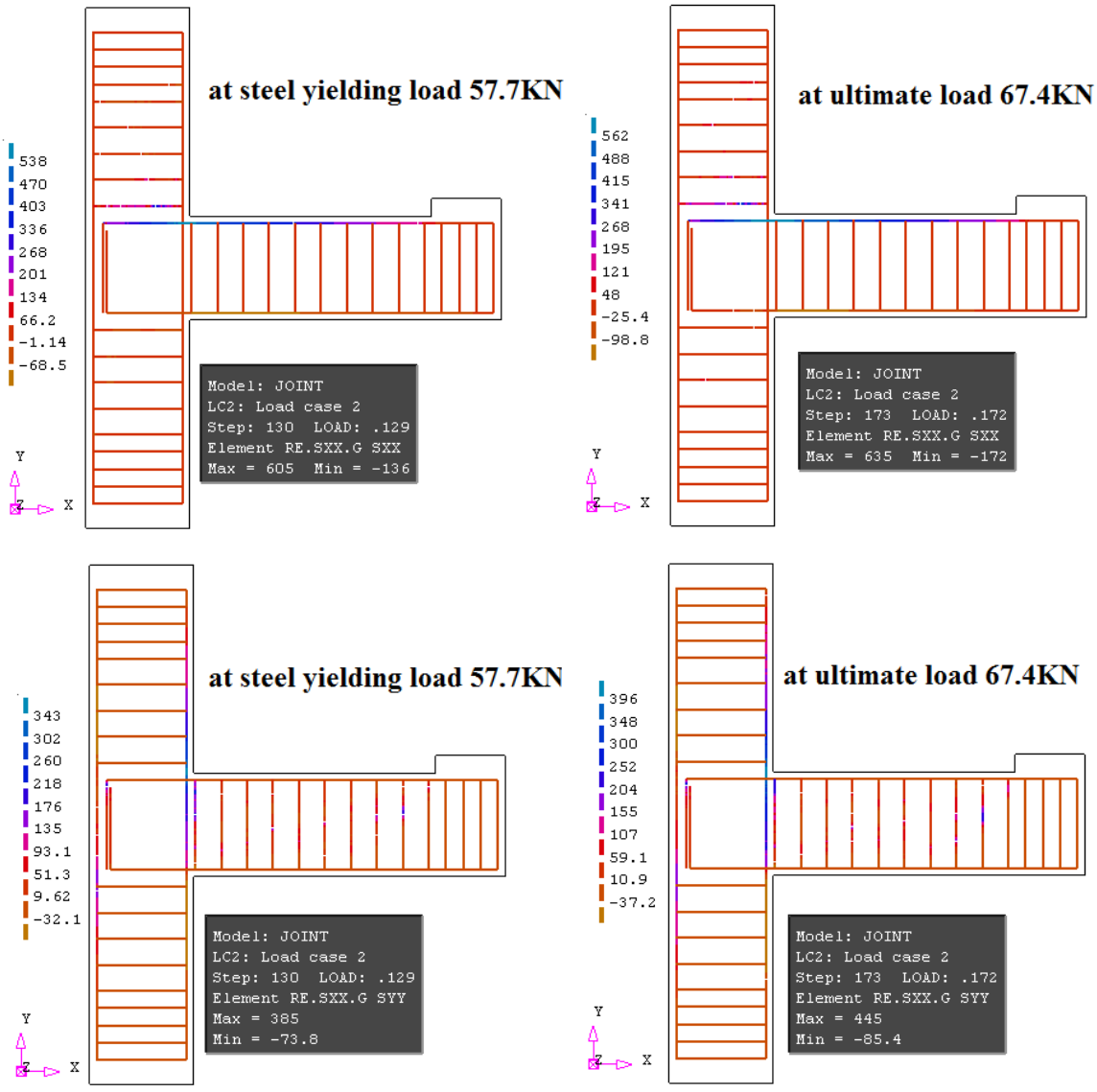

Figure 141 Stress in Steel Sxx & Syy for J-BI-12 in Diana

The stresses σx, σy and σxy in concrete at steel yielding load (57.7KN) and at ultimate load (67.4KN) are shown in "Figure 142 & 143". The stresses in concrete shows the similar behavior of stresses formed in concrete as it was observed in experimental test and the joint region of beam-column joint is found to be more critical as it was in actual test. The diagonal crack pattern at the joint closely resembles the crack pattern observed in experimental program as shown in "Figure 144".

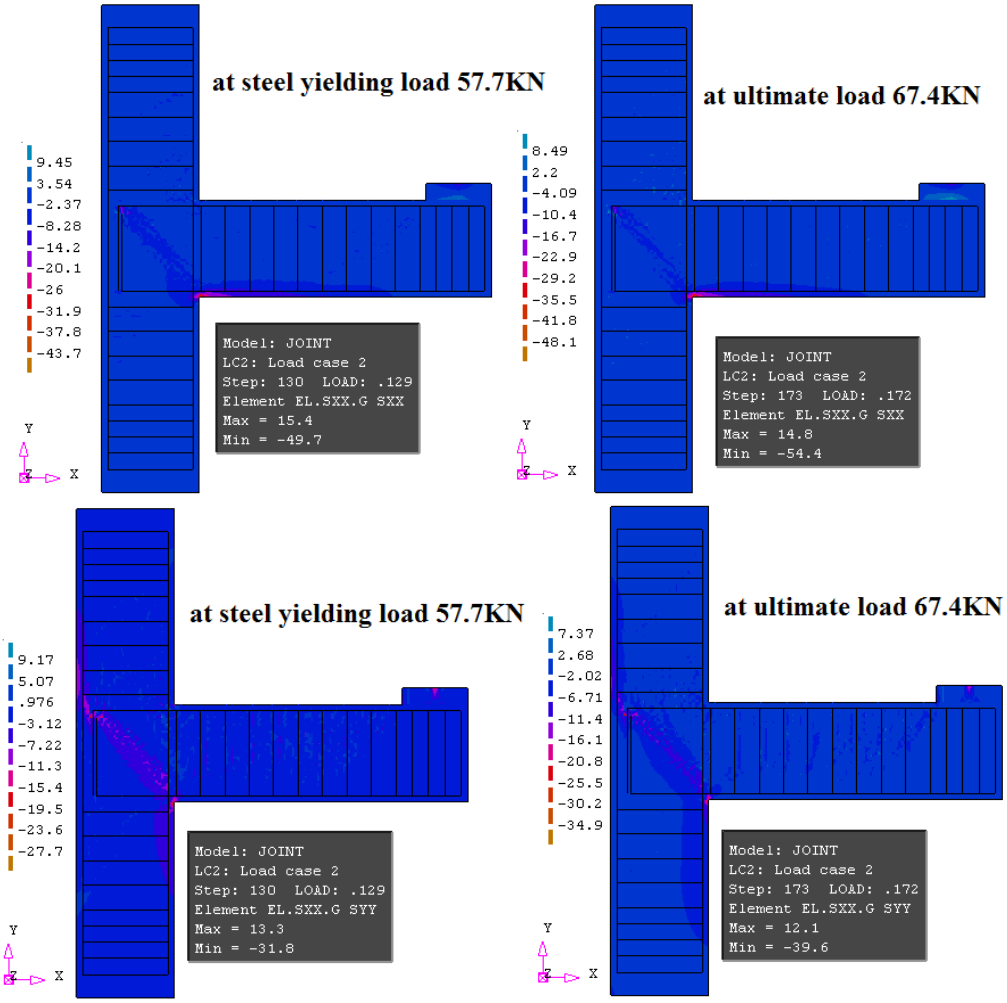

Figure 142 Stress in Concrete Sxx & Syy for J-BI-12 in Diana

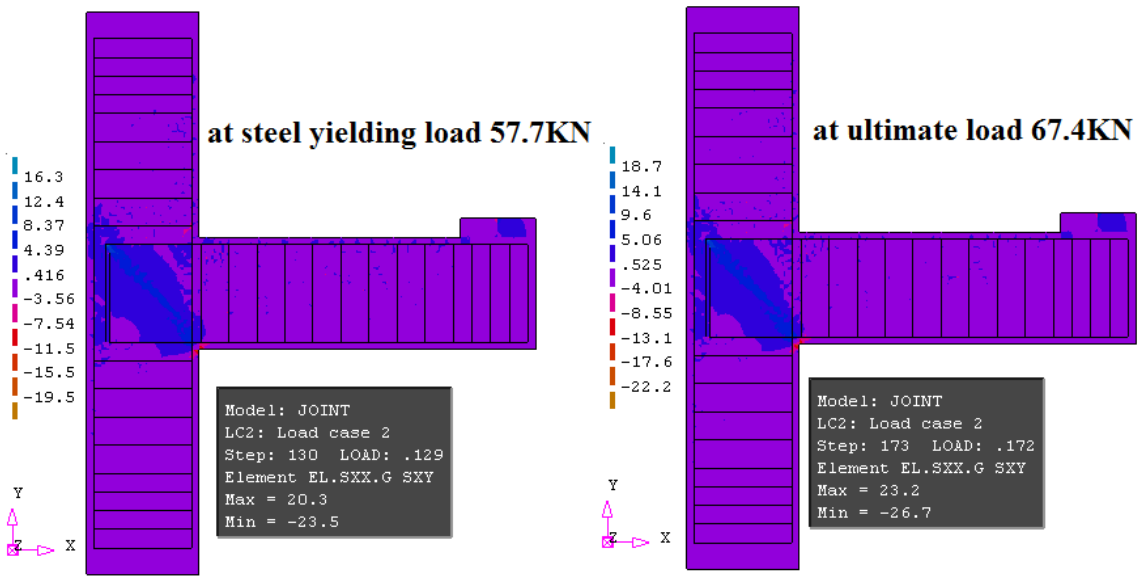

Figure 143 Stress in Concrete Sxy for J-BI-12 In Diana

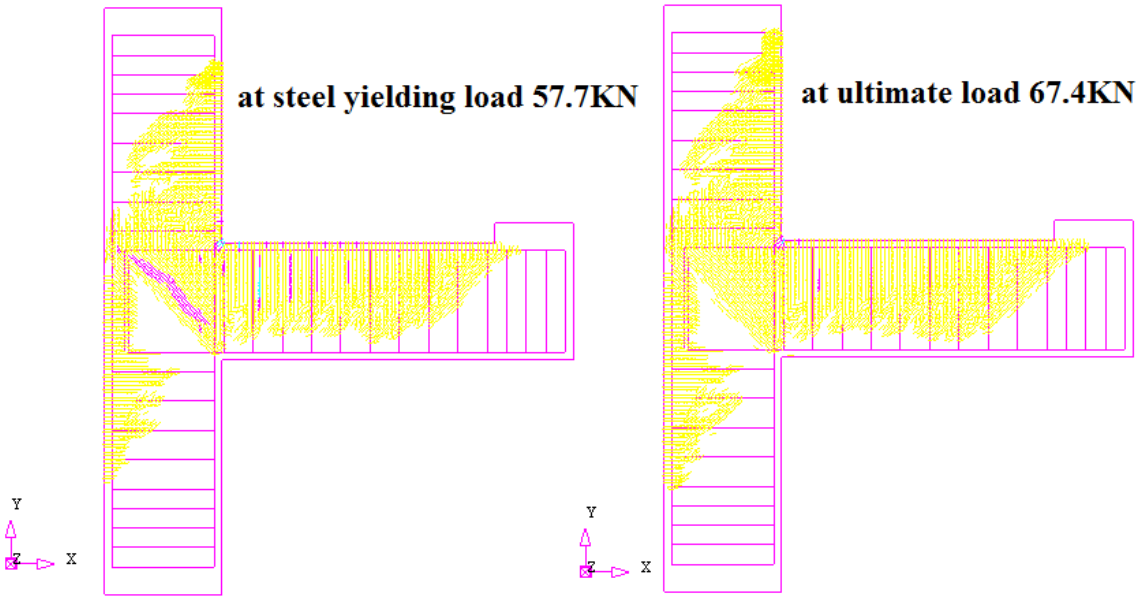

Figure 144 Crack Patterns for J-BI-12 in Diana

7.6 FINITE ELEMENT ANALYSIS FOR J-BI-18

Model was made in DIANA and the load displacement graphs were plotted to compare the results of experiment and finite element results as shown in “Figure 145, 146 & 147”.

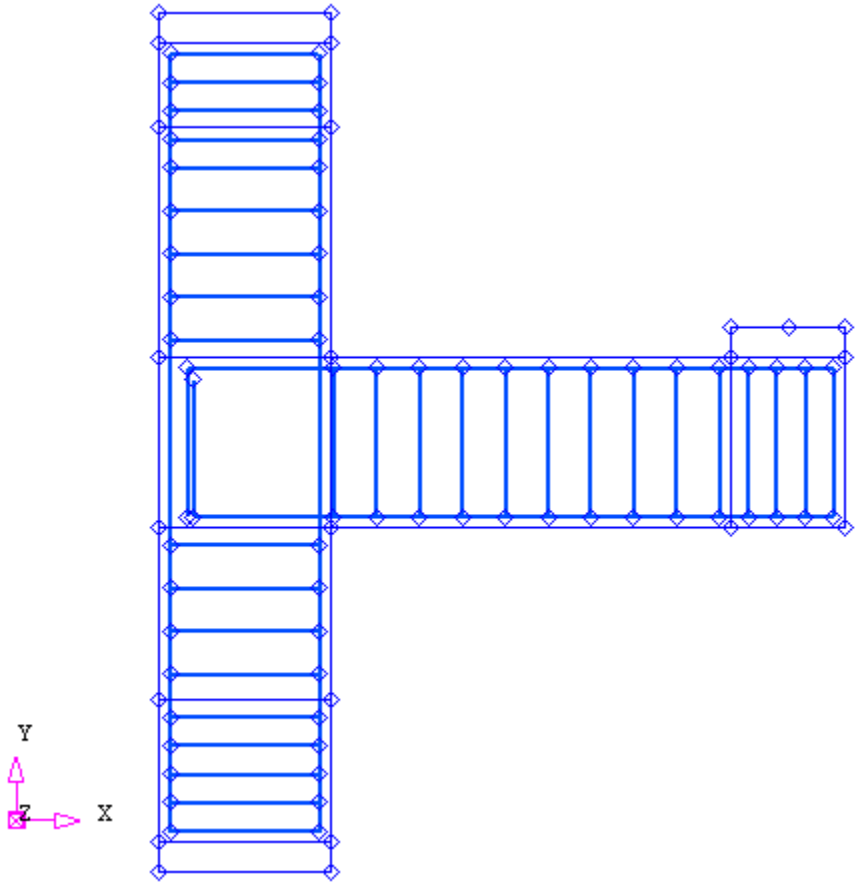

Figure 145 Diana Model of Specimen J-Bi-18

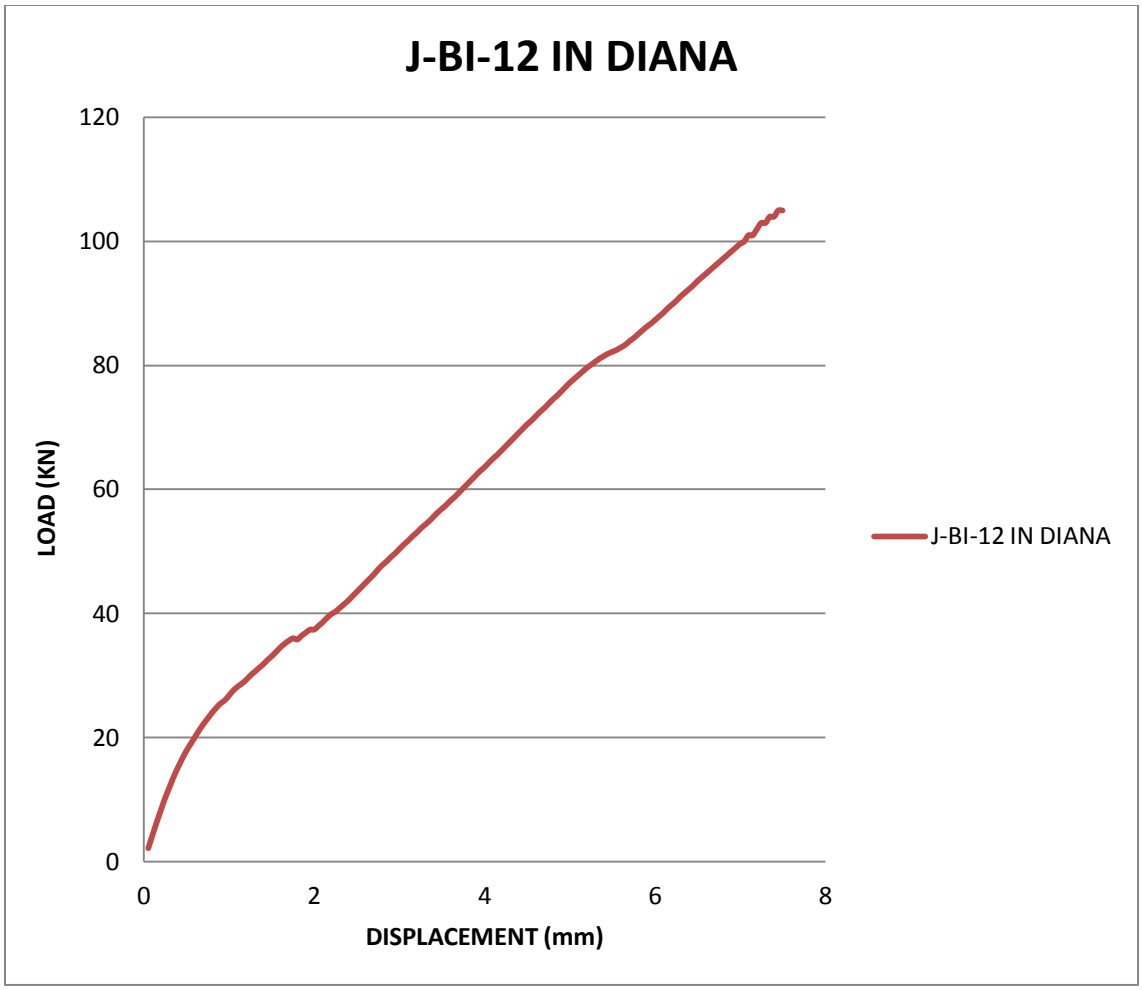

Figure 146 Load Vs Displacement Graph for Specimen J-Bi-18 in Diana

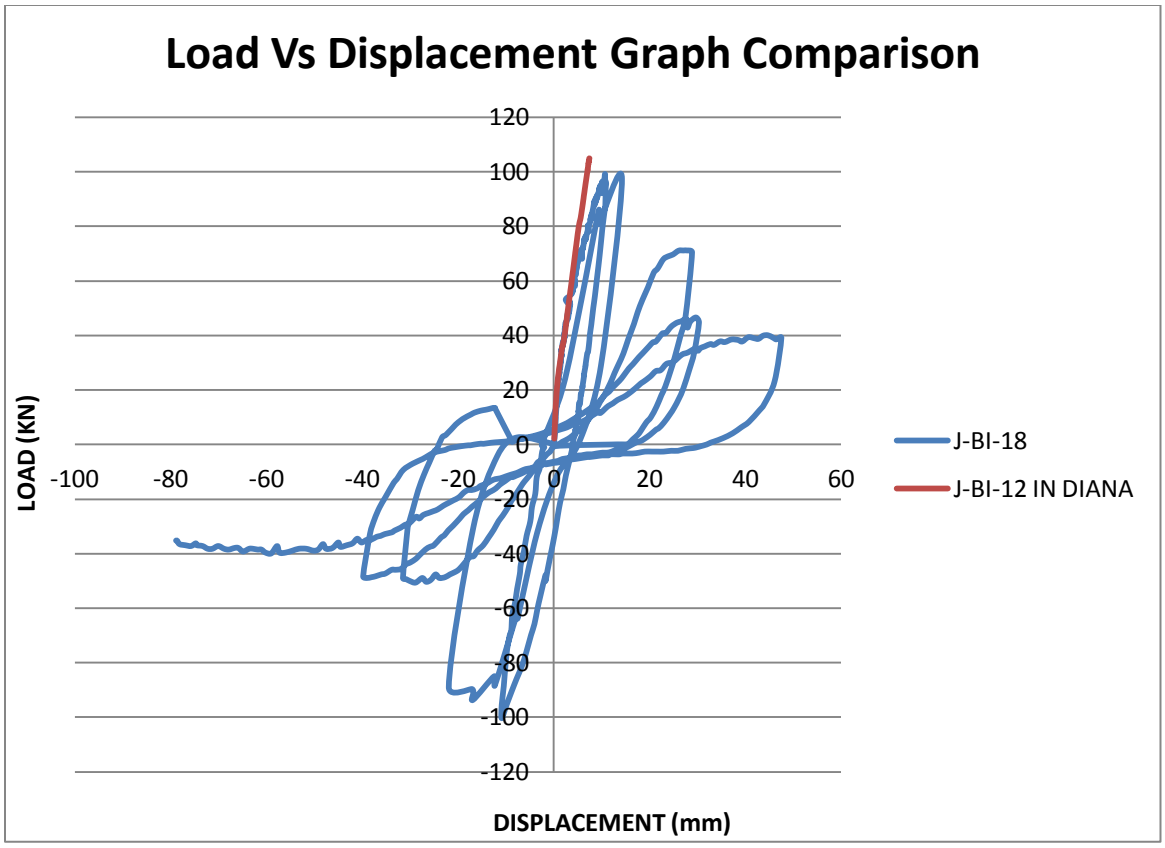

Figure 147 Load Vs Displacement Graph Comparison

The experimental results of cyclic load test on the beam-column joint carried at KFUPM are shown “Figure 147”. For numerical simulation the envelope of the load displacement curve is considered. The result of finite element simulation matches closely with experimental results as shown in “Figure 147”. Diana is not able to capture the softening as reported by Bindhu et al [14] & Mitra et al [15].

The stresses in steel in x and y directions at ultimate load that is 105KN is shown in "Figure 148". The stress in top steel of the beam at ultimate load is 526MPa. The stress in steel for column on tension side at ultimate load is 348MPa.

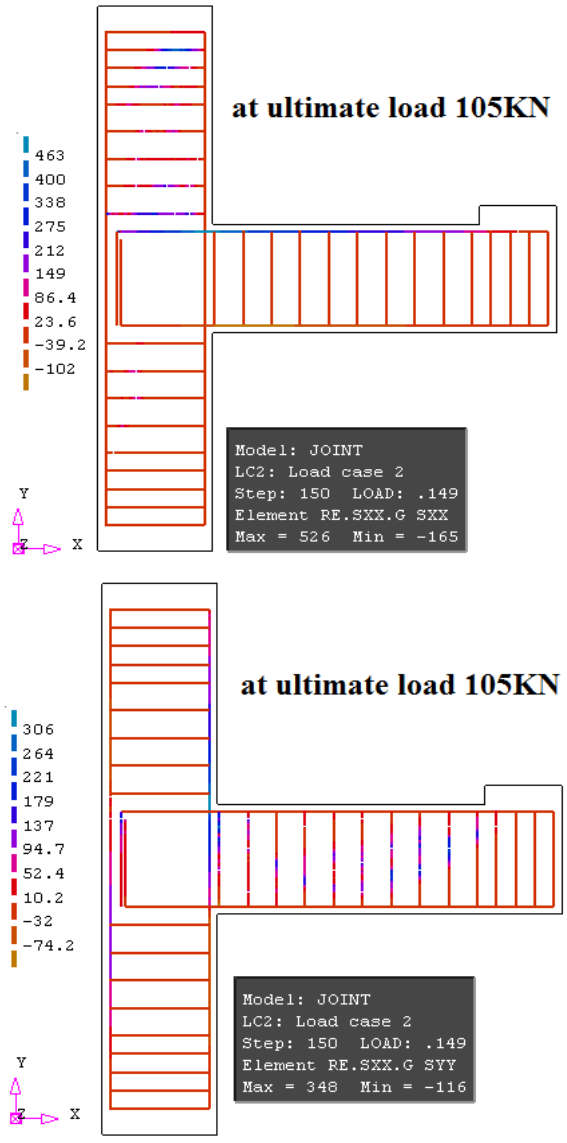

Figure 148 Stress in Steel Sxx & Syy for J-BI-18 in Diana

The stresses σx, σy and σxy in concrete at at ultimate load (105KN) are shown in "Figure 149 & 150". The stresses in concrete shows the similar behavior of stresses formed in

concrete as it was observed in experimental test and the joint region of beam-column joint is found to be more critical as it was in actual test. The diagonal crack pattern at the joint closely resembles the crack pattern observed in experimental program as shown in "Figure 151".

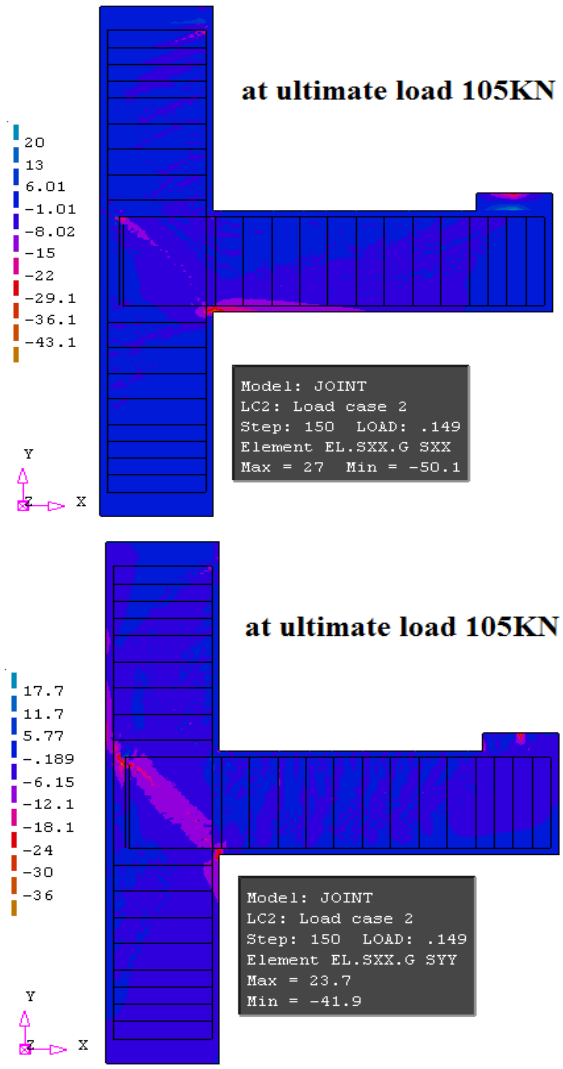

Figure 149 Stress in Concrete Sxx & Syy for J-Bi-18 in Diana

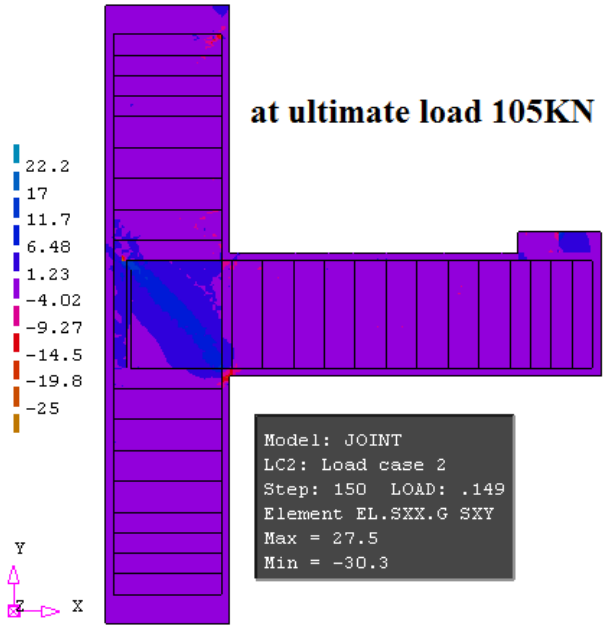

Figure 150 Stress in Concrete Sxy for J-Bi-18 in Diana

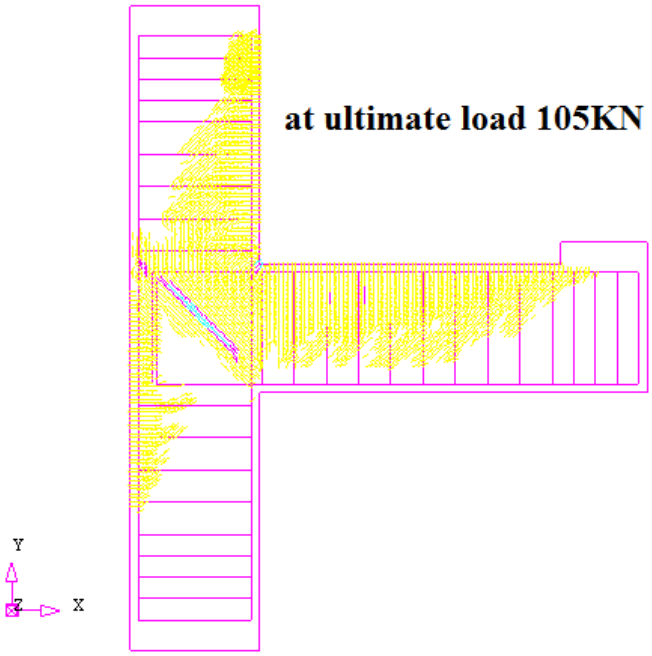

Figure 151 Crack Patterns for J-Bi-18 in Diana

CHAPTER 8

FINITE ELEMENT ANALYSIS OF ITU SPECIMENS

USING DIANA

In a collaboration program between Istanbul Technical University and King Fahd University of Petroleum and Minerals in the area of seismic behavior of RC structures, an experimental program is being conducted on the beam-column joints constructed in early eighties in Saudi Arabia. The concrete strength used in RC structures was very low and detailing at joints was non-existent; this is similar to situation which exists in many seismically active areas of Turkey.

Finite element simulation of a typical exterior beam-column joint using a very low strength concrete (8.6MPa).The results from experimental program conducted at Istanbul Technical University on a typical low strength concrete beam-column joint is used to validate the finite element model.

8.1 TEST PROGRAM

Ilki et. al. [19 & 20]tested eight exterior beam-column joints in two series of tests using low-strength concrete and plain reinforcing bars to represent the conditions of joints of existing deficient reinforced concrete building structures.

8.1.1 Test Specimens

The configuration is common to all specimens; a cross section of the columns is 250 mm x 500 mm and a cross section of the beams is 250 mm x 500 mm. Eight plain bars of 16mm diameter were used in the column for longitudinal reinforcement and 8mm diameter closed ties at a spacing of 150mm were used as transverse reinforcement. For beams, four plain bars of 16 mm diameter were used for both the top and bottom longitudinal reinforcement and 8mm diameter closed ties with spacing of 100 were used for transverse reinforcement in beam. Details of specimen's geometry and reinforcement are given in "Figure 152".

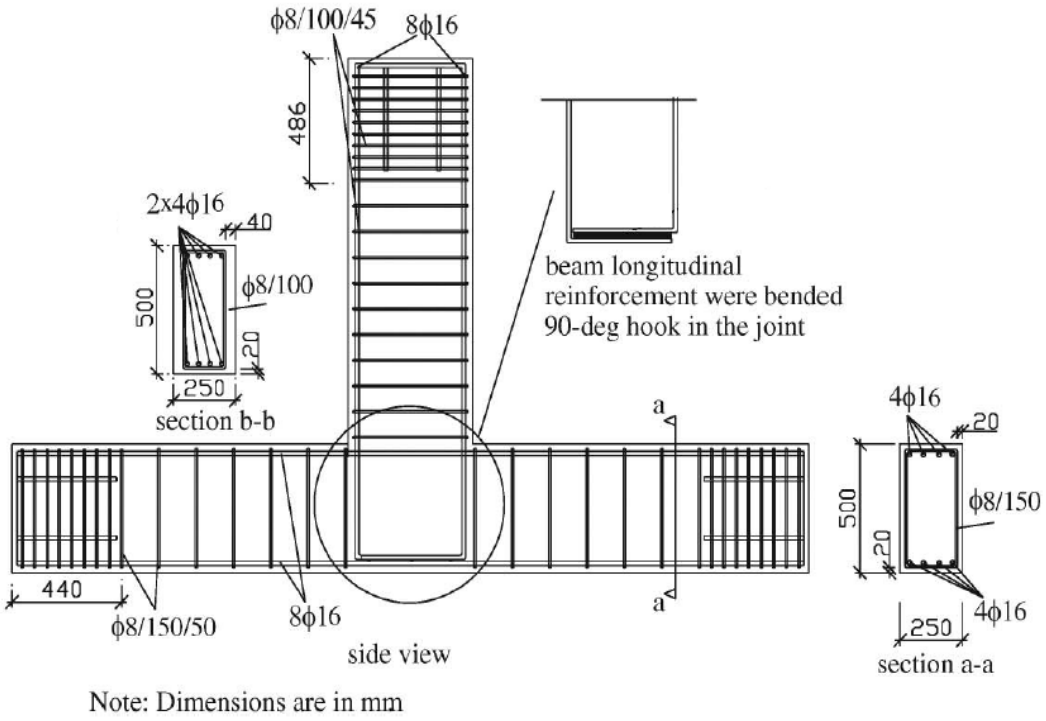

Figure 152 Geometry and Reinforcement Details of Specimens [19, 20]

The specimens referred to as JW was the major target for the numerical study, where JW is from the series of reference

8.1.2 Material Properties

The mechanical properties of the reinforcing bars and concrete were determined in the experimental program and are presented in Tables 5. and 6.

Table 5 Mechanical Properties of Reinforcing Bars

Reinforcement	Diameter (mm)	f_y, Mpa	$\varepsilon_y = f_y/E_s$	ε_{sh}	f_{smax} Mpa	ε_{smax}	f_{su} Mpa	ε_{su}
Φ16	16	333	0.0017	0.03	470	0.20	335	0.34
Φ8	8.4	315	0.0016	0.03	433	0.20	265	0.34

Table 6 Material Properties of Concrete

f'c (Mpa)	Ec (Mpa)
8.3	13000

8.1.3 Experimental Program

Specimens were tested under the combine action of constant axial load on the column and cyclic load on the tip of beam. The axial load is applied at one end of the column by using hydraulic jack and the cyclic load is applied at the free end of the beam using 250KN servo-controlled hydraulic actuator. Specimens were tested on the horizontal frame as shown in "Figure 153"

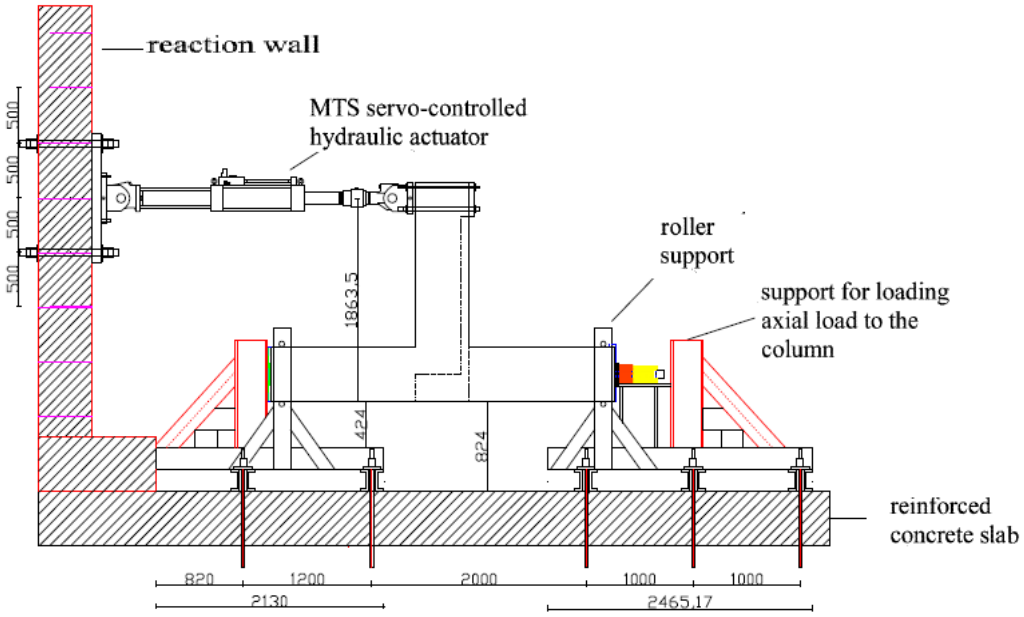

Figure 153 Horizontal Frame for Test Specimens [19, 20]

The test was displacement controlled, lateral displacements were imposed until the selected target drift ratios were reached as given in "Figure 154". The movements of the specimens in the vertical and horizontal directions were measured using variable displacement transducers (LVDTs).

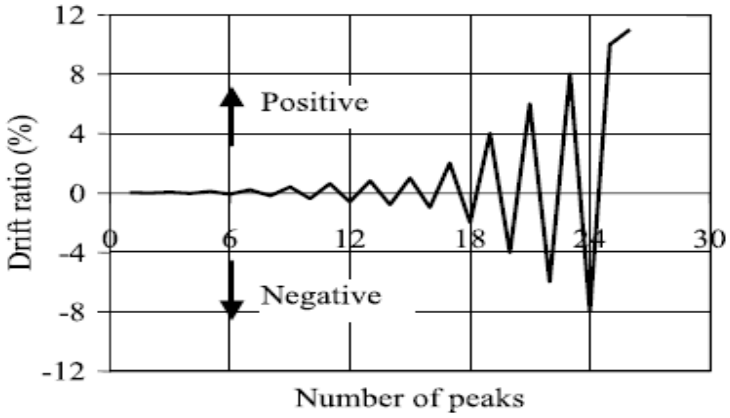

Figure 154 Displacement History [19, 20]

8.2 FINITE ELEMENT ANALYSIS OF ITU SPECIMEN

8.2.1 Material Properties in DIANA

Material properties for concrete f_t=0.73MPa at 28 days, c= 2.15MPa (calibrated to match experimental data, Φ=Ψ=10º, beta=0.9 (smaller values lead to premature curtailment of P-Δ curve), modulus of elasticity of concrete E= 12000 MPa, steel hardening diagram and modulus of elasticity of steel taken from actual test results.

8.2.2 Mesh

The mesh scheme and density is shown in "Figure 155"

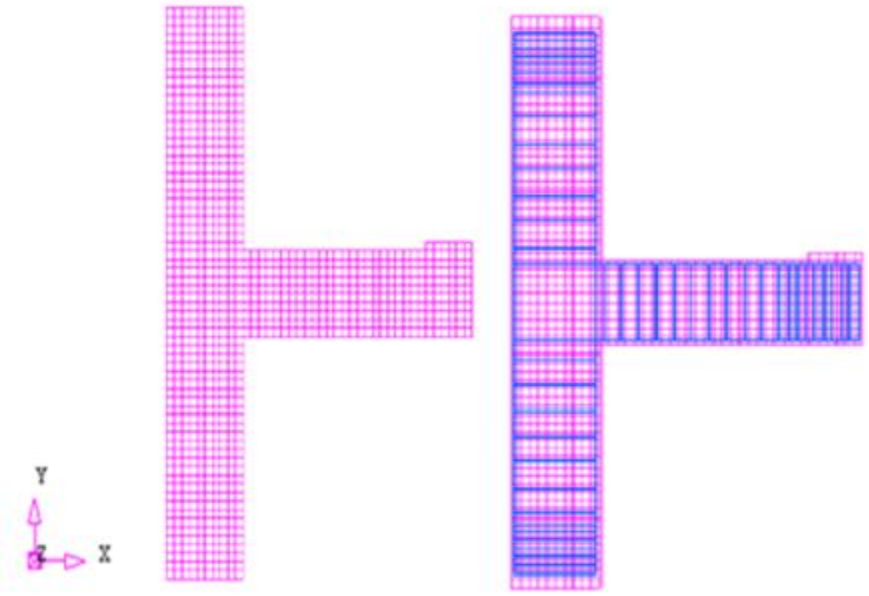

Figure 155 Specimen with Mesh & Reinforcement

8.2.3 Boundary Conditions and Loading Details

"Figure 156" shows the top end of the column surface is constrained in x and y-direction. Bottom end of the column is constrained in x-direction and free in y-direction due to upward axial pressure (0.125*f'c). The tip of beam is constrained in y-direction for application of displacement which is 50mm.

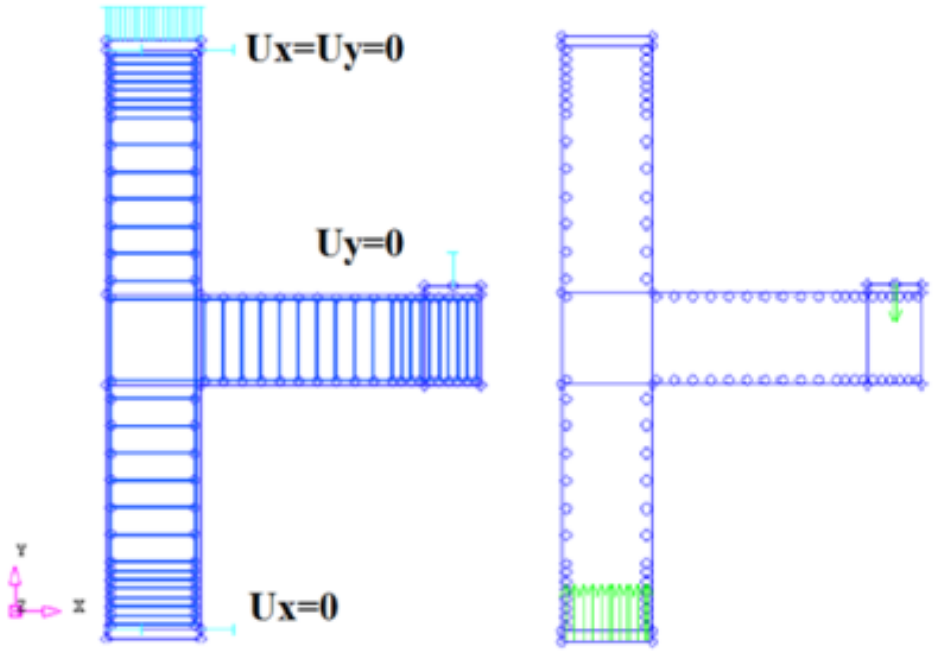

Figure 156 Boundary Conditions and Loading Details

8.3 RESULTS FROM EXPERIMENT AND ANALYSIS

8.3.1 Beam Column Joint JW2

The experimental results of cyclic load test on the beam-column joint carried at ITU are shown "Figure 157a". For numerical simulation the envelope of the load displacement

curve is considered. The result of finite element simulation matches closely with experimental results as shown in “Figure 157b”. Diana is not able to capture the softening as reported by Bindhu et al [14] & Mitra et al [15]

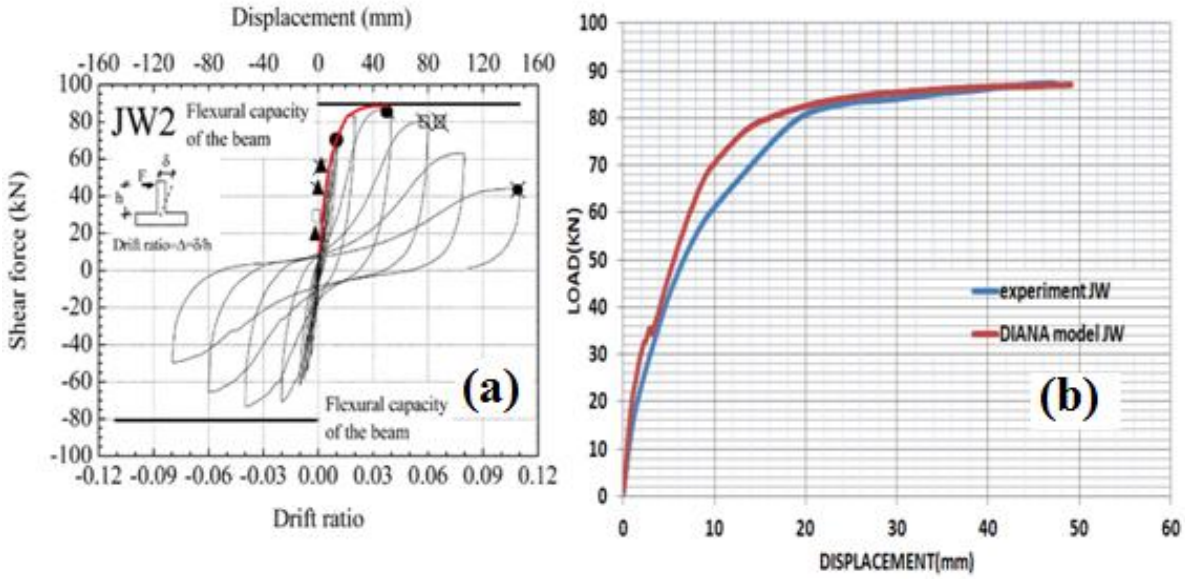

Figure 157 (a) Envelope for Hysteresis & (b) Comparison of Load Displacement Graph from DIANA for Specimen JW2 [19, 20]

The stresses in steel in x and y directions at steel yielding load that is 75KN and at ultimate load that is 86.91K is shown in “Figure 158”. The stresses in top steel of the beam at steel yielding load and at ultimate load are 279MPa and 292MPa. The stresses in steel in column on tension side at steel yielding load and at ultimate load are 379MPa and 441MPa.

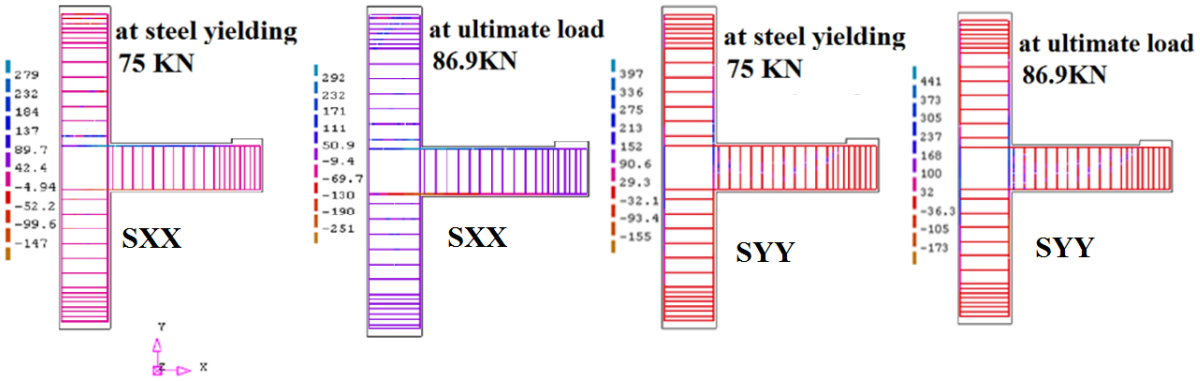

Figure 158 Stress Sxx & Syy in steel from DIANA

The stresses σx, σy and σxy in concrete at steel yielding load (75KN) and at ultimate load (86.9KN) are shown in "Figure 159". The stresses in concrete shows the similar behavior of stresses formed in concrete as it was observed in experimental test and the joint region of beam-column joint is found to be more critical as it was in actual test. The diagonal crack pattern at the joint closely resembles the crack pattern observed in experimental program as shown in "Figure 160".

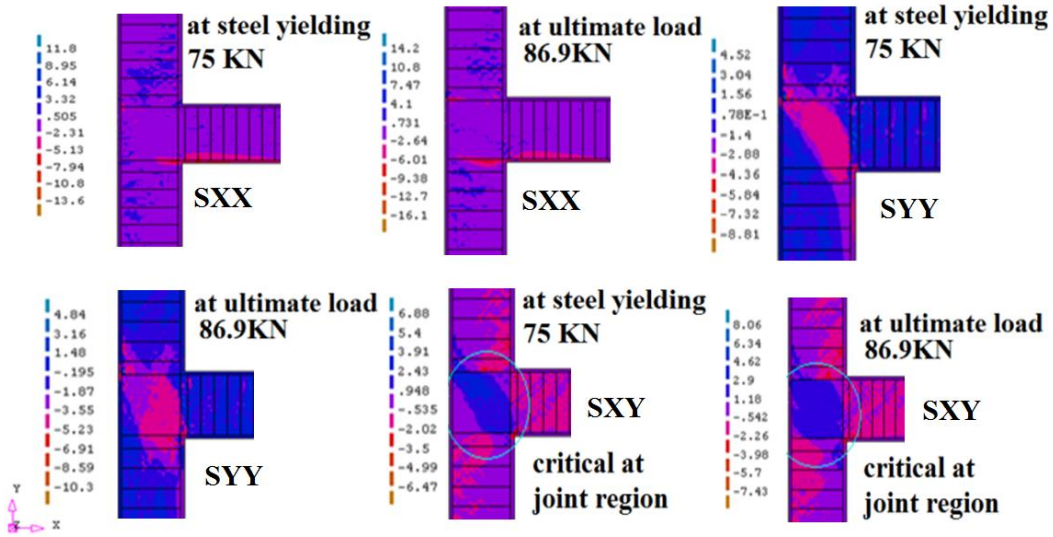

Figure 159 Stresses Sxx, Syy & Sxy in Concrete from DIANA

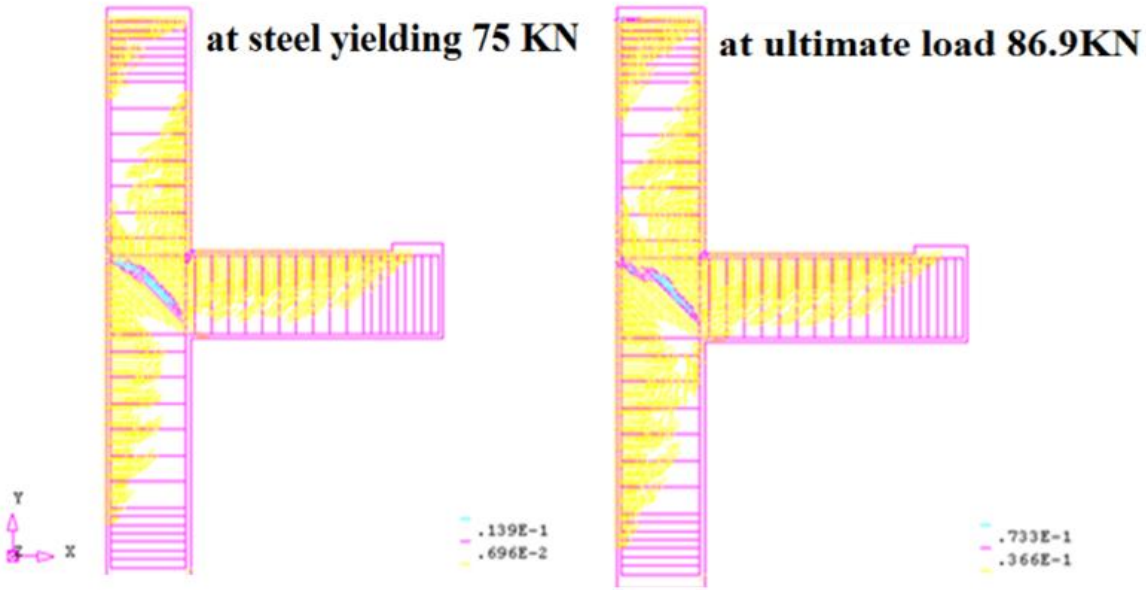

Figure 160 Crack Patterns Obtained From DIANA

CHAPTER 9

RETROFITTING OF EXTERIOR BEAM COLUMN JOINT

OF ITU SPECIMENS

Finite element simulation of a typical exterior beam-column joint using a very low strength concrete (8.6 Mpa) strengthened with CFRP sheets retrofitting .The results from experimental program conducted at Istanbul Technical University on a typical low strength concrete beam-column joint is used to validate the finite element model, testing procedure, geometry, reinforcement and material details are the same as it was used in the chapter 8

The specimen referred to as JWC-D-2 is the major target for the numerical study, where JWC-D-2, belong to FRP-retrofitted specimen (2 plies of CFRP-200mm diagonal strips) as shown in “Figure 161”.

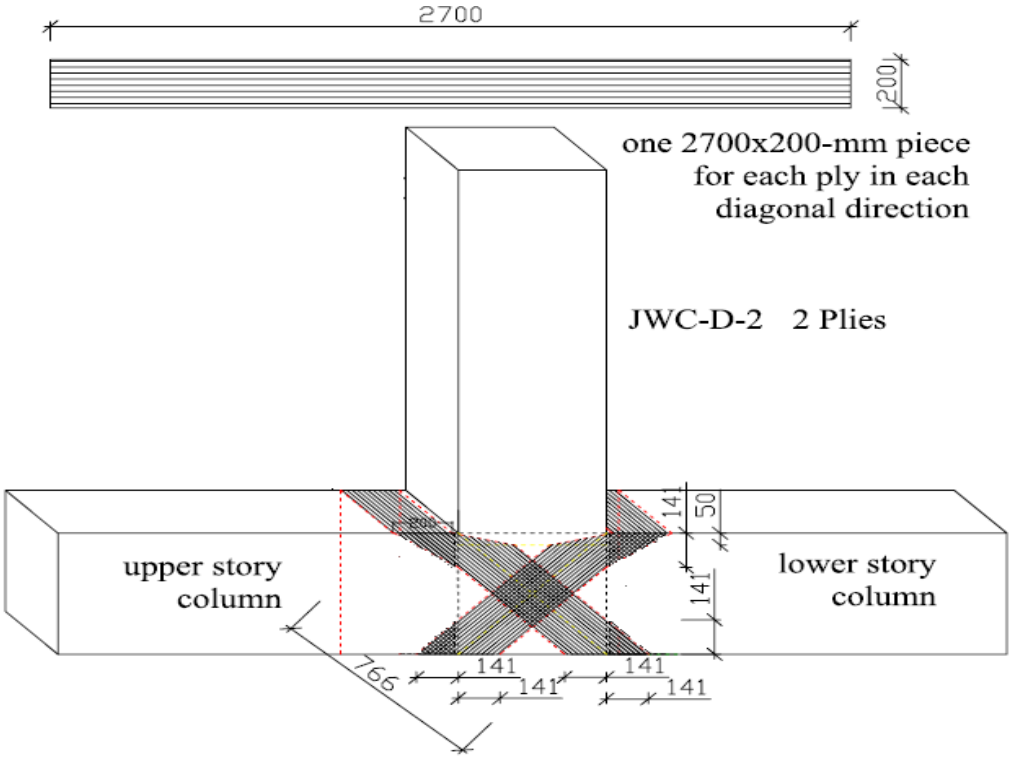

Figure 161 Retrofit of ITU Test Specimen [19, 20]

9.1 RETROFIT OF TEST SPECIMEN

The specimen JWC-D-2 was retrofitted with 2 plies of 200mm wide FRP sheets in diagonal directions (±45º). FRP sheets were bonded only on the external side of joints as shown in "Figure 161". All the corners were rounded before application to avoid stress concentration. Tensile strength, elasticity modulus, rupture strain, effective thickness and unit weight of carbon-FRP sheets were 3800Mpa, 240Gpa, 1.55%, 0.176mm and 330g/m2 respectively.

9.2 RETROFIT OF TEST SPECIMEN

The surface preparation and the application of CFRP on the specimen is given in “Figure 162”

Figure 162 Surface Preparation and Application of CFRP

9.3 COMPARISON OF EXPERIMENTAL TEST RESULTS

The load verses displacement graph were plotted for both retrofitted JWC-D-2 and non retrofitted JW2 specimens from chapter 8 of ITU and it can be scene clearly that the application of CFRP retrofitting increases the flexural capacity of specimen by 13% .as shown in “Figure 163”.

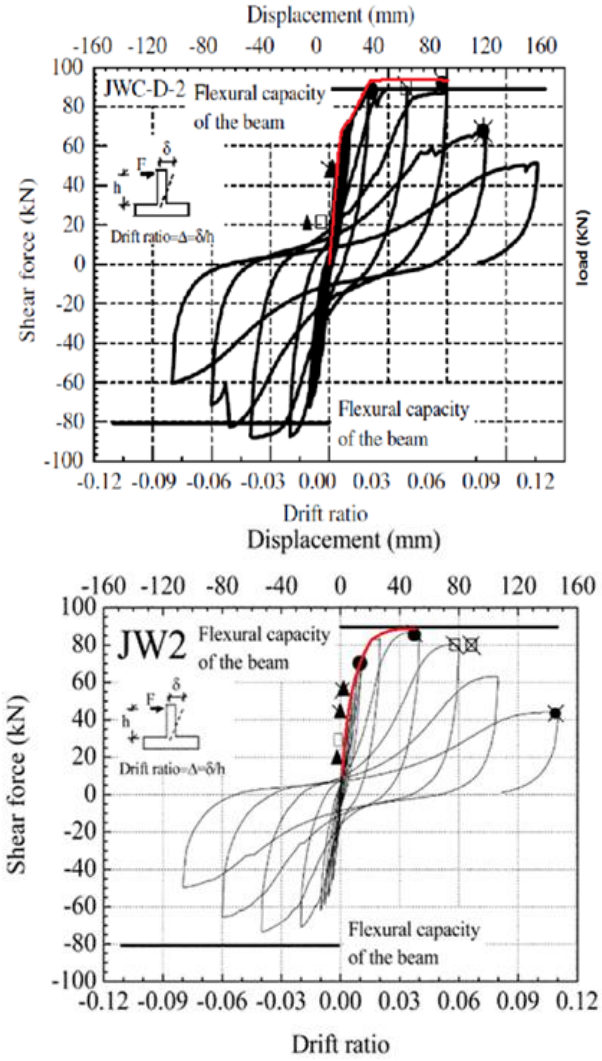

Figure 163 Comparison of Experimental Test Results [19, 20]

9.4 MESH

The mesh scheme and density for retrofitted specimen is shown in Figure “Figure 164”.

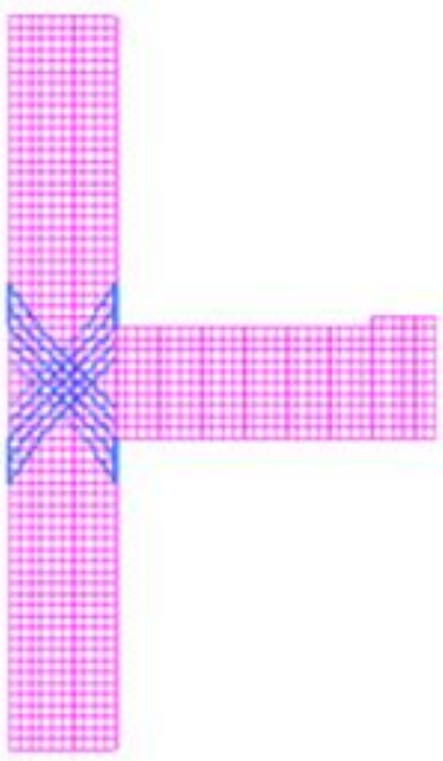

Figure 164 Specimen with Mesh and CFRP Retrofitting

9.5 RESULTS FROM EXPERIMENT AND ANALYSIS

9.5.1 Beam Column Joint Strengthened With CFRP

The hysteresis envelopes obtained in experimental programs for the beam-column joint strengthened with CFRP (Fig.165) in diagonal direction is shown in Fig.165. The stress in steel and CFRP is shown in Fig.166. It can be seen that the maximum stresses occurred in CFRP for both σx and σy. The ultimate load capacity of the beam-column joint strengthened by CFRP sheets increased by 13%. The stress in concrete is shown in Fig.167. The shear stress in the joint decreases due to application of CFRP sheets. The crack pattern of CFRP strengthened beam-column joint changes and failure occurs by cracking at beam column interface with no significant cracking in the joint "Figure 168".

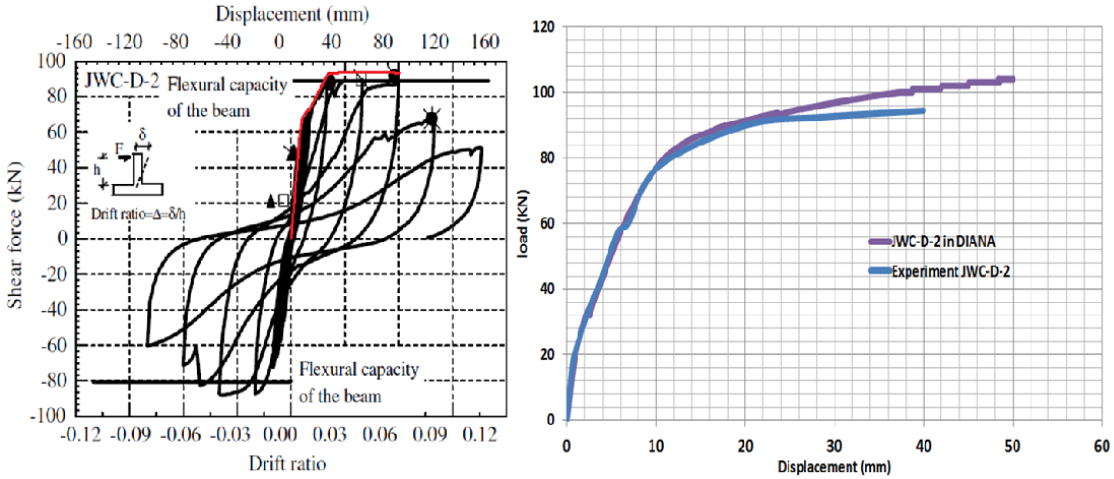

Figure 165 Envelope for Hysteresis & Comparison of Load Displacement Graph from DIANA for Specimen JWC-D-2 [19, 20]

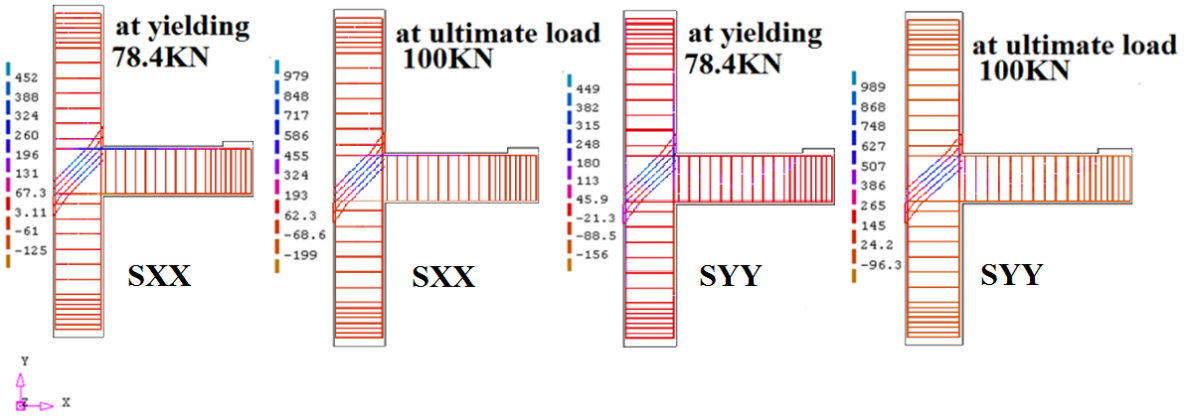

Figure 166 Stress Sxx & Syy in Steel and CFRP from DIANA

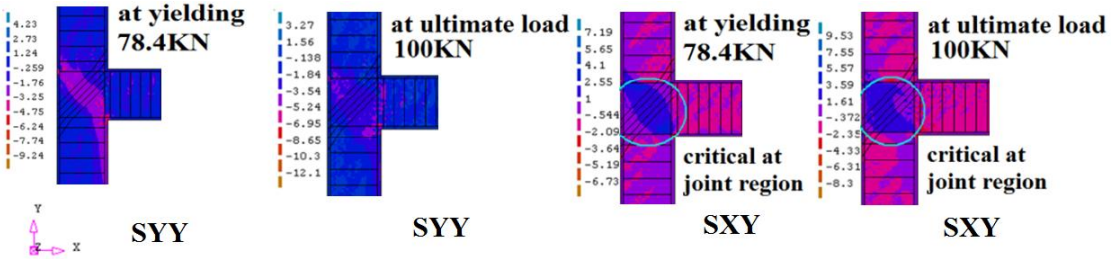

Figure 167 Stresses Syy & Sxy in Concrete from DIANA

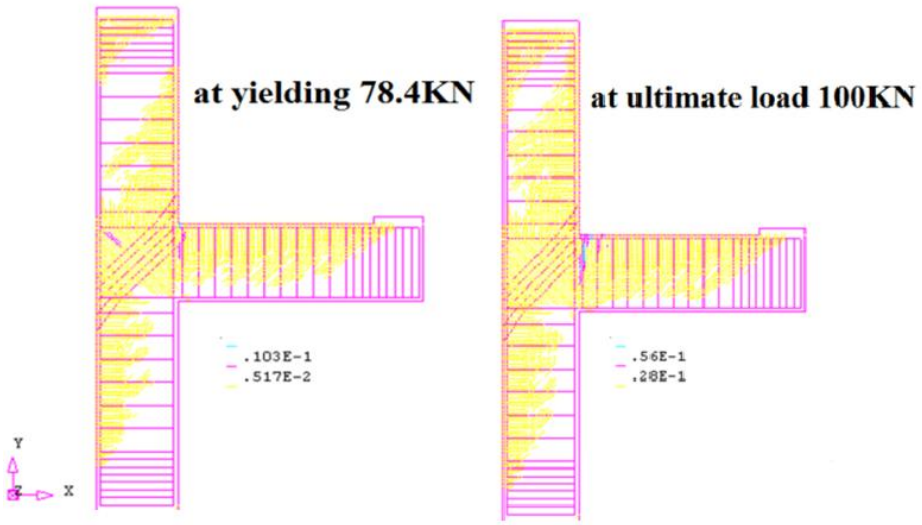

Figure 168 Crack Patterns Obtained from DIANA

CHAPTER 10

CONCLUSIONS

Based on the experimental, mechanistic and computational modeling carried out for the three exterior reinforced concrete beam-column joint specimens at KFUPM and one ITU specimen, following conclusions may be drawn:

- The actual mode of failure in the joint is dictated by the geometry of the beam, the column, and the joint, and the amount of reinforcement in the beam, together with reinforcement detailing of joint.
- Two cracking loads have been identified. One is associated with flexural cracking of the beam and the other with a diagonal crack in the joint which results when the maximum principal stress exceeds the tensile strength of concrete. For the specimen considered in this task, the P_{cr} due to flexure < P_{cr} due to joint shear.
- For specimens designed with ρ=0.0045 (J-BU-12 & J-BI-12), the experimental results showed that the ultimate capacity of the specimen was reached when the load corresponded to the flexural capacity of the beam. This was further confirmed by mechanistic model calculations in conjunction with experimental data of reinforcement strains and by the results obtained from computational model under DIANA environment.
- Stresses in the beam, column and joints are matchable and model predicts good result for stress which indicates that beam- column joint is well modeled by Drucker-Prager with tension cut-off and tension softening.

- For specimen designed with higher ρ=0.01 (J-BI-18) experimental results showed that the specimen collapsed due to failure of joint under shear, as the collapse load was lower than the flexural capacity of the beam (27.59% lower). That was confirmed from the combined mechanistic/ experimental computations and also further corroborated from DIANA results.
- Based on experimental results of specimens with ρ=0.01 (J-BI-18) a value of "γ" of approximately 9 from the expression $\emptyset V_{nj} = 0.75\gamma\sqrt{f_c'}A_j$ was obtained, in contrast to the suggested values of "γ" from 12 to 15 in the ACI code for properly detailed joints subjected to seismic loading. In this study, the joint detailing did not meet ACI specifications as the work was simulating joints in old buildings not conforming to the code.
- In order to study retrofitting of beam-column connections failing prematurely due to the collapse of joint, the ITU specimens with very low compressive strength concrete were modeled in the DIANA environment by using CFRP strips similar to reinforcement steel used as stirrups. Reasonable correlations between experimental and finite element results were obtained both for control and retrofitted ITU specimens.
- The FEM modeling using Drucker – Prager in a DIANA environment was noted to yield reasonably accurate results for the beam-column joint specimens. It appears that the non-associated theory of plasticity gives better results for the behavior of concrete in compression. Further, the angle of internal friction was noted to change, depending on whether the component was under dominant uniaxial or biaxial state of stress.

References

[1] Shigeru Hakuto. Seismic Load Tests on Interior and Exterior Beam-Column. *ACI Structural Journal* , Title no. 97-S02. (2000).

[2] Chris P Pantelides. Rehabilitation Of R/C Building Joints With FRP Composites. *12th World Conference Earthquake Engineering.* (2000).

[3] M.Gencoglu. The Strengthening of the Deficient RC Exterior Beam-Column Joints Using CFRP for Seismic Excitation. *Structural Engineering,Mechanics and Computation.* Cape Town, South Africa: Millpress, The Netherlands. (2007).

[4] Kien Le-Trung . Experimental study of RC beam–column joints strengthened using CFRP composites. *Composites: Part B* , 76-85. (2010).

[5] S. Pampanin. Seismic Behaviour Of R.C. Beam-Column Joints Designed For Gravity Loads. *12th European Conference on Earthquake Engineering* (p. Paper Reference 726). Barbican Centre, London, UK: Elsevier Science. (2003).

[6] Robert Ravi.S. Experimental Investigation on Behavior of Reinforced Concrete Beam Column Joints Retrofitted with GFRP & AFRP. *International Journal Of Civil And Structural Engineering* , 245-253. (2010).

[7] A. Ghobarah. Seismic rehabilitation of beam–column joint using GFRP sheets. *Engineering Structures* , 1397–1407. (2002).

[8] Franco Braga. R/C Existing Structures with Smooth Reinforcing Bars: Experimental Behaviour of Beam-Column Joints Subject to Cyclic Lateral Loads. *The Open Construction & Building Technology Journal* , 52-67. (2009).

[9] Saptarshi Sasmal. Seismic retrofitting of nonductile beam-column sub-assemblage using FRP wrapping and steel plate jacketing. *Construction and Building Materials* , 175–182. (2011).

[10] Saleh H. Alsayed. Seismic Behavior of As-built, ACI-complying and CFRP-repaired Exterior RC Beam-Column Joints. *Journal of Composites for Construction* , 1943-5614. (2010).

[11] D. Mostofinejad. Finite Element Modeling Of Rc Connections Strengthened With FRP Laminates. *Iranian Journal of Science & Technology* , Vol. 30, No. B1. (2006).

[12] Robert Ravi.S. Finite Element Modeling on behavior of Reinforced Concrete Beam Column Joints Retrofitted with Carbon Fiber Reinforced Polymer sheets. *International Journal Of Civil And Structural Engineering* , 576-582. (2010).

[13] G. Sagbas. Computational Modeling of the Seismic Performance of Beam-Column Subassemblies. *Journal of Earthquake Engineering* , 15:640–663. (2011).

[14] K.R. Bindhu. Strength And Behaviour Of Exterior Beam Column Joints With Diagonal Cross Bracing Bars. *Asian Journal Of Civil Engineering (Building And Housing)* , 397-410. (2010).

[15] Mitra. Continuum Model For Rc Interior Beam-Column Connection Regions. *The 14th World Conference on Earthquake Engineering.* Beijing, China: WCEE. (2008).

[16] DeWitte. *DIANA - Finite Element Analysis DIANA - Finite Element Analysis.* The Netherlands.: TNO Building and Construction Research, Delft. (2005).

[17] Imran, Plasticity model for concrete under. *J. Engrg. Mech., ASCE* , 281–290. (2001).

[18] Smith, S. W. Concrete over the top, or is there life after peak? *ACI Mat.* , 491–497. (1989.).

[19] Alper Ilki. Behavior of Deficient Joints with Plain Bars and Low-Strength Concrete. *ACI Structural Journal* , 300-310. (2010).

[20] Alper Ilki. Behavior of FRP Retrofitted Joints Built with Plan Bars and Low-Strength Concrete. *Journal Of Composites For Construction © ASCE* . (2011).

[21] Priestley, M. Displacement-based seismic assessment of reinforced concrete. *Journal of Earthquake Engineering* , 157-192. (1997).

[22] Borst, P. *Non-associated plasticity for soil, concrete and rock.* Netherlands: HERON. (1984)

APPENDIX A

DESIGN OF SPECIMEN J-BI-18

DESIGN PARAMETERS:

CONCRETE COMPRESSIVE STRENGTH: f'c	**4350**	**30**	**MPa**	**concrete cover: (in)**	**0.590551181**	15 mm
STEEL LONGITUDINAL REBER YIELD STRENGTH: fy	**95700**	**660**	**Mpa**			
STEEL TRANSVERSE REBAR YIELD STRENGTH: fy_h	**69600**	**480**	**Mpa**			
STEEL MODULUS OF ELASTICITY: Es	**29000000**	**200000**	**Mpa**			
SHEAR STRENGTH REDUCTION FACTOR: ϕv	**0.75**					
MAX. CONCRETE COMPRESSIVE STRENGTH STRAIN: εc	**0.003**					
Increase factor for yield stress in beam tensile rebar (ACI 21.5.1.1) : α	**1.25**					
Joint shear strength factor based on confinement (ACI 21.5.3.1) : ɣ	**15**					

COLUMN DESIGN :

COLUMN DIMENSIONS:

	b in	h in	Ag in2	Lcol in
	9.84252	11.81102362	116.2502325	55.11811024
mm	250	300	75000	1400

LONGITUDINAL REINFORCEMENT:

	bar loc.(in)	bar size (#)	bar area (in2)	no. bars
levels of reinforcement:	1.06988189	5.669291339	0.394586503	3
	0	0	0	0
	10.74114173	5.669291339	0.394586503	3

TRANSVERSE REINFORCEMENT :

Diameter of transverse reinforcing bars:	dtr: (in)	0.375
Area of transverse reinforcing bars:	Atr: (in2)	0.110491071
Number of closed hoops:	nclosed	1
Total area of transverse reinforcing steel:	Asv: (in2)	0.220982143

Steel Reinforcement Layout:

Area of steel at each level: (in2)	As	1.18375951	763.7142857mm^2
		0	0
		1.18375951	763.7142857mm^2
Total area of steel: (in2)	Ast	2.367519021	
Reinforcement ratio:		0.020365714	
Nominal axial load capacity: (Kips)		647.6529034	2882.05KN
12.5% of P0: (Kips)		32.38264517	144.10KN

Flexure Design:

Equivalent stress block factor:	β1	0.8325		
Location of neutral axis: (in)	c	2.789	69.52872048	mm
Strain in each level of rebar: (+) tension, (-) compression:	εS = εc.(d-c)/c	-0.001758966		
		-0.003		
		0.008703257		
Stress in each level of reber: (+) tension, (-) compression:	fs=Es.εS (Ksi)	-51.01001654	-351.793218	Mpa
		-87	-600	Mpa
		95.7	660	Mpa
Forces in each level of reber: (+) tension, (-) compression:	Fs=As.fs (Kips)	-60.3835922	-268.706985	KN
		0	0	KN
		113.2857851	504.1217439	KN
Compressive axial force in effective concrete stress block:	Fc=0.85f'c.b.(β1.c) (kips)	82.93335553	369.0534321	KN
Sum of axial forces to show that the sum is appx zero:	Fc-∑Fs-Pn (lb)	0.0028		

Moment capacity of column:	∑[Fs.(d-a/2)]+0.85.f'c.b.(β1.c).(h/2-β1c/2) (Kips.in)	1454.0832	164355	KN-mm

Beam Design

Beam		hb (in)	bb (in)	Agb (in2)	lb(in)

Dimensions:	11.81102362	9.842519685	116.2502325	35.43307087
	mm 300	250	75000	900

Beam Reinforcement:

level of reinforcement:	bar loc (in)	bar size (#)	bar area (in2)	no.bars
	1.13238189	5.669291339	0.394586503	3
	10.67864173	5.669291339	0.394586503	3

Transverse Reinforcement:

Diameter of transverse reinforcing bars :	dtrb (in)	0.375
Area of transverse reinforcing bars:	Atrb (in2)	0.110491071
number of closed hoops:	nclosedb	1
total area of transverse reinforcing steel:	Asvb (in2)	0.220982143

Steel Reinforcement Layout:

Area of steel at each level:	Asb (in2)	1.18375951	763.7142857mm^2
		1.18375951	763.7142857mm^2

Total area of steel:	Astb (in2)	2.367519021

Reinforcement ratio:	0.010182857

Flexure Design:

Location of neutral axis:	cb (in)	2.1392633	54.33728782 mm

Strain in each level of rebar: (+) tension, (-) compression:	εSb = εc.(dbeam-cb)/cb	-0.001412002	
		0.011975214	

Stresses in each level of rebar: (+) tension, (-) compression:	fsb=Es.εSb (Ksi)	-40.94806034	-282.4004161	Mpa
		95.7	660	Mpa

Forces in each level of rebar: (+) tension, (-) compression:	Fsb= (Asb.fsb) (Kips)	Fcs	-48.47265586	-215.70KN
		T	113.2857851	504.12KN

compressive axial force in effective concrete stress block:	Fcb=0.85f'c.bb.(β1.cb) (Kips)	64.81312439	288.4184035	KN
Sum of axial forces to show that the sum is appx zero:	Fcb+Fcs-T=0	4.89405E-06		

Moment capacity of beam:	Mnb (Kips-in)	(Fcb(d-(β1.cb)/2))+Fcs(d-d')	1097.13	124009.131	KN-mm	KN load 137.7879238

Joint Shear Design:

Tensile force in beam rebar:	**Tn=α.fy.Astb (Kips)**	**141.6072314**
Joint area	**Aj=bb.h (in2)**	**116.2502325**
Length of column to inflection points, used to calculate shear in column:	**Ipc= Lcol (in)**	**55.11811024**
Shear in column:	**Vcol=Mnb/Ipc (Kips)**	**0**
Total shear force in joint:	**Vuj=Tn-Vcol (kips)**	**141.6072314**
Design shear strength of joint:	**ϕVnj=0.75.ɣ.√(f'c).Aj (kips)**	**86.25633101**

Beam shear design:

length of beam from load point to column face: (in)	**beam-length**	**35.43307087**	**900mm**
load required to reach design moment: Pmax (Kips)	**Mnb/beam-length**	**30.96357838**	**137.78KN**
Max. shear load in beam: (Kips)	**Vu = Pmax**	**30.96357838**	**137.78KN**
Design shear strength: (Kips)	**Vn=Vu/ϕv**	**41.28477118**	**183.71KN**
Shear strength of concrete: (kips)	**Vc=2.√(f'c).bb.db**	**13.8642676**	**61.69KN**
Required steel reinforcing shear strength: (Kips)	**Vsreq=Vn-Vc**	**27.42050358**	**122.02KN**
Min spacing factor: Ψ	**2 if Vsreq≥2.√(f'c).bb.db or else 1**	**1**	
Area of transverse reinforcing per hoop: (in2)	**Av=2.Atrb**	**0.220982143**	**142.56mm^2**
Required spacing of shear reinforcement: (in)	**s=Av.Fyh.dbeam/Vsreq**	**5.989726746**	**152.13mm**
Minimum spacing requirments (ACI 21.3.3.2): (in)	**Sreqb=min{s,dbeamNb/2Ψ,24in}**	**5.339320866**	**135.61mm**

column shear design:

max. shear load in column: (kips)	**Vcu=Vcol**	**19.90515753**	**88.57KN**
design shear strength: (kips)	**Vnc=Vuc/ϕv**	**26.54021004**	**118.10KN**
shear strength of concrete: (kips)	**Vcc=2{1+Pn/2000.Ag}.√f'c .dN.b**	**15.79528163**	**70.28KN**
required steel reinforcing shear strength: (kips)	**Vsc=max((Vnc-Vcc,0.001kip)**	**10.74492842**	
Min spacing factor: Ψ	**Ψ=2 if Vsc≥4.√(f'c).b.dcol or else 1**	**1**	
Required spacing of shear reinforcement: (in)	**Sc=Av.fyh.dN/Vsc**	**15.28547397**	
Min stirrup spacing: (in)	**Sreqc=min{Sc,dcol/2.Ψ,16dbb,48.dtrb,24in,bb}**	**5.339320866**	**135.61mm**

DESIGN OF SPECIMENS J-BU-12 & J-BI-12

DESIGN PARAMETERS:

CONCRETE COMPRESSIVE STRENGTH: f'c	**4350**	**30**	**MPa**	**concrete cover: (in)**	**0.590551181**	15 mm
STEEL LONGITUDINAL REBER YIELD STRENGTH: fy	**88450**	**610**	**Mpa**			
STEEL TRANSVERSE REBAR YIELD STRENGTH: fy_h	**69600**	**480**	**Mpa**			
STEEL MODULUS OF ELASTICITY: Es	**29000000**	**200000**	**Mpa**			
SHEAR STRENGTH REDUCTION FACTOR: ϕv	**0.75**					
MAX. CONCRETE COMPRESSIVE STRENGTH STRAIN: εc	**0.003**					
Increase factor for yield stress in beam tensile rebar (ACI 21.5.1.1) : α	**1.25**					
Joint shear strength factor based on confinement (ACI 21.5.3.1) : ɣ	**15**					

COLUMN DESIGN :

COLUMN DIMENSIONS:

	b in	h in	Ag in2	Lcol in
	9.84252	11.81102362	116.2502325	55.11811024
mm	250	300	75000	1400

LONGITUDINAL REINFORCEMENT:

	bar loc.(in)	bar size (#)	bar area (in2)	no. bars
levels of reinforcement:	0.951771654	3.779527559	0.175371779	3
	0	0	0	0
	10.85925197	3.779527559	0.175371779	3

TRANSVERSE REINFORCEMENT :

Diameter of transverse reinforcing bars:	**dtr: (in)**	**0.375**
Area of transverse reinforcing bars:	**Atr: (in2)**	**0.110491071**
Number of closed hoops:	**nclosed**	**1**
Total area of transverse reinforcing steel:	**Asv: (in2)**	**0.220982143**

Steel Reinforcement Layout:

Area of steel at each level: (in2)	**As**	**0.526115338**	**339.4285714**
		0	**0**
		0.526115338	**339.4285714**
Total area of steel: (in2)	**Ast**	**1.052230676**	
Reinforcement ratio:		**0.009051429**	
Nominal axial load capacity: (Kips)		**519.014415**	**2309.614147 KN**
12.5% of P0: (Kips)		**33.03526752**	**147.0069404 KN**

Flexure Design:

Equivalent stress block factor:	β1	0.8325		
Location of neutral axis: (in)	c	1.880294	47.7594676	mm
Strain in each level of rebar: (+) tension, (-) compression:	εS = εc.(d-c)/c	-0.001481453		
		-0.003		
		0.014325884		
Stress in each level of reber: (+) tension, (-) compression:	fs=Es.εS (Ksi)	-42.96213472	-296.290584	Mpa
		-87	-600	Mpa
		88.45	610	Mpa
Forces in each level of reber: (+) tension, (-) compression:	Fs=As.fs (Kips)	-22.60303803	-100.583519	KN
		0	0	KN
		46.53490164	207.0803123	KN
Compressive axial force in effective concrete stress block:	Fc=0.85f'c.b.(β1.c) (kips)	56.96714795	253.5038084	KN
Sum of axial forces to show that the sum is appx zero:	Fc-∑Fs-Pn (lb)	1.68183E-05		

Moment capacity of column:	∑[Fs.(d-a/2)]+0.85.f'c.b.(β1.c).(h/2-β1c/2) (Kips.in)	748.6284532	84617.47	KN-mm

Beam Design

Beam Dimensions:	hb (in)	bb (in)	Agb (in2)	lb(in)
	11.81102362	9.842519685	116.2502325	35.43307087

mm 300 250

bar loc (in)	bar size (#)	bar area (in2)	no.bars
1.014271654	3.779527559	0.175371779	3
10.79675197	3.779527559	0.175371779	3

dtrb (in)	0.375
Atrb (in2)	0.110491071
nclosedb	1
Asvb (in2)	0.220982143

Asb (in2)	0.526115338	339.42mm^2
	0.526115338	339.42mm^2

Astb (in2)	1.052230676

0.004525714

Flexure Design:

Location of neutral axis:	**cb (in)**	**1.250532**	**31.7635128**	**mm**

Strain in each level of rebar: (+) tension, (-) compression:	**εSb = εc.(dbeam-cb)/cb**	**-0.000566784**		
		0.022901181		
Stresses in each level of rebar: (+) tension, (-) compression:	**fsb=Es.εSb (Ksi)**	**-16.43672464**	**-113.35**	**Mpa**
		88.45	**610**	**Mpa**

Forces in each level of rebar: (+) tension, (-) compression:	**Fsb= (Asb.fsb) (Kips)**	**Fcs**	**-8.64761294**	**-38.48**	**KN**
		T	**46.53490164**	**207.08**	**KN**

compressive axial force in effective concrete stress block:	**Fcb=0.85f'c.b b.(β1.cb) (Kips)**	**37.88728861**	**168.59**	**KN**

Sum of axial forces to show that the sum is appx zero:	**Fcb+Fcs-T=0**	**8.58616E-08**

Moment capacity of beam:	**Mnb (Kips-in)**	**(Fcb(d-(β1.cb)/2))+Fcs(d-d')**	**473.93**	**53568.663**	**KN-mm**	**KN load**
						59.52

Joint Shear Design:

Tensile force in beam rebar:	**Tn=α.fy.Astb (Kips)**	**58.16862705**
Joint area	**Aj=bb.h (in2)**	**116.2502325**
Length of column to inflection points, used to calculate shear in column:	**Ipc= Lcol (in)**	**55.11811024**
Shear in column:	**Vcol=Mnb/Ipc (Kips)**	**0**
Total shear force in joint:	**Vuj=Tn-Vcol (kips)**	**58.16862705**
Design shear strength of joint:	**ϕVnj=0.75.ɣ.√(f'c).Aj (kips)**	**86.25633101**

Beam shear design:

length of beam from load point to column face: (in)	beam-length	35.43307087	900	mm
load required to reach design moment: Pmax (Kips)	Mnb/beam-length	13.37544644	59.52	KN
Max. shear load in beam: (Kips)	Vu = Pmax	13.37544644	59.52	KN
Design shear strength: (Kips)	Vn=Vu/ϕv	17.83392858	79.36	KN
Shear strength of concrete: (kips)	Vc=2.√(f'c).bb.db	14.01761219	62.37	KN
Required steel reinforcing shear strength: (Kips)	Vsreq=Vn-Vc	3.816316391	16.98	KN
Min spacing factor: Ψ	2 if Vsreq≥2.√(f'c).bb.db or else 1	1		
Area of transverse reinforcing per hoop: (in2)	Av=2.Atrb	0.098214286	63.36	mm^2
Required spacing of shear reinforcement: (in)	s=Av.Fyh.dbeam/Vsreq	19.33893946	491.20	mm
Minimum spacing requirments (ACI 21.3.3.2): (in)	Sreqb=min{s,dbeamNb/2Ψ,24in}	5.398375984	137.11	mm

column shear design:

max. shear load in column: (kips)	**Vcu=Vcol**	**8.598501281**	**38.26KN**
design shear strength: (kips)	**Vnc=Vuc/ϕv**	**11.46466838**	**51.01KN**
shear strength of concrete: (kips)	**Vcc=2{1+Pn/2000.Ag}.√f'c .dN.b**	**16.10200555**	**71.65KN**
required steel reinforcing shear strength: (kips)	**Vsc=max((Vnc-Vcc,0.001kip)**	**0.001**	
Min spacing factor: Ψ	**Ψ=2 if Vsc≥4.√(f'c).b.dcol or else 1**	**1**	
Required spacing of shear reinforcement: (in)	**Sc=Av.fyh.dN/Vsc**	**74230.74**	

Min stirrup spacing: (in)	**Sreqc=min{Sc,dcol/2.Ψ,16dbb,48.dtrb,24in,bb}**	**5.429625984**	**137.91mm**

Vitae

Name	: Danish Ahmed
Nationality	: Pakistani
Date of Birth	:6/16/1985
Email	: danish_cv@hotmail.com
Contact Number	: 00966551745895
Address	: P.O.BOX # 8665, 31261 Dhahran Saudi Arabia
Permanent Address	: R-27, Hina Homes, Block-21,F.B.Area, Karachi,Pakistan
Academic Background	:Bachelor of Engineering Science, Major Civil Engineering, Sir Syed University of Engineering and Technology, Karachi, Pakistan, 2009. Master of Science, Major Structural Engineering, King Fahd University of Petroleum and Minerals, Dhahran, Saudi Arabia, 2012.